

LASER INTERFEROMETER GRAVITATIONAL WAVE OBSERVATORY
- LIGO -

=====

LIGO SCIENTIFIC COLLABORATION

Technical Note	LIGO-T1500060-v1	July 2017
aLIGO Output Mode Cleaner: Optical Testing and Results		
Koji Arai, Jeffery Lewis, William Z. Korth		

Distribution of this document:

LIGO Scientific Collaboration

California Institute of Technology
LIGO Project, MS 100-36
Pasadena, CA 91125
Phone (626) 395-2129
Fax (626) 304-9834
E-mail: info@ligo.caltech.edu

Massachusetts Institute of Technology
LIGO Project, Room NW22-295
Cambridge, MA 02139
Phone (617) 253-4824
Fax (617) 253-7014
E-mail: info@ligo.mit.edu

LIGO Hanford Observatory
Route 10, Mile Marker 2
Richland, WA 99352
Phone (509) 372-8106
Fax (509) 372-8137
E-mail: info@ligo.caltech.edu

LIGO Livingston Observatory
19100 LIGO Lane
Livingston, LA 70754
Phone (225) 686-3100
Fax (225) 686-7189
E-mail: info@ligo.caltech.edu

Contents

1 Objective and scope	9
2 Test of individual optical components	9
2.1 Characterization of the curved mirrors	9
2.1.1 Curvature radii for the curved mirrors	9
2.1.2 Thickness of the curved mirrors	17
2.1.3 Characterization of the curvature center	17
2.2 Characterizations of the OMC prism mirrors	19
2.2.1 Wedge angle measurement	19
2.2.2 Prism perpendicularity test	23
2.2.3 Data sheet values for the mirror reflectivities and transmissivities . .	27
2.2.4 Measurement of the mirror transmissivities	29
2.2.5 Mirror scattering measurement at Caltech	32
2.2.6 Mirror scattering measurement at UC Fullerton	32
2.3 Characterization of the PZTs	36
2.3.1 PZT Wedge angle	36
2.3.2 PZT actuator DC response & length-to-angle coupling	37
2.3.3 Determination of the mirror arrangement for the PZT subassemblies .	38
2.3.4 PZT endurance test 1: High repetition test	43
2.3.5 PZT endurance test 2: Reverse voltage test	45
2.4 Photodiode and photodetector test	47
2.4.1 DCPD diode test	47
2.4.2 DCPD diode response test	53
2.4.3 Dependence of the photodiode response on the incident angle	54
2.4.4 DCPD preamp test	55
2.4.5 High QE DCPD diode test	55
2.4.6 High QE DCPD response measurement	56
2.4.7 High QE DCPD dark current measurement	56
2.4.8 High QE DCPD dark noise measurement	56
2.4.9 Effect of air-baking on high QE DCPD	56

2.5	Miscellaneous measurements	56
2.5.1	Breadboard size measurement	56
2.5.2	UV epoxy thickness	56
3	Test of the integrated OMC breadboards	58
3.1	Experimental setup	58
3.2	Cavity geometry test	61
3.2.1	Cavity absolute length measurement with detuned locking	61
3.2.2	Cavity length and finesse measurement with RFAM injection	62
3.2.3	Transverse-mode spacing measurement	63
3.2.4	Cavity geometry test results: L1 OMC	63
3.2.5	Cavity geometry test results: H1 OMC	65
3.2.6	Cavity geometry test results: 3rd IFO OMC	70
3.3	Power budget	71
3.4	PZT characterization	71
3.4.1	PZT response	71
3.5	Diode alignment	71
3.5.1	SHIM HEIGHT MEASUREMENT	71
3.5.2	PD/QPD ALIGNMENT photos	71
3.5.3	QPD ALIGNMENT	75
3.6	Misc measurement	78
3.6.1	Weight	78
3.6.2	Spot positions	78
3.7	Backscatter measurement	78
3.8	Vibrational test	79
Appendices		80
A	Mirror List	80
B	DCPD dimensions	82
C	Cavity axis alignment	82

List of Figures

1	Optical setup for the mirror curvature measurement.	11
2	Electrical setup for the mirror curvature measurement.	11
3	Measured TMS/FSR of the curved mirror C1	12
4	Measured TMS/FSR of the curved mirror C2	13
5	Measured TMS/FSR of the curved mirror C3	13
6	Measured TMS/FSR of the curved mirror C4	14
7	Measured TMS/FSR of the curved mirror C5	14
8	Measured TMS/FSR of the curved mirror C6	15
9	Measured TMS/FSR of the curved mirror C7	15
10	Measured TMS/FSR of the curved mirror C8	16
11	Measured TMS/FSR of the curved mirror C9	16
12	Precession of the reflected beam due to axial asymmetry of a curved mirror	18
13	Setup for curvature center measurement	18
14	Definition of the mirror angles	19
15	Geometrical analysis of the curvature center measurement.	20
16	Measurement of the reflected beam precession.	20
17	Graphical representation of the derived positions of the curvature minimum.	21
18	Horizontal wedge measurement	22
19	Vertical wedge measurement	22
20	Principle of the perpendicularity test.	25
21	The test setup for the prism perpendicularity.	26
22	Typical view of the autocollimator and the result analysis.	26
23	Coating A specification.	29
24	Coating B specification.	29
25	Coating C specification.	29
26	Coating D specification.	30
27	Coating E specification.	30
28	AR Coating ACD specification.	30
29	AR Coating BE specification.	30
30	Scattering measurement for the two flat OMC cavity mirrors	34

31	Scattering measurement for the two curved OMC cavity mirrors	35
32	Measured thicknesses of the PZTs	37
33	PZT assembly No.1 gluing sheet	40
34	PZT assembly No.2 gluing sheet	40
35	PZT assembly No.3 gluing sheet	40
36	PZT assembly No.4 gluing sheet	41
37	PZT assembly No.5 gluing sheet	41
38	PZT assembly No.6 gluing sheet	41
39	PZT assembly No.3 gluing sheet actual	42
40	PZT assembly No.4 gluing sheet actual	42
41	PZT endurance test: Driving voltage monitor.	44
42	PZT endurance test: Teperature monitor setup.	44
43	Thermal vision of the PZTs before the actuation.	45
44	Thermal vision of the PZTs during the actuation.	45
45	Teperature change of the PZTs	45
46	Reverse voltage test of the PZT	46
47	Test result of DCPD SN:4, typical good diode performance	50
48	Test result of DCPD SN:1	51
49	Test result of DCPD SN:2	51
50	Test result of DCPD SN:3	51
51	Test result of DCPD SN:5	51
52	Test result of DCPD SN:6	51
53	Test result of DCPD SN:7	51
54	Test result of DCPD SN:8	52
55	Test result of DCPD SN:9	52
56	Test result of DCPD SN:10	52
57	Test result of DCPD SN:11	52
58	Test result of DCPD SN:12	52
59	Test result of DCPD SN:13	52
60	Measured quantities on the photodiode efficiency.	53
61	Optical setup for the OMC test.	59

62	Mode-matching telescope for the OMC cavity.	59
63	The actual setting of the mode matching telescope.	59
64	Beam profile measurement for the OMC cavity mode-matching.	60
65	Photo of the transmission monitor CCD when the cavity is locked.	60
66	Photo of the reflection monitor CCD when the cavity is locked.	60
67	Electrical setup for the OMC test.	61
68	Electrical setup for the OMC test.	64
69	Electrical setup for the OMC test.	65
70	L1 OMC Vertical HOM measurement with $V_{PZT1} = 0V$ and $V_{PZT2} = 0V$	66
71	L1 OMC Horizontal HOM measurement with $V_{PZT1} = 0V$ and $V_{PZT2} = 0V$	66
72	L1 OMC Vertical HOM measurement with $V_{PZT1} = 50V$ and $V_{PZT2} = 0V$	66
73	L1 OMC Horizontal HOM measurement with $V_{PZT1} = 50V$ and $V_{PZT2} = 0V$	66
74	L1 OMC Vertical HOM measurement with $V_{PZT1} = 100V$ and $V_{PZT2} = 0V$	66
75	L1 OMC Horizontal HOM measurement with $V_{PZT1} = 100V$ and $V_{PZT2} = 0V$	66
76	L1 OMC Vertical HOM measurement with $V_{PZT1} = 150V$ and $V_{PZT2} = 0V$	67
77	L1 OMC Horizontal HOM measurement with $V_{PZT1} = 150V$ and $V_{PZT2} = 0V$	67
78	L1 OMC Vertical HOM measurement with $V_{PZT1} = 200V$ and $V_{PZT2} = 0V$	67
79	L1 OMC Horizontal HOM measurement with $V_{PZT1} = 200V$ and $V_{PZT2} = 0V$	67
80	L1 OMC Vertical HOM measurement with $V_{PZT1} = 0V$ and $V_{PZT2} = 0V$	68
81	L1 OMC Horizontal HOM measurement with $V_{PZT1} = 0V$ and $V_{PZT2} = 0V$	68
82	L1 OMC Vertical HOM measurement with $V_{PZT1} = 0V$ and $V_{PZT2} = 50V$	68
83	L1 OMC Horizontal HOM measurement with $V_{PZT1} = 0V$ and $V_{PZT2} = 50V$	68
84	L1 OMC Vertical HOM measurement with $V_{PZT1} = 0V$ and $V_{PZT2} = 100V$	68
85	L1 OMC Horizontal HOM measurement with $V_{PZT1} = 0V$ and $V_{PZT2} = 100V$	68
86	L1 OMC Vertical HOM measurement with $V_{PZT1} = 0V$ and $V_{PZT2} = 150V$	69
87	L1 OMC Horizontal HOM measurement with $V_{PZT1} = 0V$ and $V_{PZT2} = 150V$	69
88	L1 OMC Vertical HOM measurement with $V_{PZT1} = 0V$ and $V_{PZT2} = 200V$	69
89	L1 OMC Horizontal HOM measurement with $V_{PZT1} = 0V$ and $V_{PZT2} = 200V$	69
90	Electrical setup for the OMC test.	70
91	FSR/DETUNING L1	72
92	AM INJ L1	72

93	FSR/DETUNING H1	73
94	AM INJ H1	73
95	FSR/DETUNING 3IFO	74
96	AM INJ 3IFO	74
97	DCPD dimensions	82
98	Definition of the parameters for the cavity axes and mirror alignment	83
99	Preamp SNs and arrangement at LLO	85
100	Preamp SNs and arrangement at LHO	85
101	OMC Wiring - diagram as built	85
102	OMC Wiring - diagram as built (OLD)	86
103	OMC Wiring - diagram as built (OLD)	86

List of Tables

1	Summary of the curvature radii of the C mirrors	12
2	Derived positions of the curvature minimum.	21
3	Result of the wedge angle measurement.	24
4	Perpendicularity measurement for the mounting prisms.	27
5	Perpendicularity measurement for the Mirror As.	28
6	Perpendicularity measurement for the Mirror Bs.	28
7	Perpendicularity measurement for the Mirror Es.	28
8	Mirror transmission measurement for Mirror A.	32
9	Mirror transmission measurement for Mirror C.	33
10	Mirror transmission measurement for Mirror E.	33
11	Mirror transmission measurement for Mirror B.	36
12	PZT actuator response and length-to-angle coupling	38
13	Measured impedances of the 3mm, 2mm, and 1mm photodiodes.	49
14	Dark noise/current measurement for the 3mm InGaAs photodiodes	50
15	Measurement of the quantum efficiencies for the DCPD photodiodes.	54
16	Estimated responsivities and quantum efficiencies of the DCPD photodiodes.	55
17	The dimensions and masses of the OMC glass breadboards	57
18	Summary of the cavity geometry tests for L1 OMC	64
19	Summary of the cavity geometry tests for H1 OMC	65
20	Summary of the cavity geometry tests for 3rd IFO OMC	67
21	List and location for OMC breadboards and Mounting Prisms	80
22	List and location for Mirror A & B	80
23	List and locations for Mirror C & PZTs	81
24	List and locations for Mirror E	81

1 Objective and scope

The Advanced LIGO Output Mode Cleaner (OMC) is a suspended glass optical cavity for filtering radio-frequency optical sidebands and higher-order modes in the output beam of the interferometer. The cavity optics, peripheral optics, suspension interface, diodes for signal readout, and interface for electrical connections are built on a single fused silica glass breadboard.

The goal of this report is to provide a one-stop documentation that describes various optical tests of the OMCs before they are installed at the sites.

The structure of this document is as follows:

- Section 2 describes various component tests that have been done before they were integrated to the OMC breadboard.
- Section 3 describes various tests for the integrated OMC cavity on the glass breadboard.
- Appendix describes additional information to keep the record of the optics inventory and installation information, as well as some results of useful calculations.

2 Test of individual optical components

2.1 Characterization of the curved mirrors

[External Link]

LIGO-E1101088: aLIGO OMC Curved Optics Specification

2.1.1 Curvature radii for the curved mirrors

Radii of curvature of the curved mirrors were evaluated by measuring a round-trip gouy phase of a fabry-perot cavity.

[External Link]

http://nodus.ligo.caltech.edu:8080/OMC_Lab/22
http://nodus.ligo.caltech.edu:8080/OMC_Lab/30
http://nodus.ligo.caltech.edu:8080/OMC_Lab/31
http://nodus.ligo.caltech.edu:8080/OMC_Lab/41
http://nodus.ligo.caltech.edu:8080/OMC_Lab/42
http://nodus.ligo.caltech.edu:8080/OMC_Lab/49

[Description]

The curved mirrors of the OMC are designed to have the radius of curvature of 2.5m. This number was necessary to be confirmed with a measurement. A Fabry–Perot cavity was formed by a curved mirror and a flat prism mirror of the OMC. The curvature of the curved

mirror was estimated from the ratio between the free spectral range (FSR) and the transverse mode spacing (TMS) of the cavity, assuming the flat mirror has negligibly small curvature.

[Experimental method]

The setup was built on the optical table at ATF. The optical and electrical setups are shown in Figure 1) and Figure 2), respectively. A Fabry–Perot cavity was formed by an OMC flat mirror (“A” coating) and a curved mirror (“C” coating). The cavity was locked with the PDH technique. The phase modulation was applied at 32.7MHz with a resonant EOM. The reflected light from the cavity was detected by a broadband photodetector (Thorlabs PDA255, BW~50MHz). The output signal was demodulated at the LO frequency. Newport LB1005 Servo Box was used for the servo filter. The laser frequency was actuated with the laser fast PZT.

In order to measure the FSR and TMS of the cavity, the technique in [1] was used. The additional phase modulation was applied using an broadband EOM with the modulation frequency scanned by a network analyzer. The input beam of the cavity was misaligned in pitch or yaw. The broadband photodetector (BBPD: Newfocus 1801, BW: 125MHz, Si photodiode) is placed at the cavity transmission. The network analyzer measured the transfer function between the excitation to the BB EOM and the BBPD output. The transfer function exhibited the peaks associated with the transverse modes when the clipping is introduced to the BBPD.

The transfer function has a repetitive structure with the spacing by the FSR. In addition, the transfer function becomes symmetric with regard to the TEM00 resonances, because the phase modulation by an EOM introduces symmetric modulation sidebands to the carrier. For example, the peaks associated with the 1st-order higher-order modes, appears at $f = n f_{\text{FSR}} \pm f_{\text{TMS}}$. The FSR and the TMS can be obtained by measuring the frequency of the first three peaks for the 1st-order higher-order modes. Once f_{FSR} and f_{TMS} are obtained separately, the curvature of the curved mirror is obtained from the following formula, assuming the flat mirror has sufficiently large radius of curvature:

$$R_{\text{RoC}} = \frac{L}{1 - \cos^2(\pi f_{\text{TMS}}/f_{\text{FSR}})}$$

[Result]

The measured transfer functions are shown as Figures 3~11 together with the peak fitting data. Each peak was fitted with a Lorentzian $H(f)$:

$$H(f) = \frac{a_0}{\sqrt{1 + (f - f_0)^2/\gamma^2}},$$

where a_0 , f_0 , and γ are the fitting parameters.

The summary of the curvature measurement is found in Table 1. The average RoC is

$$\overline{R_{\text{RoC}}} = 2.575 \pm 0.005 \text{ [m]},$$

when C2, C7, C8 are excluded.

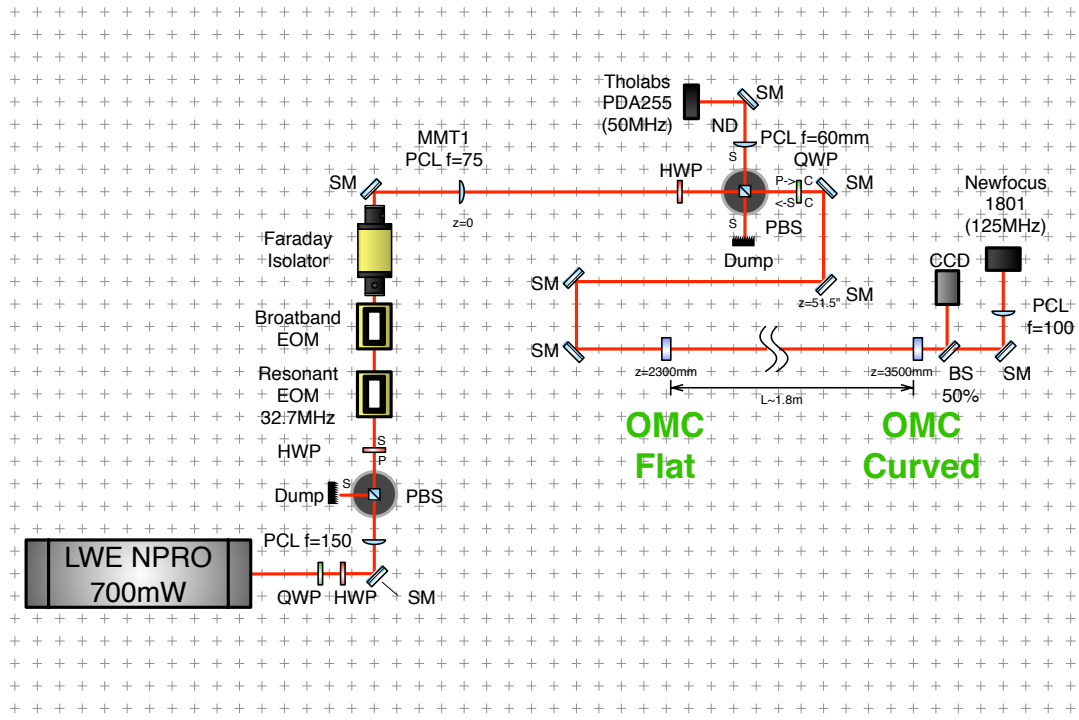


Figure 1: Optical setup for the mirror curvature measurement.

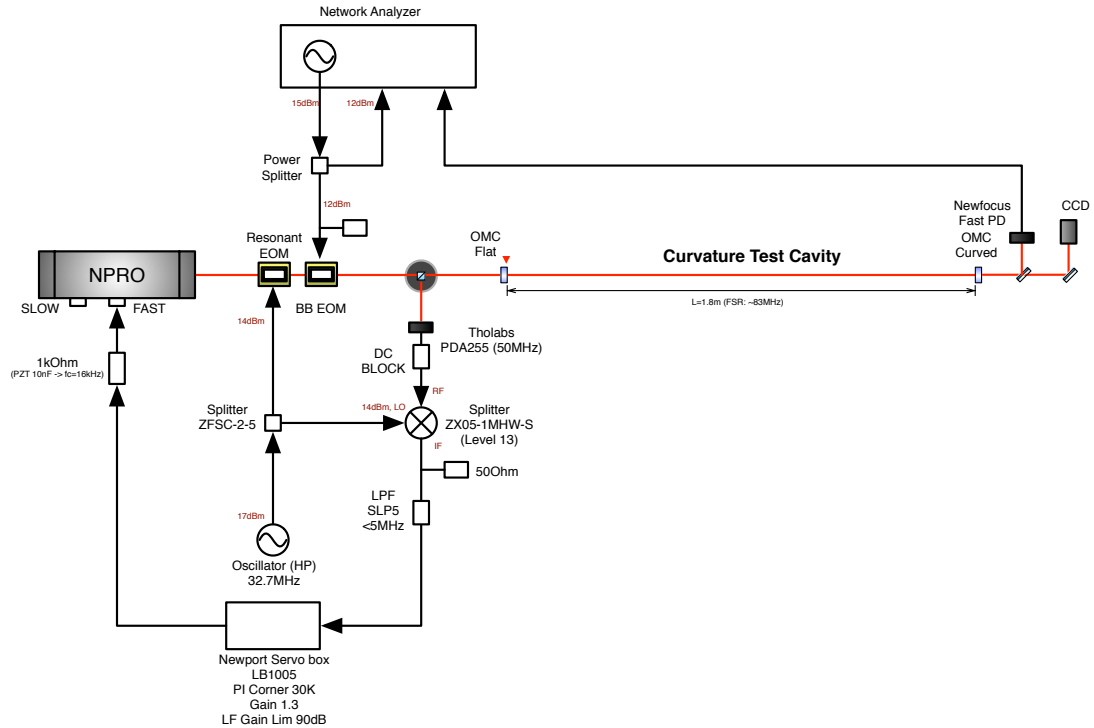


Figure 2: Electrical setup for the mirror curvature measurement.

Mirror serial	RoC [m]	note
C1	$2.57845 \pm 4.2 \times 10^{-5}$	
C2	$2.54363 \pm 4.9 \times 10^{-5}$	excluded
C3	$2.57130 \pm 6.3 \times 10^{-5}$	
C4	$2.58176 \pm 6.8 \times 10^{-5}$	
C5	$2.57369 \pm 9.1 \times 10^{-5}$	
C6	$2.57321 \pm 4.2 \times 10^{-5}$	
C7	$2.56244 \pm 4.0 \times 10^{-5}$	excluded
C8	$2.56291 \pm 4.7 \times 10^{-5}$	excluded
C9	$2.57051 \pm 6.7 \times 10^{-5}$	

Table 1: Summary of the curvature radii of the C mirrors

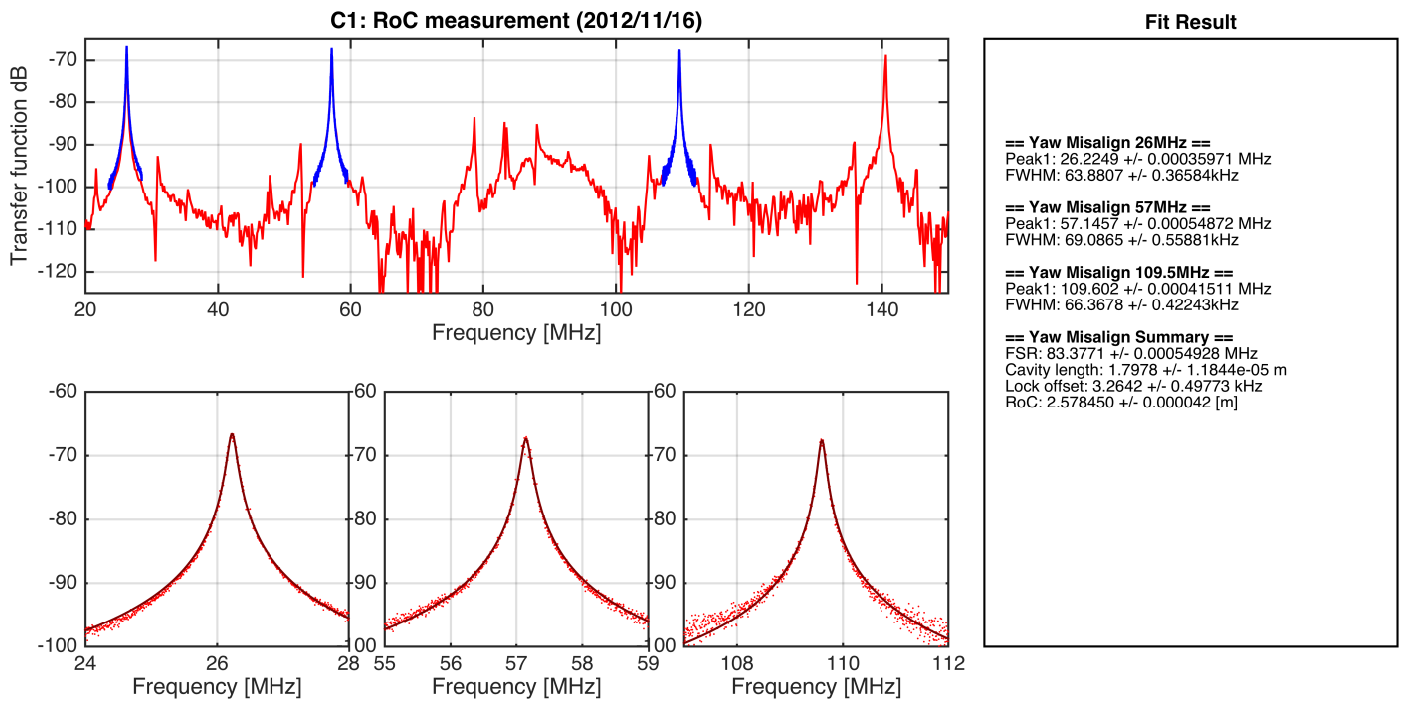


Figure 3: Measured TMS/FSR of the curved mirror C1

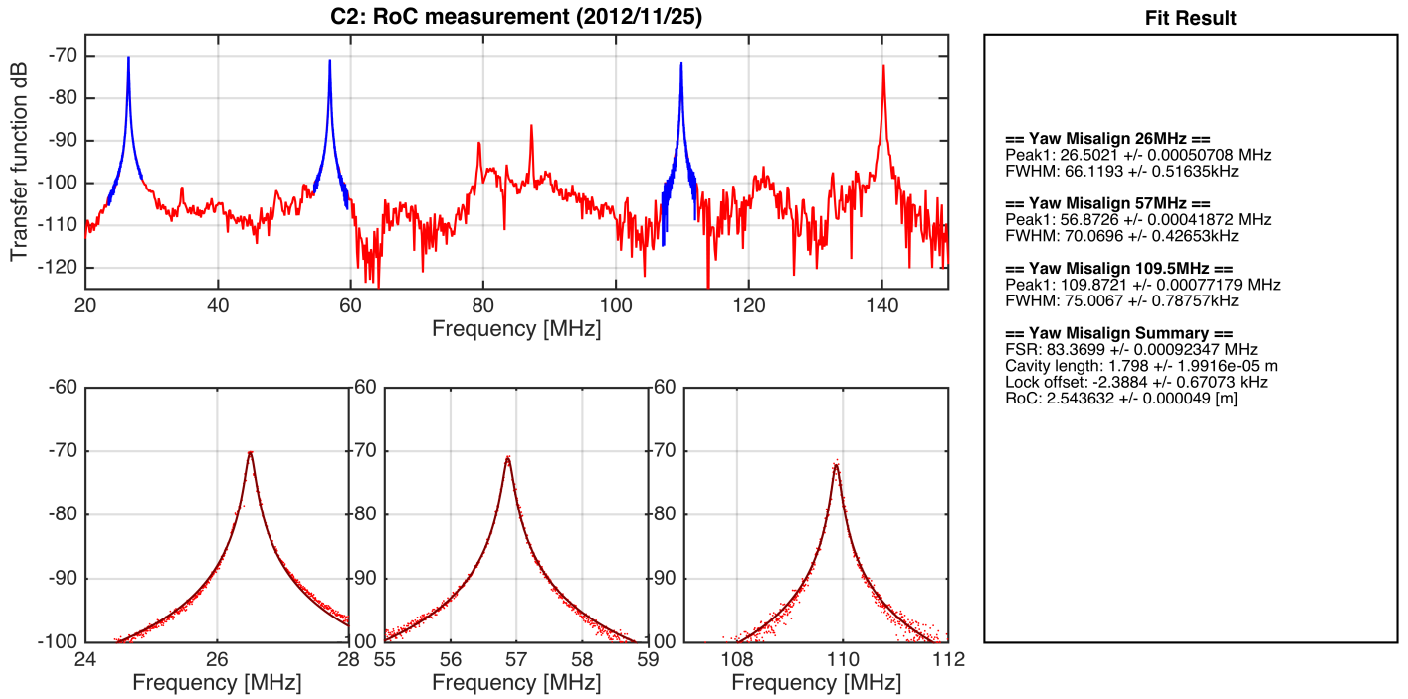


Figure 4: Measured TMS/FSR of the curved mirror C2

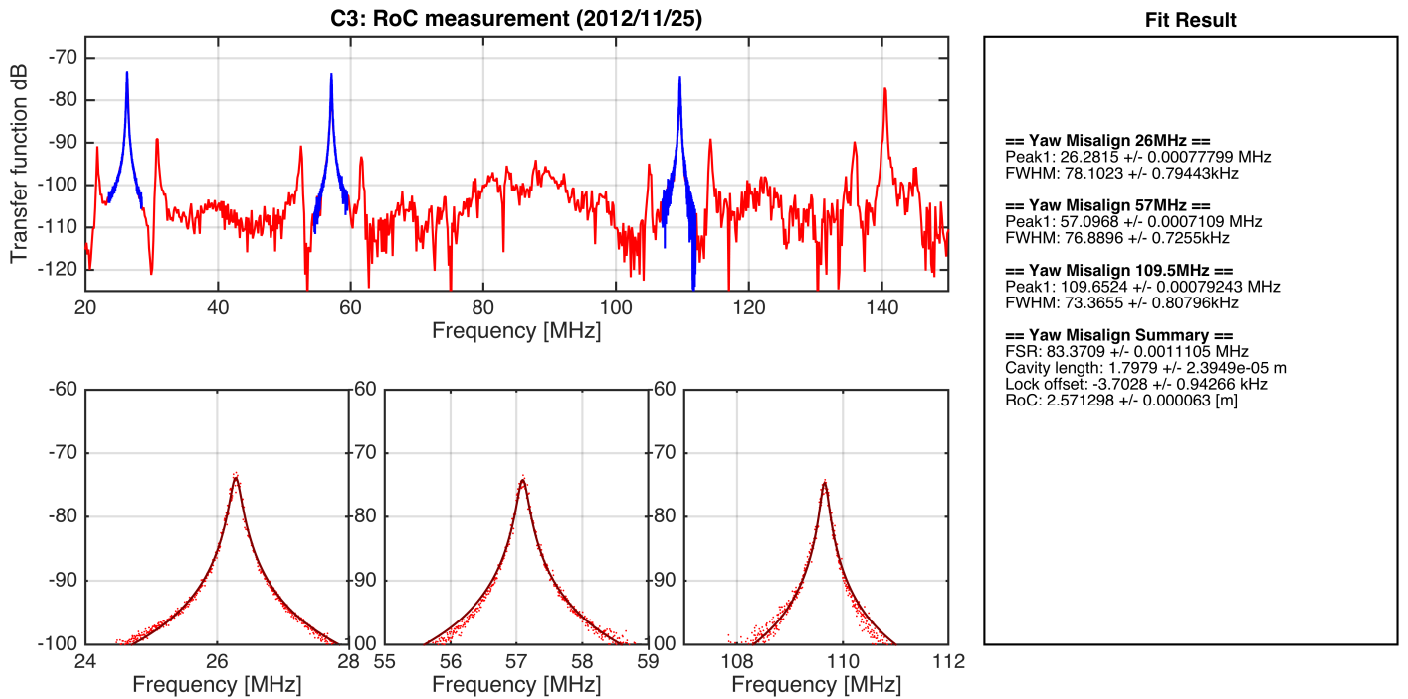


Figure 5: Measured TMS/FSR of the curved mirror C3

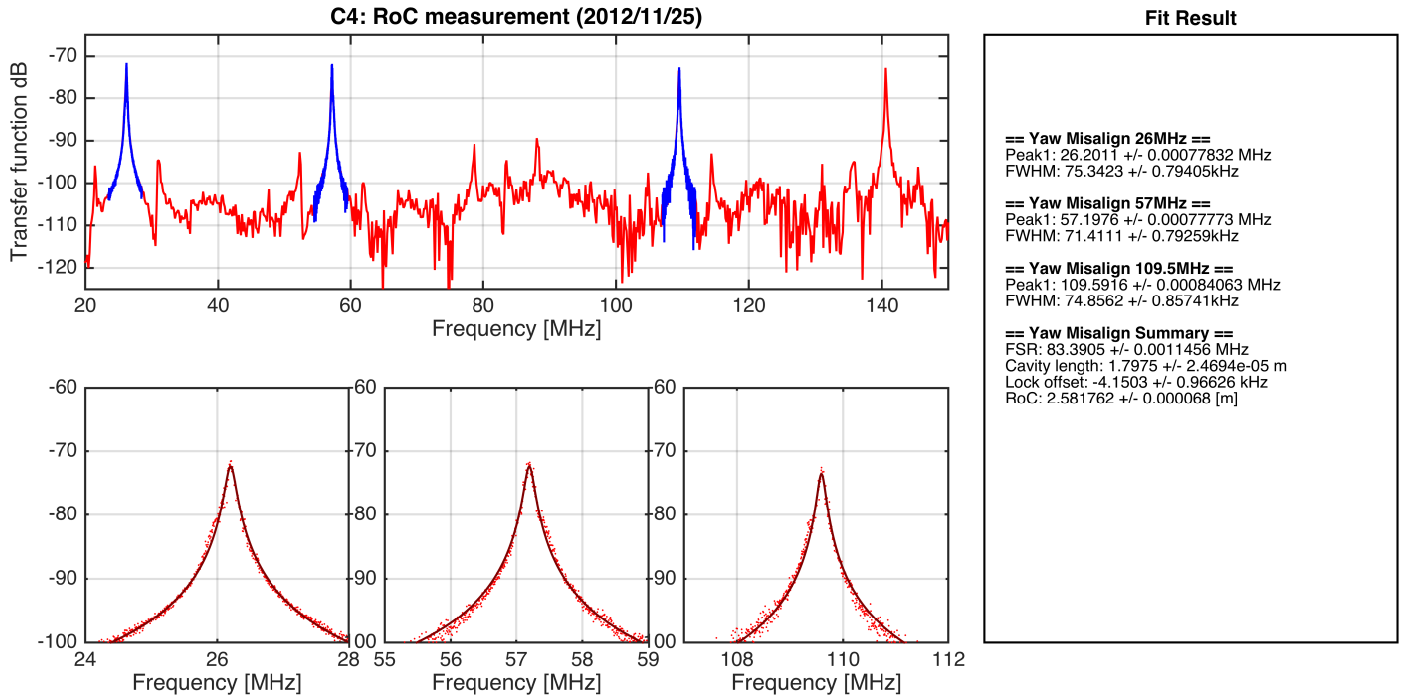


Figure 6: Measured TMS/FSR of the curved mirror C4

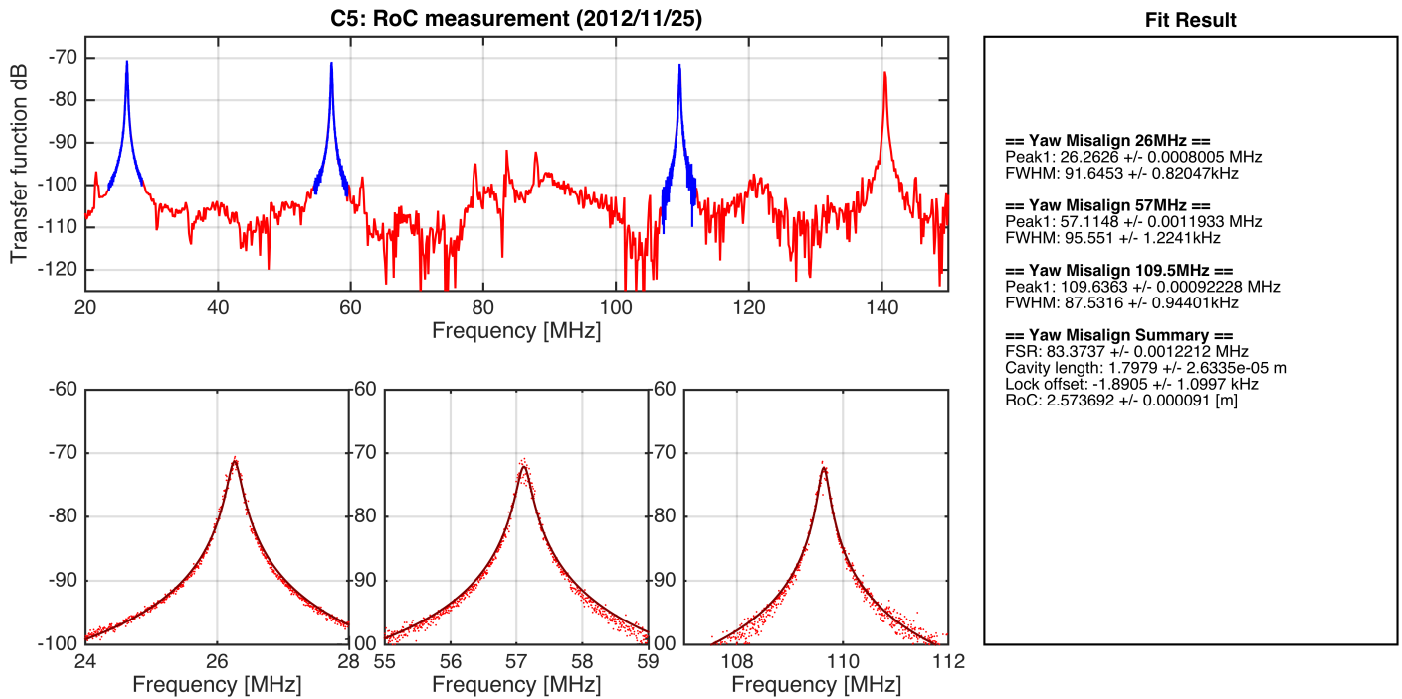


Figure 7: Measured TMS/FSR of the curved mirror C5

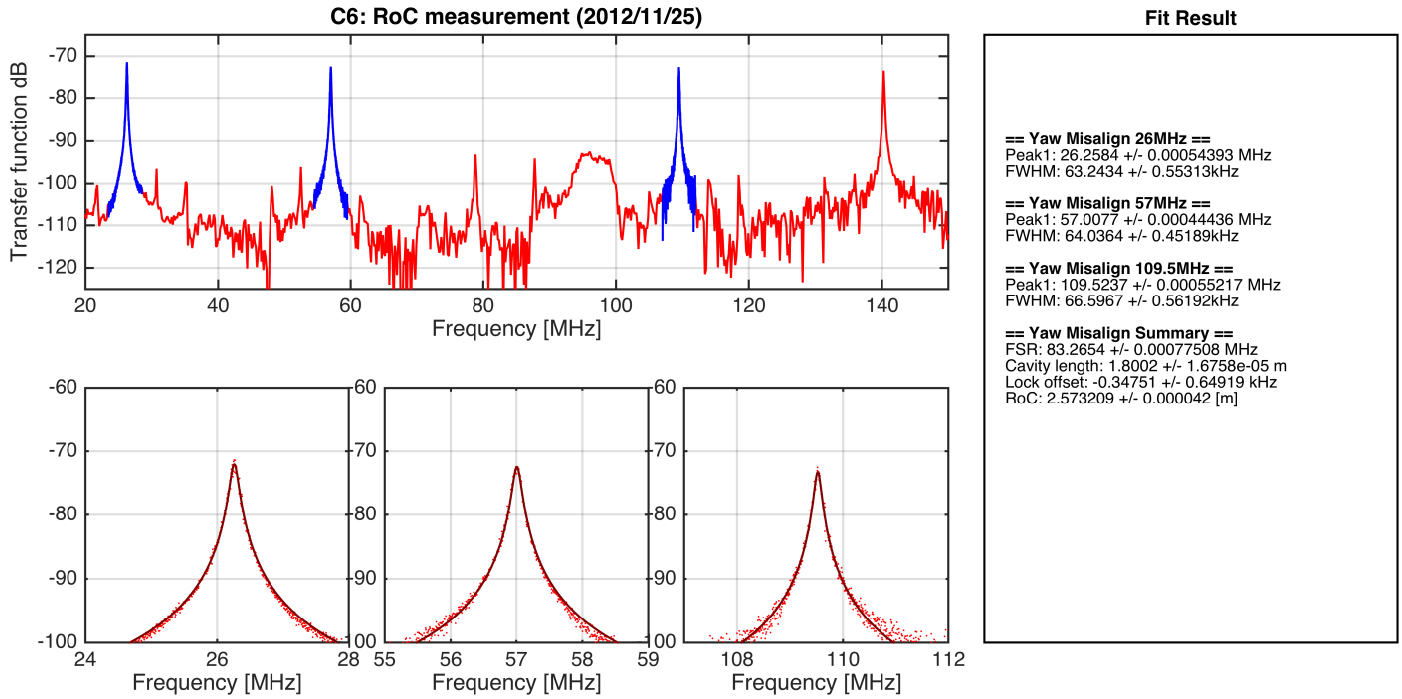


Figure 8: Measured TMS/FSR of the curved mirror C6

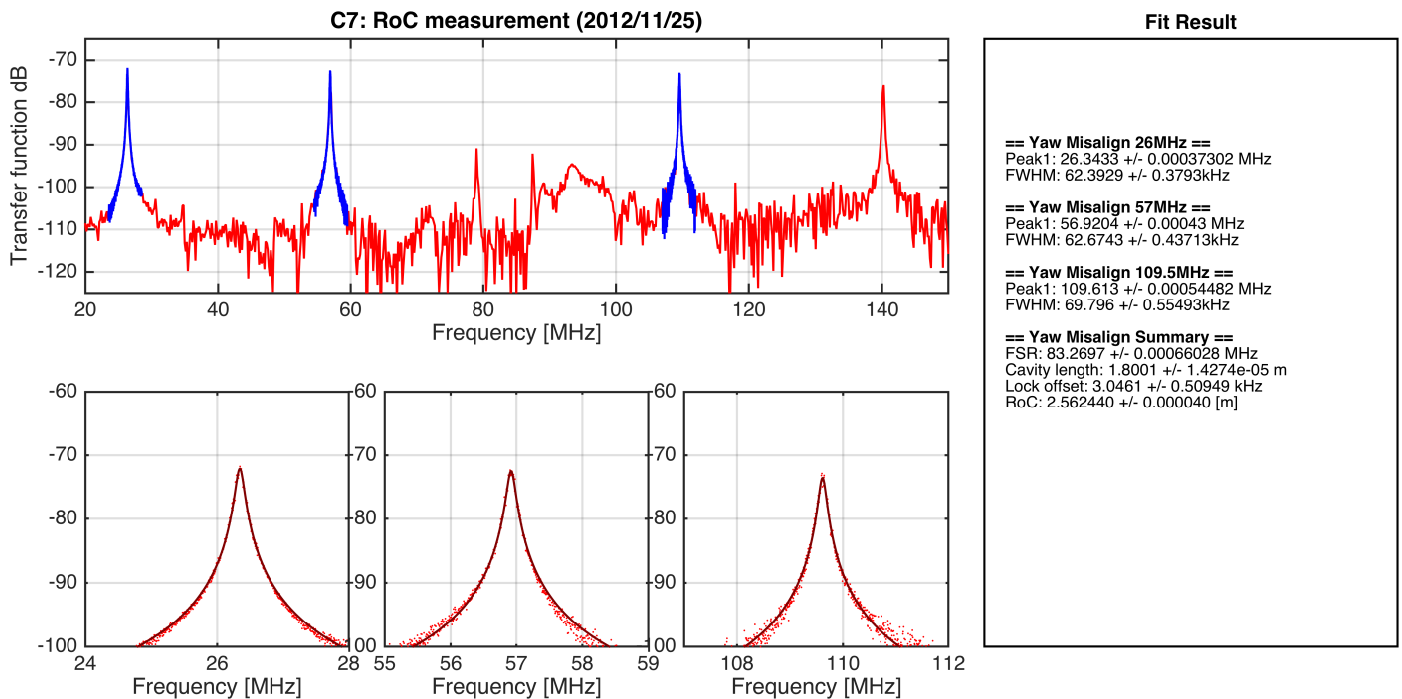


Figure 9: Measured TMS/FSR of the curved mirror C7

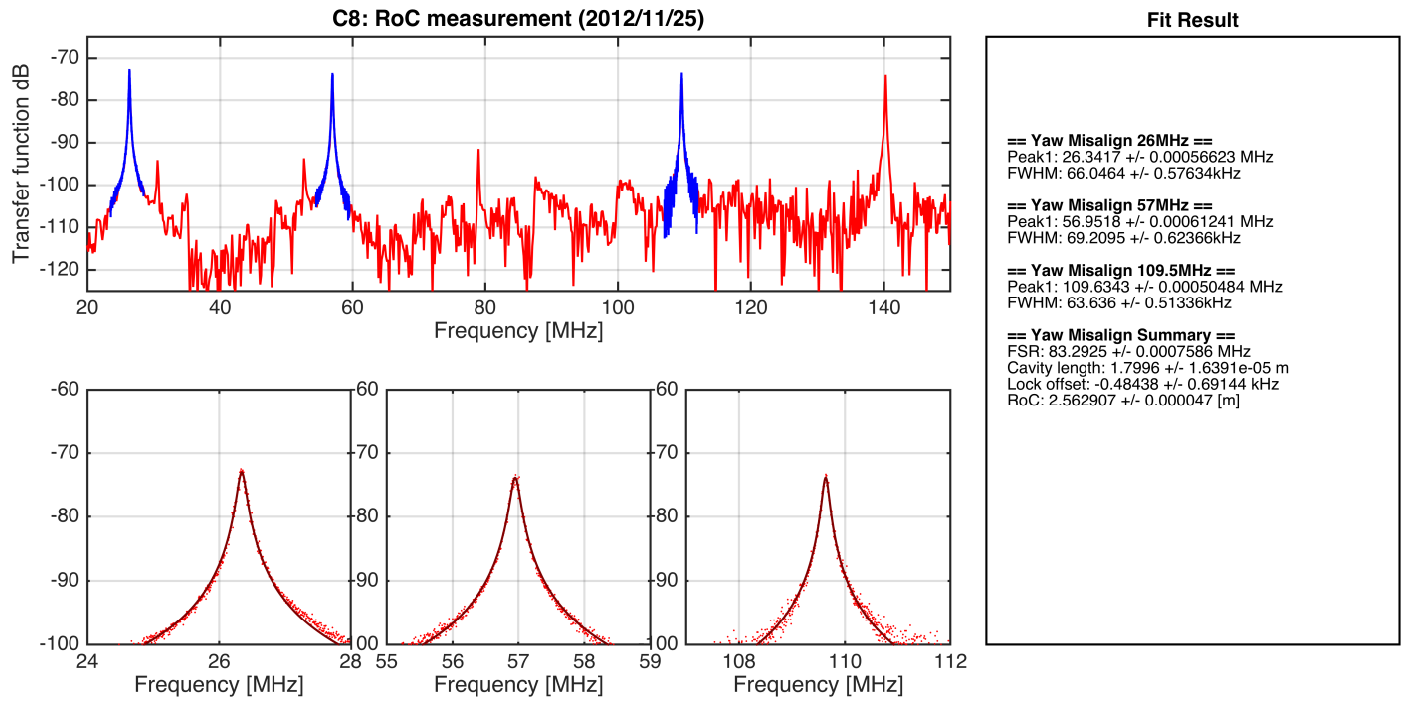


Figure 10: Measured TMS/FSR of the curved mirror C8

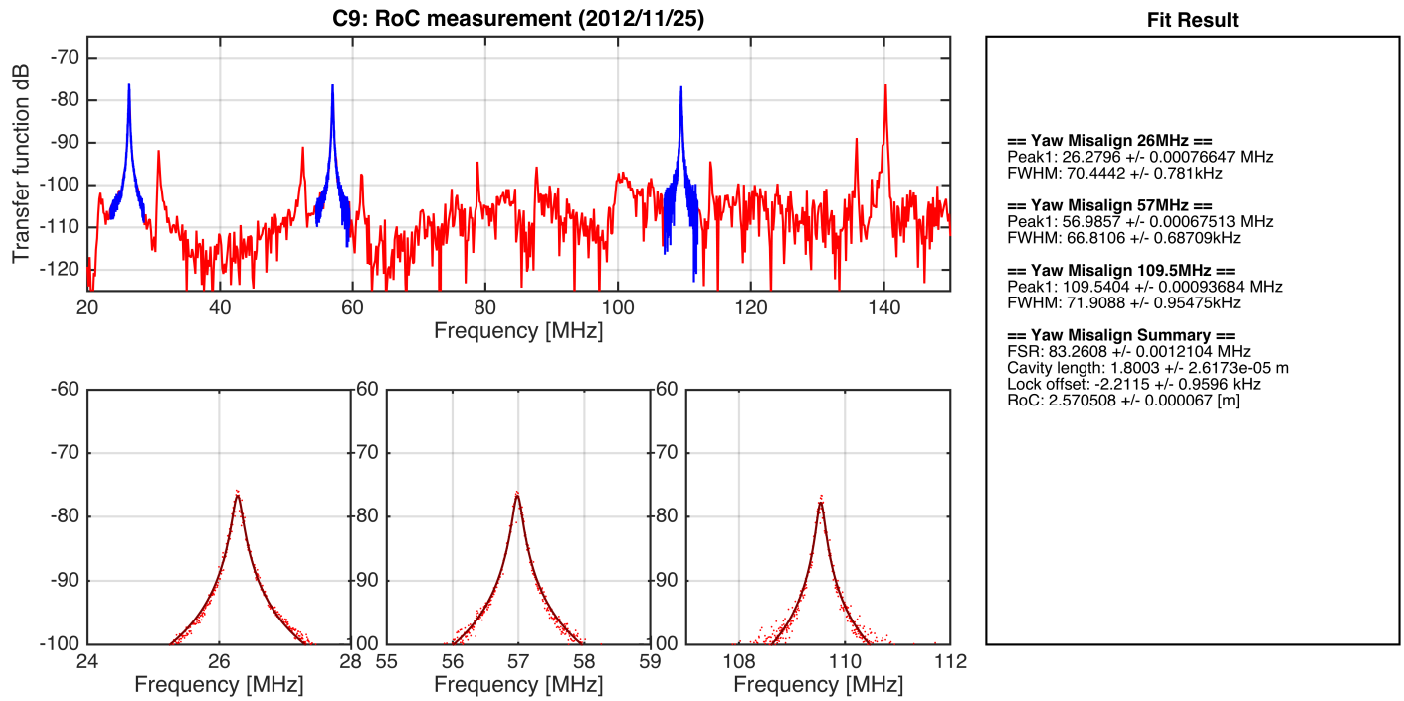


Figure 11: Measured TMS/FSR of the curved mirror C9

2.1.2 Thickness of the curved mirrors

[External Link]

http://nodus.ligo.caltech.edu:8080/OMC_Lab/50

[Description]

The curved mirror specification (E1101088) does not specify precise thickness of the curved mirror. We need to specify the position of the reflecting surface for the OMC cavity, we needed to know the thickness of the curved mirrors.

[Experimental method]

A micrometer gauge was used to measure the thickness of a curved mirror. Therefore this measurement has a risk to be destructive for the reflecting coating. Therefore, one of the worst mirrors in terms of the curvature (Section 2.1.1) was preselected for this measurement.

Took three points of the mirror edges separated by 120 degree to have some statistics.

[Result]

The curved mirror “C2” was used for this measurement.

Micrometer readings: (0.2478, 0.2477, 0.2477) in inch \Rightarrow (6.294, 6.292, 6.292) in mm

This gives us the thickness of 6.3mm.

2.1.3 Characterization of the curvature center

Locations of the curvature minimum on the OMC curved mirrors have been measured.

[External Link]

LIGO-D1300185: aLIGO OMC Curved Mirror Bonding Fixture Assembly

http://nodus.ligo.caltech.edu:8080/OMC_Lab/91

[Description]

When a curved mirror is misaligned, the location of the curvature center moves. We have to be aware of this effect because our curved mirror is going to be attached on a mounting prism (via a PZT) with the back surface of the mirror. This means that each curved mirror has inherent misalignment if the curvature minimum of the curved mirror is shifted from the center of the mirror. Since we have no ability to control mirror pitch angle once it is glued on the prism, the location of the curvature minimum should be characterized so that we can push all of the misalignment in the horizontal direction.

[Experimental method]

- Principle

When a curved mirror is completely axisymmetric (in terms of the mirror shape), any rotation of the mirror does not induce change on the axis of the reflected beam. If the curvature minimum deviates from the center of the mirror, the reflected beam suffer precession. As

we want to precisely rotate the mirror, we use the gluing fixture for the PZT subassembly (D1300185). In this method, the back surface of the curved mirror is pushed on the mounting prism, and the lateral position of the mirror is precisely defined by the fixture. As you rotate the mirror in clockwise viewing from the front, the spot moves in counter clockwise on the CCD

(Figure 12).

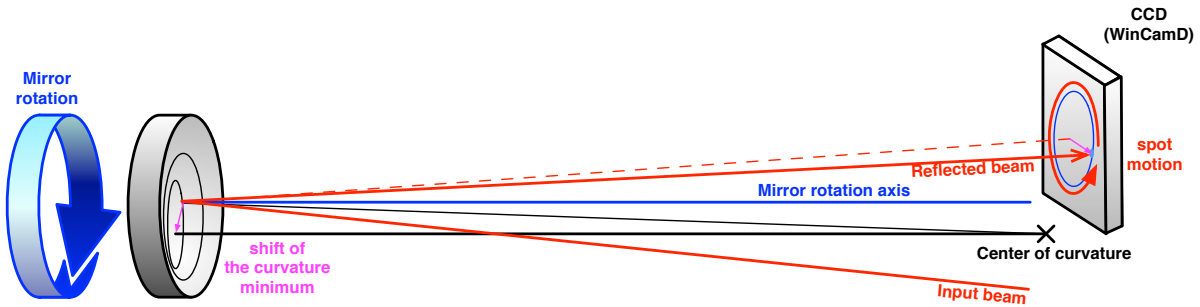


Figure 12: Precession of the reflected beam due to axial asymmetry of a curved mirror

- Setup and procedure

The measurement setup is shown in Figure 12. The mounting prism (#21) is placed on the gluing fixture. A curved mirror under the test is loaded in the fixture with no PZT, i.e. the back surface is aligned by the mounting prism. The fixing pressure is applied to the curved mirror by the front plate with spring loads. The mirror needs to be pushed from the top at least once to seat on its defined position in the fixture. The incident beam is slightly slanted for the detection of the reflected spot. The beam is aligned to hit the center of the mirror as much as possible.

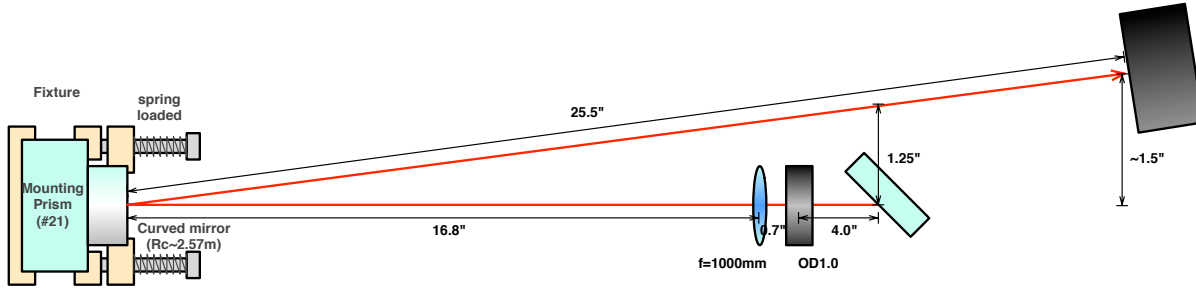


Figure 13: Setup for curvature center measurement

The position of the reflected spot on the CCD (WinCamD) is recorded, while the mirror is rotated 90 deg at once. The rotation of the mirror is defined as shown in Figure 14. The angle origin is defined by the arrow mark of the mirror and rotated in clockwise being viewed from the front face. The mirror is rotated 540 deg (8 points) to check reproducibility.

[Result]

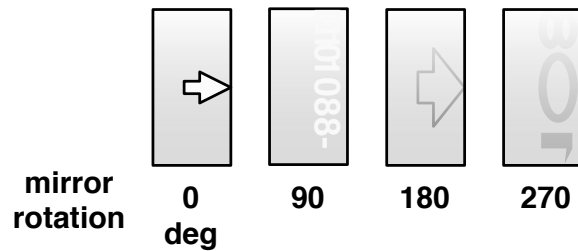


Figure 14: Definition of the mirror angles

Measured 8 points for each mirror is fitted by a circle. The fitting result provides the origin and radius of the circle, and the angle correspond to mirror angle of 0 deg.

The geometrical analysis of the measurement is shown in Figure 15. Here is the description of the symbols:

- d : distance of the curvature minimum and the mirror center (quantity to be derived)
- D : distance of the prove beam spot from the center of the mirror
- R : Radius of curvature of the mirror
- θ_R : angle of incidence/reflection

The interesting consequence is that precession diameter ($X - X'$) on the CCD does not depend on the spot position on the mirror. This ensures the precision of the measurement. In the measurement, the radius of the precession ($r = (X - X')/2$) is obtained. Therefore, we derive

$$d = \frac{rR}{2L}$$

The result of the analysis is found in Table 2. In the table, d is the distance of the curvature minimum from the mirror center, and ϕ is the angle of the minimum from the horizontal line at the center of the mirror.

2.2 Characterizations of the OMC prism mirrors

2.2.1 Wedge angle measurement

The wedge angles of the prism mirrors were measured with an autocollimator (“AC”) and a rotary stage.

[External Link]

LIGO-E1101086: OMC Optical Prisms

http://nodus.ligo.caltech.edu:8080/OMC_Lab/56

http://nodus.ligo.caltech.edu:8080/OMC_Lab/59

http://nodus.ligo.caltech.edu:8080/OMC_Lab/66

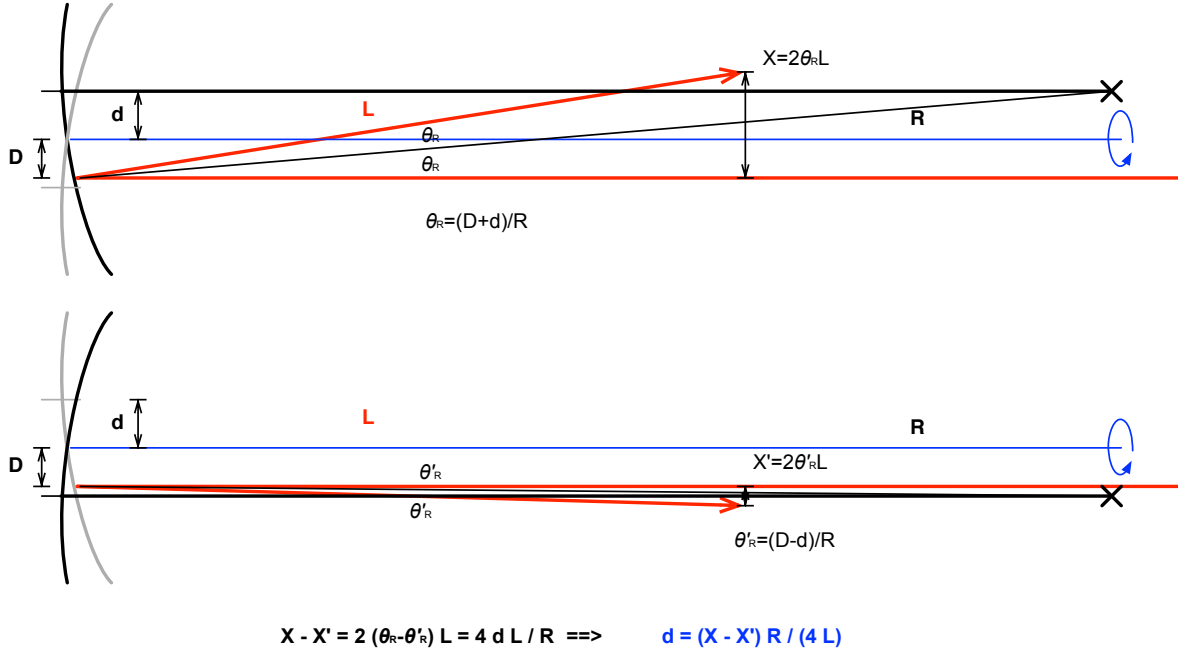


Figure 15: Geometrical analysis of the curvature center measurement. The upper figure shows the top view of the setup in the case when the curvature center is uppermost in the figure. The lower figure shows when the mirror is 180 deg rotated from the upper figure case.

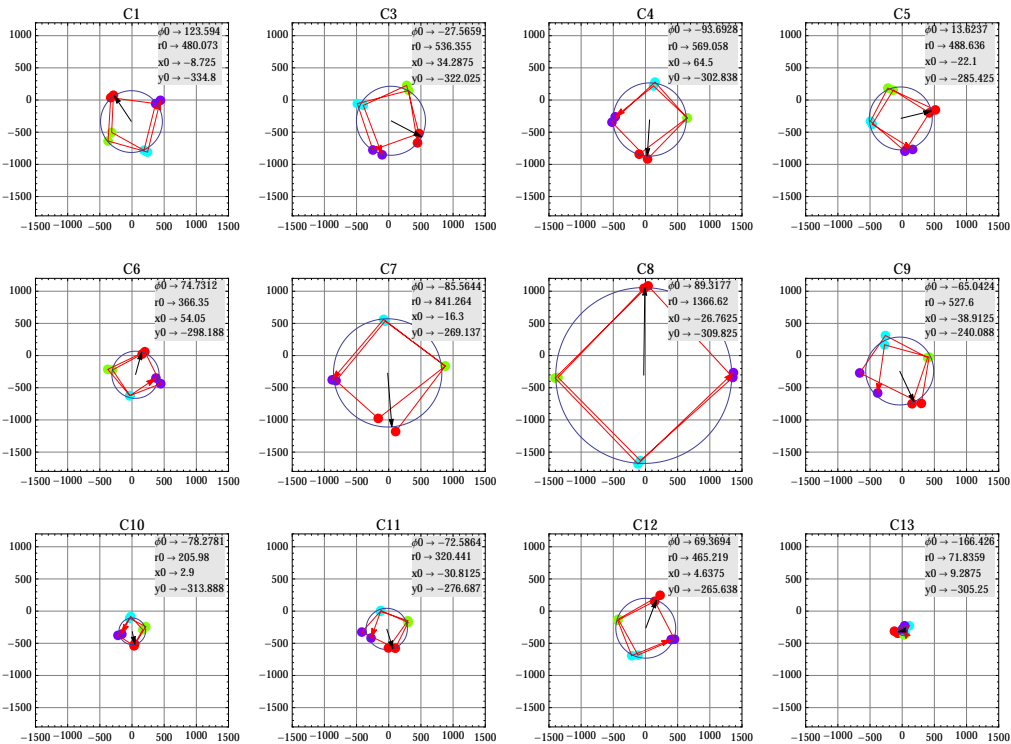


Figure 16: Measurement of the reflected beam precession. The units for the distance and angle is μm and deg.

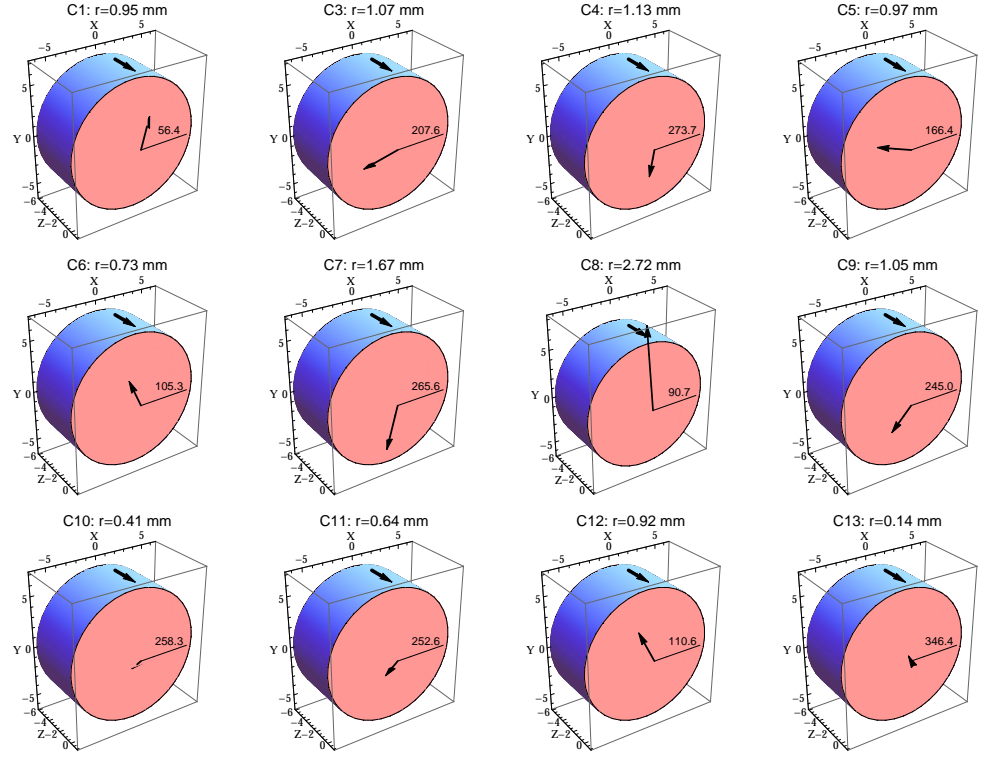


Figure 17: Graphical representation of the derived positions of the curvature minimum. The cylinder represents the curved mirror with an arrow mark at the top. The end of the arrow on the face represents the position of the curvature minimum.

Mirror serial	d [mm]	ϕ [deg]
C1	0.95	56.4
C3	1.07	207.6
C4	1.13	273.7
C5	0.97	166.4
C6	0.73	105.3
C7	1.67	265.6
C8	2.72	90.7
C9	1.05	245.0
C10	0.41	258.3
C11	0.64	252.6
C12	0.92	110.6
C13	0.14	346.4

Table 2: Derived positions of the curvature minimum.

Datasheet: HPFS Fused Silica Standard Grade, Corning

[Description]

The prism mirrors are wedged by 0.5 degree (30 arcmin). If the wedge angle is too much off from the specification, this may cause unexpected beam deflection. In order to check the wedge angle, the angle between the prompt and backside reflections were measured.

[Experimental method]

A prism mirror is set on a horizontal rotational stage. Realize the retroreflection for the front surface. Then realize the retroreflection for the back surface by rotating the stage. This angle difference α is related to the wedge angle θ_H with the following formula (see Figure 18):

$$\theta_H = \arcsin\left(\frac{\sin \alpha}{n}\right)$$

Here the refractive index is $n=1.462$ for green filter approximately at 500nm, according to the datasheet by Corning.

Horizontal wedge measurement

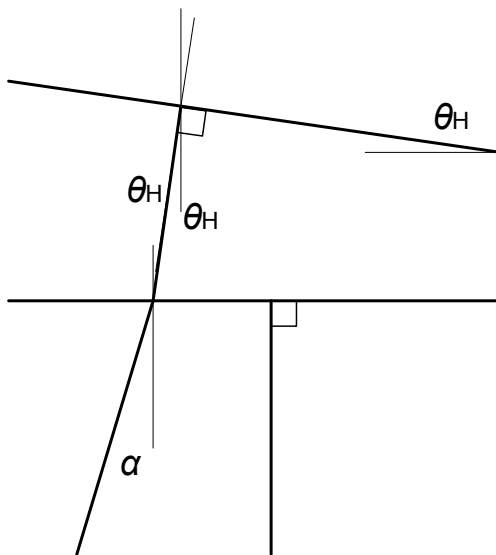


Figure 18: Horizontal wedge measurement: difference of the incident angle for retroreflection condition.

Vertical wedge measurement

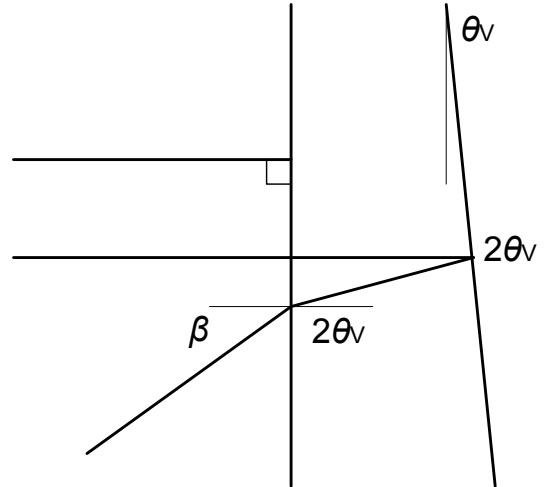


Figure 19: Vertical wedge measurement: difference between the front and back reflections.

There is no rotational adjustment in the vertical direction. Since the vertical wedge angle is expected to be small, it could be measured with the direct AC reading (Figure 19). Note that the AC is calibrated to show the angle that is required for the object to be rotated for making the view retroreflected. Therefore the direct reading angle is $\beta/2$ rather than β . The

angle β and the wedge angle θ_V have the following relationship:

$$\theta_V = \frac{1}{2} \arcsin \left(\frac{\sin \beta}{n} \right)$$

Actual procedure is listed below:

- Prism mount: Thorlabs KM100P and PM3
- Rotational stage: Newport 481-A, 0.008deg (= 0.5 arcmin) resolution
- Attach the prism mount on the rotational stage. Mount the tombstone prism on a prism mount. the rotation stage.
- Locate the prism in front of the autocollimator.
- Find the retroreflected reticle in the view. Adjust the focus if necessary.
- Confirm that the rotation of the stage does not change the height of the reticle in the view. If it does, rotate the AC around its axis to realize it. This is to match the horizontal reticle to the rotation plane.
- Use the rotation stage and the alignment knobs to find the reticle at the center of the AC. Make sure the reticle corresponds to the front surface. **Record the micrometer reading.**
- Rotate the micrometer of the rotation stage until the retroreflected reticle for the back surface.
- There maybe the vertical shift of the reticle due to the vertical wedging. **Record the vertical shift.**
- **Record the micrometer reading.** Take a difference of the two micrometer readings.

[Result]

The measurement results are shown in Table 3. A2 prism showed a particularly big number but everything else actually showed a constant smaller number from the specification (0.5deg). This A2 prism should be excluded from the assembly. The mean and standard deviation excluding A2 are 0.441 ± 0.014 [deg]. This number should be reflected to the breadboard design. As far as we use the optics with the consistent wedge angle, the design of the breadboard is not affected.

2.2.2 Prism perpendicularity test

The perpendicularity of the prism optics were measured with an autocollimator.

[External Link]

http://nodus.ligo.caltech.edu:8080/OMC_Lab/63

http://nodus.ligo.caltech.edu:8080/OMC_Lab/64

http://nodus.ligo.caltech.edu:8080/OMC_Lab/65

[Description]

Mirror Serial	α [deg]	β [arcmin]	θ_H [deg]	θ_V [deg]
A1	0.680	+0.0	0.465	+0.000
A2	0.800	-6.0	0.547	-0.034
A3	0.635	-1.6	0.434	-0.0091
A4	0.650	+0.0	0.445	+0.000
A5	0.655	+2.4	0.448	+0.014
A6	0.665	+3.0	0.455	+0.017
A7	0.635	+0.0	0.434	+0.000
A8	0.623	-0.4	0.426	-0.0023
A9	0.670	+2.4	0.458	+0.014
A10	0.605	+0.4	0.414	+0.0023
A11	0.640	+0.8	0.438	+0.0046
A12	0.625	-0.6	0.427	-0.0034
A13	0.630	+2.2	0.431	+0.013
A14	0.678	+0.0	0.464	+0.000
B1	0.665	+0.6	0.455	+0.0034
B2	0.615	+0.2	0.421	+0.0011
B3	0.620	+0.9	0.424	+0.0051
B4	0.595	+2.4	0.407	+0.014
B5	0.635	-1.8	0.434	-0.010
B6	0.640	+1.6	0.438	+0.0091
B7	0.655	+2.5	0.448	+0.014
B8	0.630	+2.8	0.431	+0.016
B9	0.620	-4.0	0.424	-0.023
B10	0.620	+1.2	0.424	+0.0068
B11	0.675	+3.5	0.462	+0.020
B12	0.640	+0.2	0.438	+0.0011
E1	0.672	+0.0	0.460	+0.000
E2	0.631	-0.3	0.432	-0.0017
E3	0.642	+0.0	0.439	+0.000
E4	0.659	+1.4	0.451	+0.0080
E5	0.695	+0.5	0.475	+0.0028
E6	0.665	-0.4	0.455	-0.0023
E7	0.652	+1.0	0.446	+0.0057
E8	0.675	+2.0	0.462	+0.011
E9	0.645	-2.4	0.441	-0.014
E10	0.640	+2.2	0.438	+0.013
E11	0.638	+1.6	0.436	+0.0091
E12	0.660	+1.6	0.451	+0.0091
E13	0.638	+0.8	0.436	+0.0046
E14	0.655	+0.4	0.448	+0.0023
E15	0.640	+1.4	0.438	+0.0080
E16	0.655	+0.6	0.448	+0.0034
E17	0.650	+0.8	0.445	+0.0046
E18	0.640	+2.4	0.438	+0.014

Table 3: Result of the wedge angle measurement.
page 24

The OMC cavity optics have no internal adjustment for the pitch alignment because the two flat mirrors and the PZT subassemblies are glued on the breadboard directly. 10 arcsec (=2.8rad) of misalignment causes about 0.1mm shift of the beam. Therefore the front and bottom surfaces of the prisms have to have good perpendicularity. We set the requirement of the perpendicularity better than 30 arcsec. This should be confirmed.

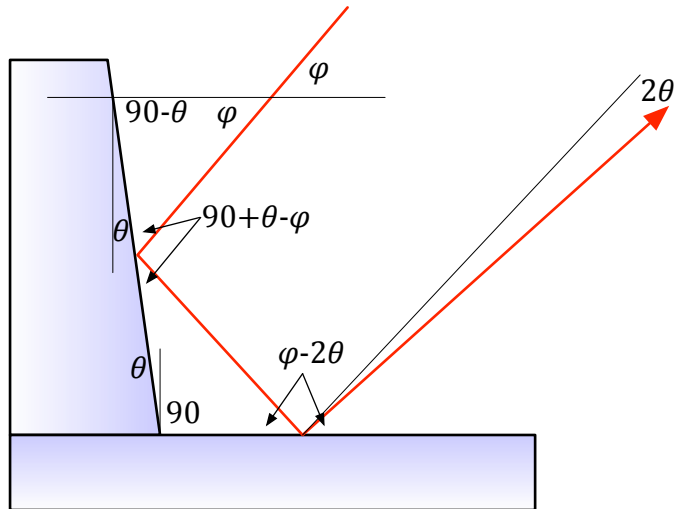


Figure 20: Principle of the perpendicularity test.

[Experimental method]

The perpendicularity of the prisms were checked with an autocollimator (AC).

Two orthogonally-joined surfaces form a 2D version of a corner cube, that retroreflects a beam towards the source regardless of the incident angle. When the joint has non-orthogonality of θ , the reflected image shows deviation from the retroreflection by 2θ (Figure 20). We can characterize this quantity with an autocollimator.

The schematic figure of the measurement setup is shown in Figure 21. In order to realize such a setup, the OMC prism optics were placed on an Al mirror. For ensuring the joint angle to be determined only by the optics, the surfaces of the joint were cleaned by Isopropanol every time when the mirror was placed. The AC illuminated the joint corner of the optics. The reflection from the optics was observed by the AC in order to determine the angle formed by the optics.

Typical view of the AC during the test is shown in Figure 22. When the image is retroreflected, only one horizontal line is observed in the view. If there is any deviation from the retroreflection, this horizontal line splits into two as the upper and lower halves have the angled wavefront by 4θ . The difference of the two horizontal bars in the view of the AC was calibrated in the angle. The deviation from the exact normal angle is a half of this measured angle between the two horizontal lines. The sign of the deviation can be determined by giving finger pressure on the mirror to tilt the prism.

[Result]

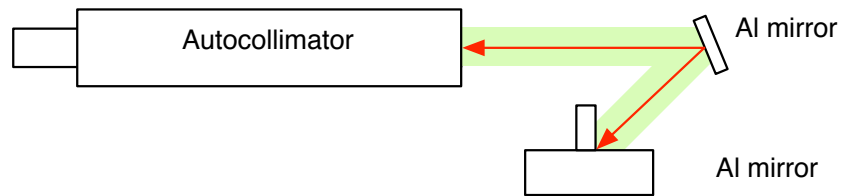


Figure 21: The test setup for the prism perpendicularity.

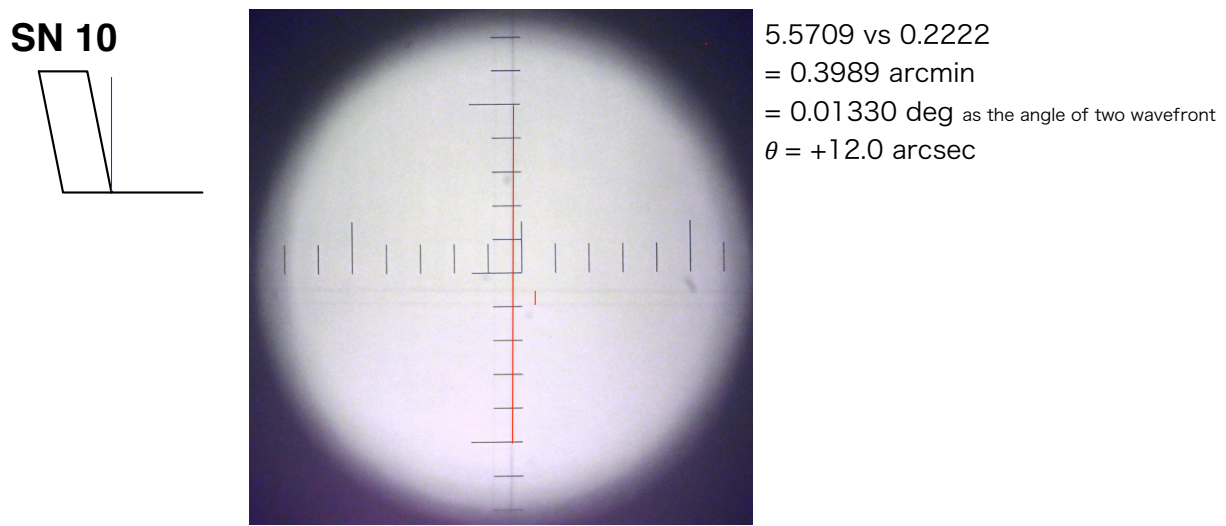


Figure 22: Typical view of the autocollimator and the result analysis.

The results of the perpendicularity measurements are shown in Tables 4, 5, 6, and 7. Table 4 also lists the perpendicularity data, which has no sign, given from the manufacturer.

When the measured (and spec if exist) value shows the deviation from the normal angle less than 30 arcsec, it is indicated as “good”. The prisms only indicated as “good” should be used.

SN #	Measurement [div]	Data Sheet [arcsec]	Note
10	0.399	12.0	29 good
11	0.220	6.6	16 good
16	0.191	5.7	5 good
20	-0.591	-17.7	5 good
21	-2.378	-71.3	15
21	-1.7	-51.	15
01	-0.5	-15.	52
02	-2.5	-75.	48
06	-1.0	-30.	15 good
07	1.7	51.	59
12	-2.2	-66.	40
13	-0.3	-9.	12 good
14	-2.8	-84.	27
15	-2.5	-75.	50
17	0.7	21.	48
22	2.9	87.	63

Table 4: Perpendicularity measurement for the mounting prisms. Requirement is the deviation of < 30arcsec.

2.2.3 Data sheet values for the mirror reflectivities and transmissivities

[External Link]

[LIGO-E1101095: Advanced LIGO Output Mode Cleaner Coating Specifications](#)

[Description]

Coating data sheets from G&H were inspected.

[Experimental method]

Estimate the coating specs from the data sheet. There are five HR surface coatings (A/B/C/D/E) and two AR coating runs (ACD for 4deg AOI and BE for 45deg AOI). From their wavelength dependence curves for transmission/reflection, the values are extracted.

[Result]

[HR coatings]

The coating spec from the vendor for HR coating A is shown in Figure 23. It shows the transmission of 7931 ppm.

SN	Measurement	Note
#	[div]	[arcsec]
A1	-0.5	-15.
A3	0.5	15.
A4	0.9	27.
A5	0.4	12.
A6	0.1	3.
A7	0.0	0.
A8	0.0	0.
A9	0.0	0.
A10	1.0	30.
A11	0.3	9.
A12	0.1	3.
A13	0.0	0.
A14	0.6	18.

Table 5: Perpendicularity measurement for the Mirror As.

SN	Measurement	Note
#	[div]	[arcsec]
B1	-0.9	-27.
B2	-0.6	-18.
B3	-0.9	-27.
B4	0.7	21.
B5	-1.1	-33.
B6	-0.6	-18.
B7	-1.8	-54.
B8	-1.1	-33.
B9	1.8	54.
B10	1.2	36.
B11	-1.7	-51.
B12	1.1	33.

Table 6: Perpendicularity measurement for the Mirror Bs.

SN	Measurement	Note
#	[div]	[arcsec]
E1	-0.8	-24.
E2	-0.8	-24.
E3	-0.2	-7.
E4	-0.5	-15.
E5	0.8	24.
E6	-1.0	-30.
E7	-0.2	-6.
E8	-0.8	-24.
E9	-1.0	-30.
E10	0.0	0.
E11	-1.0	-30.
E12	-0.3	-9.
E13	-0.8	-24.
E14	-1.0	-30.
E15	-1.2	-36.
E16	-0.7	-21.
E17	-0.8	-24.
E18	-1.0	-30.

Table 7: Perpendicularity measurement for the Mirror Es.

The coating spec from the vendor for HR coating B is sown in Figure 24. It shows the transmission of 50.385%.

The coating spec from the vendor for HR coating C is sown in Figure 25. There seemed two coating runs and the vendor data shows the transmission of 51.48ppm and 48.40ppm.

The coating spec from the vendor for HR coating D is sown in Figure 26. It shows the transmission of 4089 ppm.

The coating spec from the vendor for HR coating E is sown in Figure 27. It shows the transmission of 7400 ppm.

[AR coatings]

The coating spec from the vendor for AR coating A/C/D is sown in Figure 28. There seemed three coating runs and the vendor data shows the reflection of 765, 585, and 439 ppm. The correspondence between which AR coating and which mirror are not specified.

The coating spec from the vendor for AR coating B/E is sown in Figure 29. There is no real specification but the vendor confirmed that the reflectivity was smaller than 0.1%.

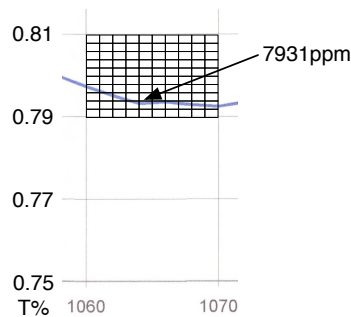


Figure 23: Coating A: Input/Output coupler, Side 1 HR, $T = 8300 \pm 800$ ppm@ 4 degrees AOI (best effort for ± 400 ppm)

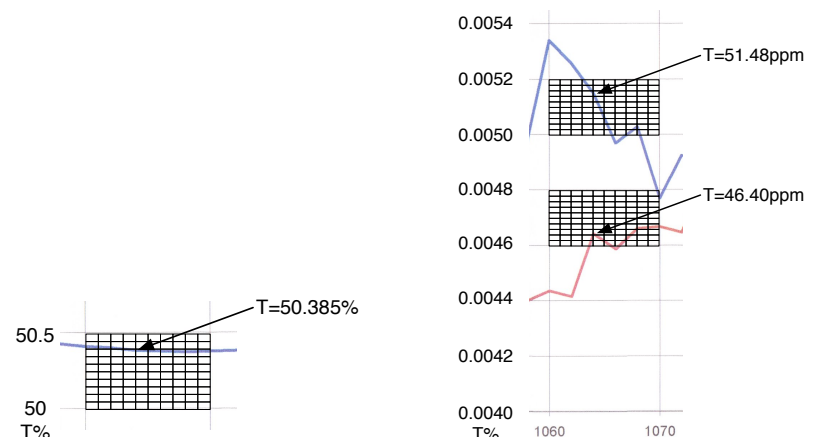


Figure 24: Coating B: Beam splitter, Side 1 50/50, $T = 50 \pm 2\%$ @ 45 degrees AOI

Figure 25: Coating C: High reflector, Side 1 HR, $T = 50 \pm 10$ ppm @ 4 degrees AOI

2.2.4 Measurement of the mirror transmissivities

[External Link]

http://nodus.ligo.caltech.edu:8080/OMC_Lab/96
http://nodus.ligo.caltech.edu:8080/OMC_Lab/100
http://nodus.ligo.caltech.edu:8080/OMC_Lab/112
http://nodus.ligo.caltech.edu:8080/OMC_Lab/114

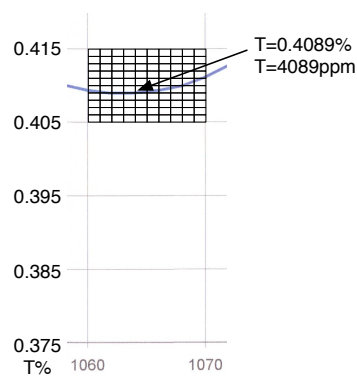


Figure 26: Coating D: Asymmetric output coupler, Side 1 HR, $T = 4150 \pm 400$ ppm @ 4 degrees AOI

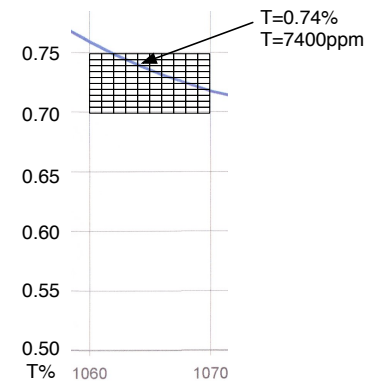


Figure 27: Coating E: High reflector, Side 1 HR, $T = 7500 \pm 2500$ ppm @ 45 degrees AOI

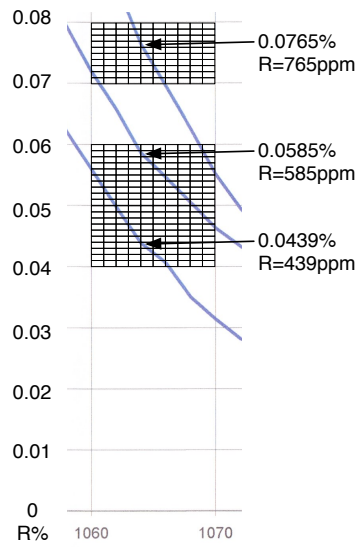


Figure 28: Coating ACD: Side 2 AR, $R < 0.1\%$, best effort < 100 ppm @ 4 degrees AOI

Theoretical 45° P-pol transmittance of AR witness is 99.2 %;
measurement agreement indicates $R < 0.1\%$

Figure 29: Coating BE: Side 2 AR, $R < 0.1\%$, best effort < 100 ppm @ 45 degrees AOI

LIGO-E1101095: Advanced LIGO Output Mode Cleaner Coating Specifications**[Description]**

Power transmissions of the prism and curved mirrors were characterized.

[Experimental method]

The measurement setup for the transmission measurement has been made at the output of the mode cleaning PM fiber.

- Made sure the output of the fiber was linearly polarized and has P-polarization by using a PBS. In fact it wasn't. Therefore the input and output fiber couplers were rotated to realize the linear P-polarization. Of course, this misaligns the input beam coupling to the fiber. Therefore some patient iteration was required.
- After some work, reasonable extinction ratio 10mW vs 100uW (100:1) with 11mW incidence. (It's curious what happened to the missing 0.9mW...)
- The P-pol (transmission) through the PBS goes into a prism mirror. The mirror is mounted on a prism mount supported by a rotational stage for precise angle adjustment. We limited the input power down to 5mW so that we can remove the attenuator on the power meter. The power meter output can depend on the position of my body. Therefore the lighting of the room had to be turned on in order to make the powermeter reading be stable.

[Result]

e.g. An example for an A mirror

- The offset of the power meter was -0.58uW
- The transmitted power for the normal incidence was 39.7uW with the incident 4.84mW.

$$[39.7 - (-0.58)]/[4.84 * 1000 - (-0.58)] * 10^6 = 8320\text{ppm}$$

- The transmitted power for the 4deg incidence was 38.0uW with the incident 4.87mW.

$$[38.0 - (-0.58)]/[4.87 * 1000 - (-0.58)] * 10^6 = 7980\text{ppm}$$

This number should be compared with the specification request for "Mirror A" (8300+/-800 ppm) and the data sheet spec (7931ppm).

The measurement results for the mirrors with 4-degree incidence are shown in Tables 8 and 9. The measurement results for the mirrors with 45-degree incidence are shown in Tables 10 and 11. Note that not all of E mirrors were inspected. None of the D mirrors were inspected.

Note on the mirror B measurements:

The initial B mirror measurements showed high number for the losses (1% ~ 3%). This inspired some investigation of the optical setup. The PBS to confine the polarization created a scattering halo around the main beam. This seemed a cause of distance dependent loss in the B mirror measurement. Therefore, the PBS was removed from the setup. Note that polarization ratio was 1:100 without the PBS. After the removal, the R&T measurement was redone. This time the loss distributed from 0.2% to 0.8% except for the one with 1.3%. Basically the loss of 0.25% is the quantization unit due to the lack of resolution.

The AR reflection was also measured for one of the B mirrors. There was a strong halo from the main specular reflection. Therefore the power from the AR reflection was measured at 0.5m distance from an iris to eliminate the halo. $33.6 \pm 0.2\mu\text{W}$ out of $39.10 \pm 0.05\text{mW}$ was observed. The offset was $-0.236\mu\text{W}$. This gives us the AR reflectivity of $865 \pm 5\text{ppm}$. This meets the spec requirement $R < 0.1\%$.

SN #	Power readings			Trans. [ppm]	Note
	Incident [mW]	Trans. [μW]	Offset [μW]		
A1	10.28	82.9	-0.205	8.08e3	
A2	—	—	—	—	@Fullerton
A3	10.00	83.2	-0.205	8.34e3	
A4	10.05	80.7	-0.205	8.05e3	
A5	9.94	81.3	-0.205	8.20e3	
A6	10.35	78.1	-0.205	7.57e3	
A7	10.35	77.8	-0.205	7.54e3	
A8	10.30	78.0	-0.205	7.60e3	
A9	10.41	84.1	-0.205	8.10e3	
A10	10.35	77.3	-0.205	7.49e3	
A11	10.33	77.9	-0.205	7.56e3	
A12	10.34	78.7	-0.205	7.63e3	
A13	10.41	85.4	-0.205	8.22e3	
A14	10.34	84.4	-0.205	8.18e3	

Table 8: Mirror transmission measurement for Mirror A. These numbers should be compared with the specification request (8300 ± -800 ppm) and the data sheet spec (7931ppm).

2.2.5 Mirror scattering measurement at Caltech

[Description]

Encountering the unexpected level of loss in the OMC cavity, the scattering measurement of the flat and curved cavity mirrors was performed at Caltech with full support of GariLynn Billingsley and Liyuan Zhang.

[Result]

The result of the measurement for the flat mirrors are shown in Figure 30. The result for the curved mirrors are shown in Figure 31.

2.2.6 Mirror scattering measurement at UC Fullerton

One mirror A and one curved mirror was sent to Joshua Smith at UC Fullerton for another scattering measurement. The below is the link to the poster posted in DCC.

[External Link]

LIGO-G1301118: Scattered Light Measurements for Advanced LIGO's Output Mode-Cleaner Mirrors (by A. Avila-Alvarez, et al.)

SN #	Power readings			Trans.	Note
	Incident [mW]	Trans. [μW]	Offset [μW]	[ppm]	
C1	10.30	0.2	-0.225	48.9	
C2	—	—	—	—	@Fullerton
C3	10.37	0.2	-0.191	41.6	
C4	10.35	0.2	-0.235	49.6	
C5	10.40	0.1	-0.235	35.9	
C6	10.34	0.1	-0.235	36.0	
C7	10.37	0.1	-0.229	35.9	
C8	10.41	0.2	-0.237	44.3	
C9	10.36	0.3	-0.230	54.8	
C10	10.39	0.3	-0.228	57.4	
C11	10.38	0.3	-0.209	56.6	
C12	10.28	0.2	-0.238	45.3	
C13	10.36	0.1	-0.234	39.8	

Table 9: Mirror transmission measurement for Mirror C. These numbers should be compared with the specification request (50+/-10 ppm) and the data sheet spec (51.48ppm or 46.40ppm, depending on the coating runs).

SN #	Power readings			Optical property		
	Incident [mW]	Trans. [μW]	Refl [mW]	Trans [ppm]	Refl	Loss [ppm]
E4	13.65 ± 0.05	0.0915 ± 0.0005	13.50 ± 0.05	6703 ± 44	0.989 ± 0.005	0.004 ± 0.005
E12	13.75 ± 0.05	0.0978 ± 0.0005	13.65 ± 0.05	7113 ± 45	0.993 ± 0.005	0.000 ± 0.005
E16	13.90 ± 0.05	0.0975 ± 0.0005	13.30 ± 0.05	7014 ± 44	0.957 ± 0.005	0.036 ± 0.005

Table 10: Mirror transmission measurement for Mirror E. These numbers should be compared with the specification request (7500+/-2500 ppm) and the data sheet spec (7400ppm).

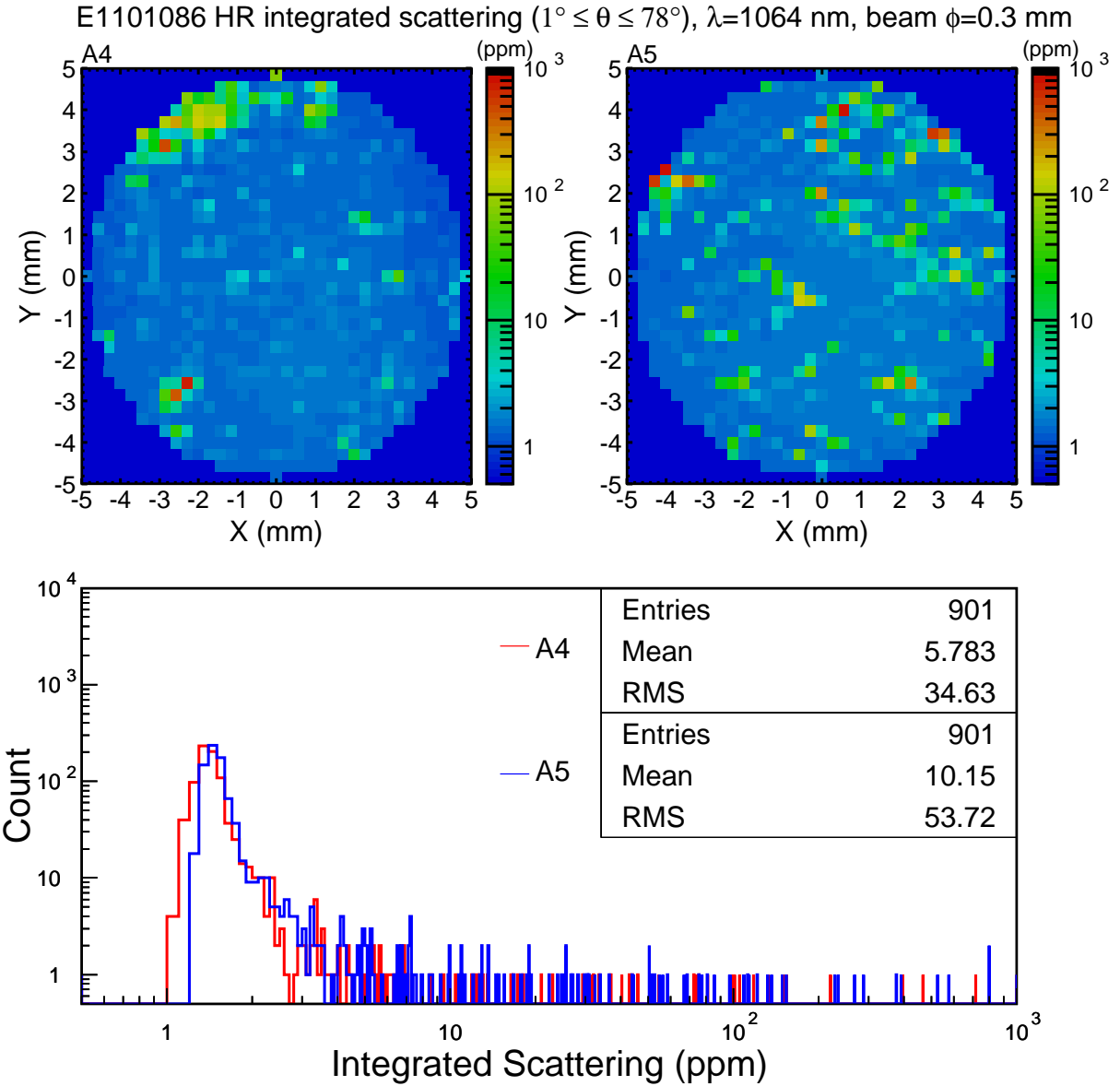


Figure 30: Scattering measurement for the two flat OMC cavity mirrors

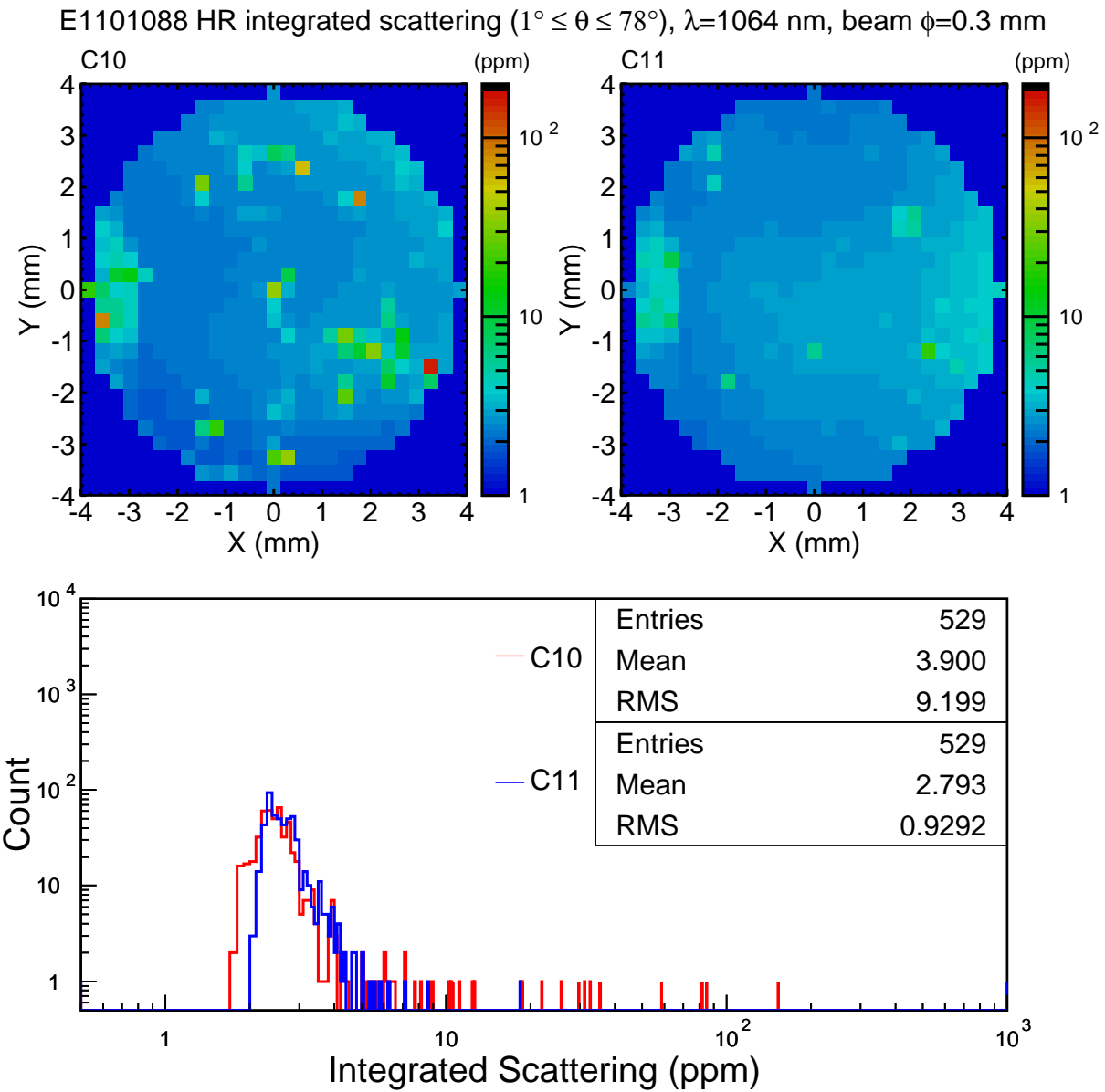


Figure 31: Scattering measurement for the two curved OMC cavity mirrors

SN #	Power readings			Optical property			Loss
	Incident [mW]	Trans. [μW]	Refl [mW]	Trans	Refl		
B1	39.10 ± 0.05	19.65 ± 0.05	19.25 ± 0.05	0.503 ± 0.001	0.492 ± 0.001	0.005 ± 0.002	
B2	39.80 ± 0.05	19.90 ± 0.05	19.70 ± 0.05	0.500 ± 0.001	0.495 ± 0.001	0.005 ± 0.002	
B3	13.87 ± 0.05	7.05 ± 0.05	6.55 ± 0.05	0.508 ± 0.004	0.472 ± 0.004	0.019 ± 0.005	
B4	39.50 ± 0.05	19.70 ± 0.05	19.30 ± 0.05	0.499 ± 0.001	0.489 ± 0.001	0.013 ± 0.002	
B5	39.50 ± 0.05	19.70 ± 0.05	19.50 ± 0.05	0.499 ± 0.001	0.494 ± 0.001	0.008 ± 0.002	
B6	39.55 ± 0.05	19.50 ± 0.05	19.95 ± 0.05	0.493 ± 0.001	0.504 ± 0.001	0.003 ± 0.002	
B7	40.10 ± 0.05	19.80 ± 0.05	20.20 ± 0.05	0.494 ± 0.001	0.504 ± 0.001	0.002 ± 0.002	
B8	40.15 ± 0.05	19.80 ± 0.05	20.20 ± 0.05	0.493 ± 0.001	0.503 ± 0.001	0.004 ± 0.002	
B9	40.10 ± 0.05	19.90 ± 0.05	19.90 ± 0.05	0.496 ± 0.001	0.496 ± 0.001	0.008 ± 0.002	
B10	40.10 ± 0.05	19.70 ± 0.05	20.30 ± 0.05	0.491 ± 0.001	0.506 ± 0.001	0.002 ± 0.002	
B11	40.20 ± 0.05	19.80 ± 0.05	20.20 ± 0.05	0.493 ± 0.001	0.502 ± 0.001	0.005 ± 0.002	
B12	40.20 ± 0.05	19.90 ± 0.05	20.20 ± 0.05	0.495 ± 0.001	0.502 ± 0.001	0.002 ± 0.002	

Table 11: Mirror transmission measurement for Mirror B. These numbers should be compared with the specification request ($T=50+/-2\%$) and the data sheet spec ($T=50.385\%$). Note that only B3 was measured before the improvement of the measurement setup.

2.3 Characterization of the PZTs

The aLIGO OMCs cavity have two Noliac NAC2124. Characterization measurements of the OMC PZTs are described in this section.

[External Link]

Noliac NAC2124

2.3.1 PZT Wedge angle

[External Link]

http://nodus.ligo.caltech.edu:8080/OMC_Lab/53

[Description]

The thickness and the wedge angle of the Noliac PZTs were measured.

[Experimental method]

For each PZT, the thickness at six points along the ring was measured with a micrometer gauge. The orientation of the PZT was recognized by the wire direction and a black marking to indicate the polarity.

[Result]

The measured thicknesses of the PZTs are shown in Figure 32.

A least square fitting of these six points determines the most likely PZT plane. Note that the measured numbers are assumed to be the thickness at the inner rim of the ring as the

micrometer can only measure the maximum thickness of a region and the inner rim has the largest effect on the wedge angle. The inner diameter of the ring is 9mm.

The measurements show all PZTs have thickness variation of 3 μm maximum.

The estimated wedge angles are distributed from 8 to 26 arcsec. The directions of the wedges seem to be random (i.e. not associated with the wires, for example)

As wedging of 30 arcsec causes at most $\sim 0.3\text{mm}$ spot shift of the cavity, the wedging of the PZTs is not critical by itself. Also, this number can be reduced by choosing the PZT orientations based on the estimated wedge directions.

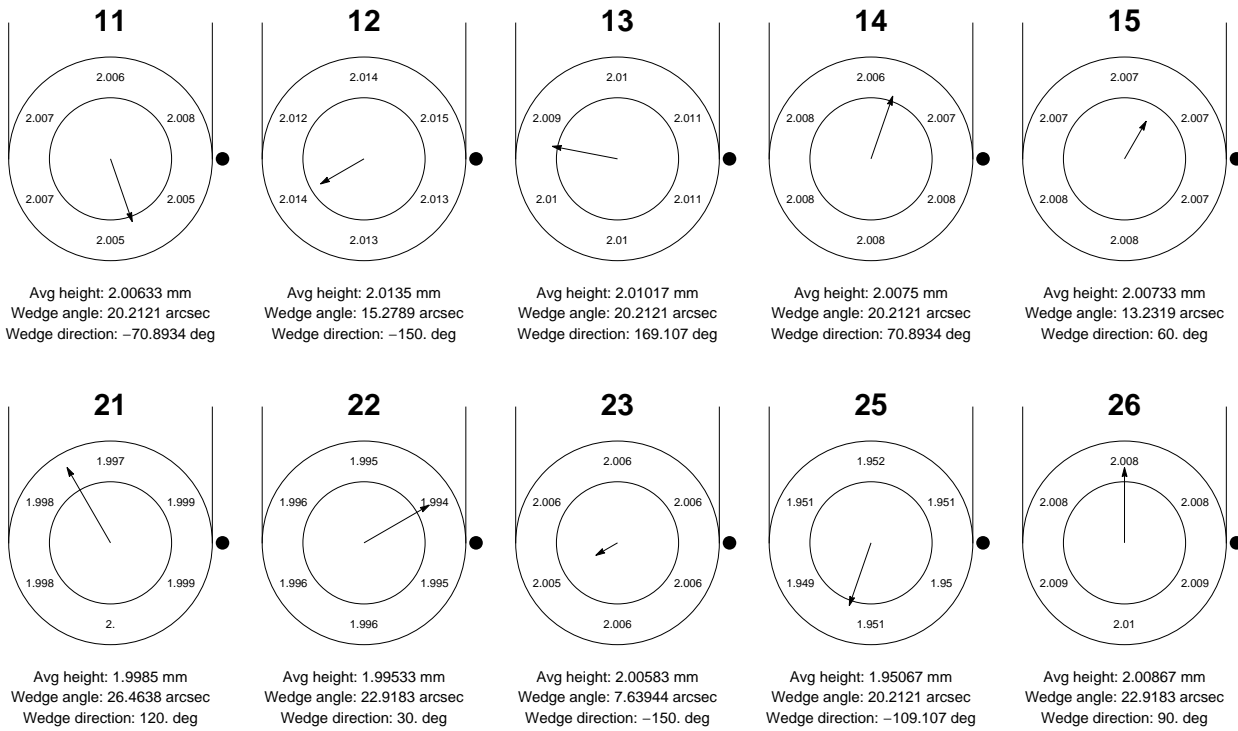


Figure 32: Measured thicknesses of the PZTs

2.3.2 PZT actuator DC response & length-to-angle coupling

[External Link]

http://nodus.ligo.caltech.edu:8080/OMC_Lab/102

aLIGO Wiki “PZT_testing”

[Description]

This is a measurement done by V. Frolov and R. DeRosa at LLO. This measurement characterized the PZTs actuation response at DC and length-to-angle coupling.

[Experimental method]

See their wiki page listed above.

[Result]

The result is summarized in Table 12. In the table, d is the distance of the curvature minimum from the mirror center, and ϕ is the angle of the minimum from the horizontal line at the center of the mirror.

PZT #	Length [nm/V]	Angle [urad/um]	Location
11	14.5	17.6	
12	13.8	17.8	
13	11.2	25.0	
14	14.5	6.6	3IFO CM1 (PZT ASSY #5)
15	12.5	10.6	3IFO CM2 (PZT ASSY #3)
21	14.5	9.7	H1 CM1 (PZT ASSY #6)
22	13.8	28.8	
23	14.5	6.8	L1 CM2 (PZT ASSY #2)
24	18.5	51.7	Used for prototyping
25	17.1	13.8	
26	14.5	6.6	L1 CM1 (PZT ASSY #1)

Table 12: PZT actuator response and length-to-angle coupling

2.3.3 Determination of the mirror arrangement for the PZT subassemblies

The combination and arrangement of a mounting prism, a PZT, and a curved mirror is determined for each PZT subassembly.

[External Link]

http://nodus.ligo.caltech.edu:8080/OMC_Lab/103
http://nodus.ligo.caltech.edu:8080/OMC_Lab/149

[Description]

The misalignment of the mirrors causes shift of the optical axis. Particularly, the vertical misalignment needs to be minimized, because the mirrors have no pitch adjustment. The pitch alignment of the prism mirrors were ensured with the perpendicularity measurement (Section 2.2.2).

However, the case for the curved mirrors is more complicated. It involves three components: a mounting prism, a PZT, and a curved mirror. The deviation of the curvature center for a curved mirror is equivalent with the misalignment. Therefore these misalignment needs to be minimized by carefully arranging these three components.

[Experimental method]

The vertical tile of each of three components are individually assessed. The sign of the angle is defined such that the positive number means the horizontal beam is reflected so that it goes away from the breadboard surface.

- The prism angle was determined by the perpendicularity measurement by an autocollimator (Section 2.2.2).
- The angle of the PZT was determined by the wedge measurement (Section 2.3.1). If the wedge angle of θ_{PZT} in arcsec is at ϕ_{PZT} in deg, the resulting vertical angle is

$$\theta_V[\text{arcsec}] = \theta_{\text{PZT}} \sin \frac{\pi \phi_{\text{PZT}}}{180}$$

For simplicity of the construction, we limit the orientation of the PZT to 0 deg and 180 deg. In the 0 deg arrangement, the wires of the PZT goes away from the breadboard.

- The curvature center was measured as described in Section 2.1.3. Suppose the center of the curvature is located at the distance of d and angle of ϕ [deg], from the horizontal line with the positive angle in CCW (cf. Figure 17). The vertical angle θ_V can be expressed as

$$\theta_V[\text{arcsec}] = \frac{180 \times 3600 \times d}{\pi R_{\text{RoC}}} \times \sin \frac{\pi(\phi - \phi_{\text{ROT}})}{180},$$

where R_{RoC} is the radius of curvature of the curved mirror, and ϕ_{ROT} is the rotation angle of the mirror in CW.

By adding these three quantities, the total vertical tilt is minimized.

[Result]

Such combinations to minimize the total vertical tilt are depicted in Figures 33 ~ 38.

For example, let's look at Figures 33.

- We use the mounting prism of #16. This has the vertical angle of +5.7arcsec.
- The PZT #26 has the wedge angle of 22.9arcsec at the angle 90deg (purely vertical). The PZT is rotated by 180 deg. Therefore the vertical angle by the PZT is -22.9arcsec.
- The C6 mirror has the curvature center at d of 0.73, mm and ϕ of 105 deg. When the mirror is rotated by 88 deg in CW, the curvature center is located at 17 deg from the horizontal line. This yields the vertical angle of +17.1arcsec.
- Therefore the total vertical angle is expected to be -0.1arcsec. That corresponds to the vertical beam shift of 1 μm .
- The right most circle shows how the curved mirror should be rotated in the gluing fixture. The curved mirror has an arrow scribe. This is the reference for the curvature center measurement. Therefore we can rotate the mirror to realize the arrow angle shown as in the figure. Note that the figure shows the front face of the mirror.

Note:

During the assembly of the #3 and #4, the curved mirrors were rotated with mistakenly calculated values. Figures 39 ~ 40 show the actual expected vertical angles. They shows -20~-30 arcsec. This corresponds to the beam shift of 25~37 μm closer to the breadboard.

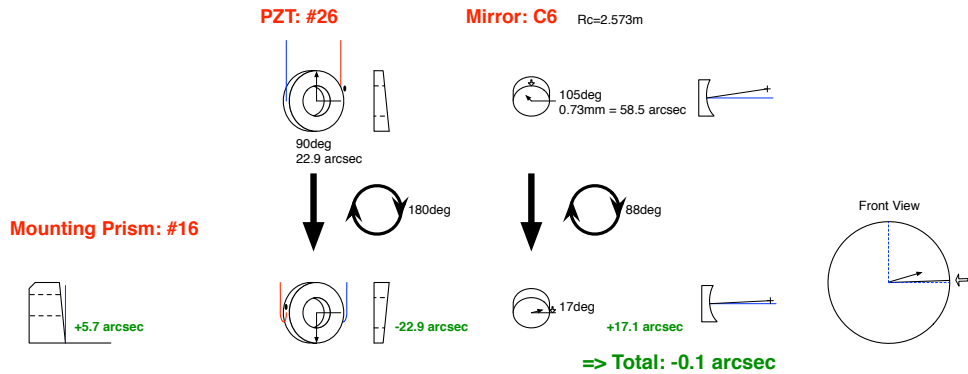
Gluing sheet: OMC PZT subassembly #1

Figure 33: PZT assembly No.1 gluing sheet

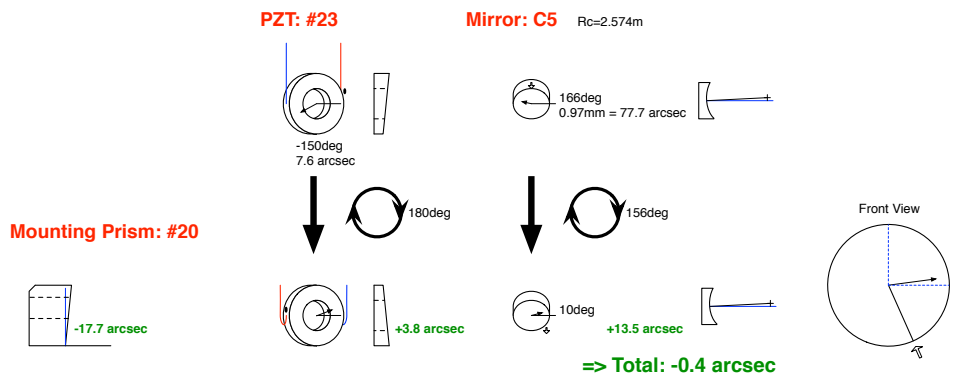
Gluing sheet: OMC PZT subassembly #2

Figure 34: PZT assembly No.2 gluing sheet

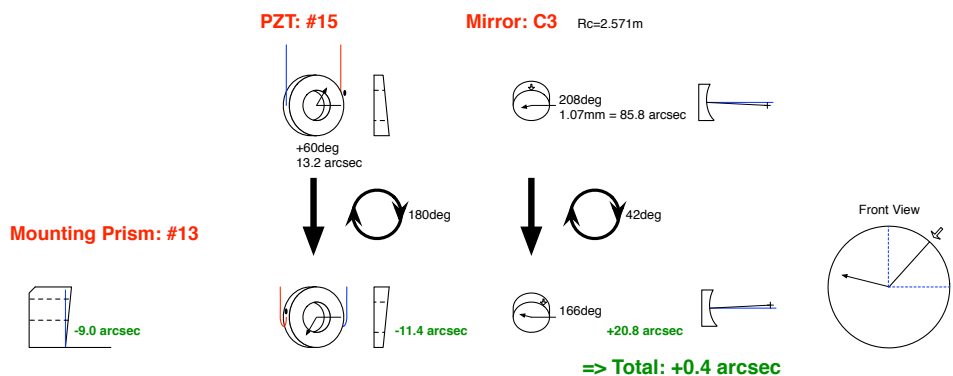
Gluing sheet: OMC PZT subassembly #3

Figure 35: PZT assembly No.3 gluing sheet

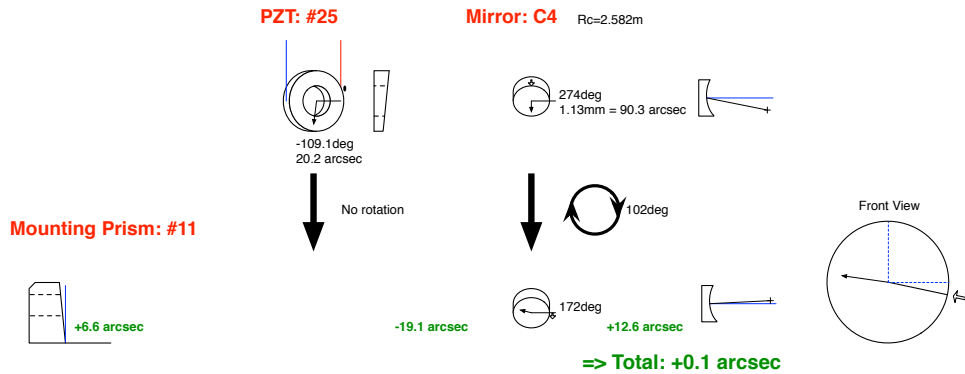
Gluing sheet: OMC PZT subassembly #4

Figure 36: PZT assembly No.4 gluing sheet

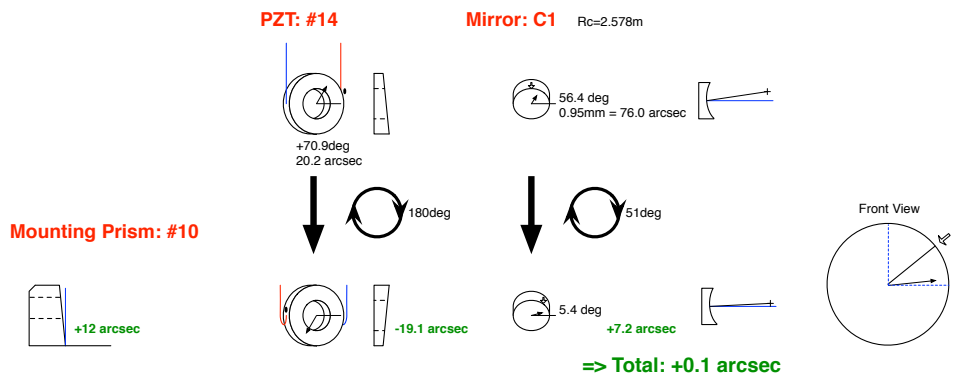
Gluing sheet: OMC PZT subassembly #5

Figure 37: PZT assembly No.5 gluing sheet

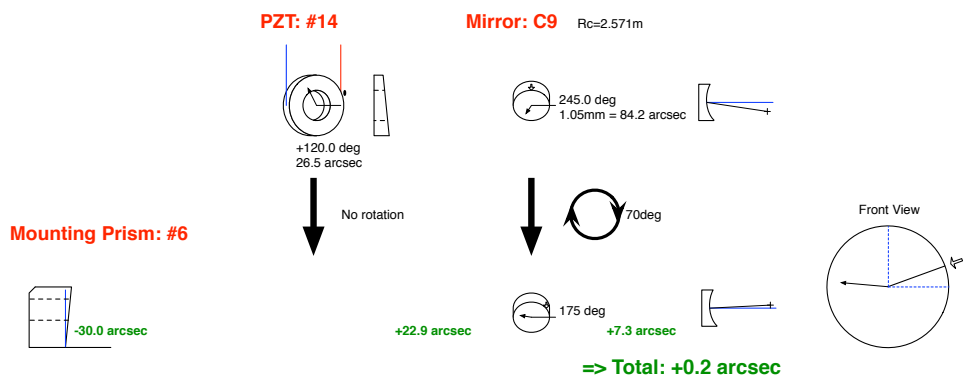
Gluing sheet: OMC PZT subassembly #6

Figure 38: PZT assembly No.6 gluing sheet

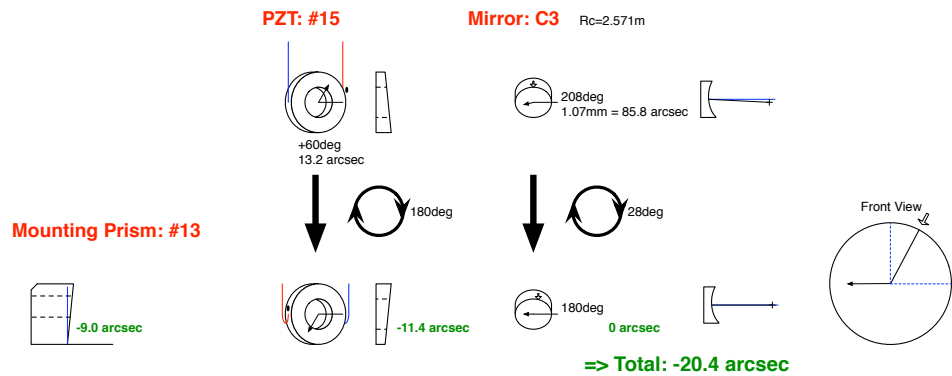
Gluing sheet: OMC PZT subassembly #3 (actual)

Figure 39: PZT assembly No.3 gluing sheet actual

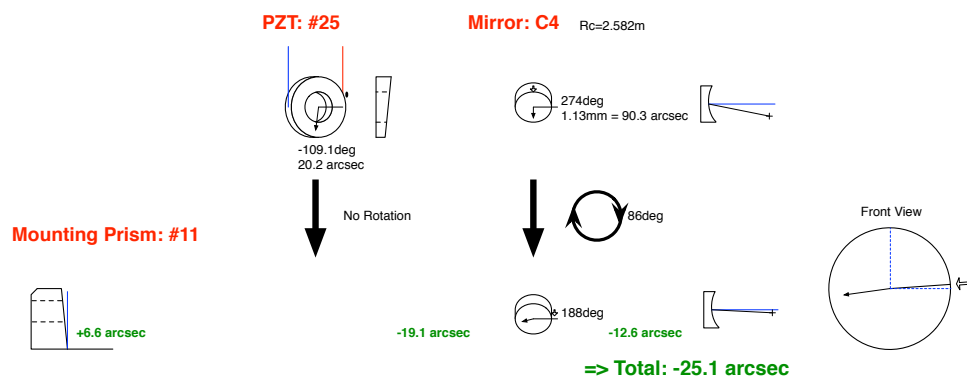
Gluing sheet: OMC PZT subassembly #4 (actual)

Figure 40: PZT assembly No.4 gluing sheet actual

2.3.4 PZT endurance test 1: High repetition test

[External Link]

http://nodus.ligo.caltech.edu:8080/OMC_Lab/156

Reliability of Piezoelectric Actuators at Extreme Operating Conditions, Noliac

[Description]

In response to the failure of one of the PZTs on L1OMC ([LLO aLOG:8366](#)), we have been taking place an endurance test of the four PZT sub-assemblies in prior to their being glued on the glass breadboard.

According to the technical note by Noliac, the common mode of PZT failure is degradation of the impedance due to cyclic actuation (like 10^7 times) with over voltage. Therefore our procedure of the test to actuate the PZTs at least 10^7 times with half voltage of the nominal operating voltage (i.e. nominal 200V) and check the degradation of the impedance.

[Experimental method]

- Driving signal

For driving the PZT, a thorlabs HV amp was used. A source signal of 3.5 Vpp with an offset of 1.7 V was produced by DS345 function generator. This signal turned to a sinusoidal signal between 0 and 100V in conjunction with the gain of 15 at the HV amp.

The maximum driving frequency is determined by the current supply limit of the HV amp (60mA). The capacitance of each PZT is $0.47\mu\text{F}$. If we decide to cycle the signal for 4 PZTs in parallel, the maximum frequency achievable without inducing voltage drop is 100Hz. This yields the test period of 28 hours in order to achieve 10^7 cycles.

- Initial impedance diagnosis

To check the initial state of the PZTs, a DC voltage of 100V was applied via 1kOhm output resistance. Note that this output resistance is used only for the impedance test. For each PZTs, both side of the resister showed 99.1V for all measurement by a digital multimeter (i.e. no measurable voltage difference). Assuming the minimum resolution (0.1V) of the multimeter, the lower limit of the resistance for each PZT was 1MOhm before the cycling test.

- Failure detection

In order to detect any impedance drop of the PZTs, the driving signal is monitored on the oscilloscope via a 1:10 probe. If there is any significant impedance drop, the driver can't provide the driving current correctly. This can be found by the deviation of the driving voltage from the reference trace on the oscilloscope (Figure 41).

- Temperature monitor

Because of the loss angle of the PZT capacitance, heating of the PZTs is expected. In order to check the temperature rise, an IR Viewer (FLIR) was used. We did not take care of careful calibration for the PZT emissivity as what we want was a rough estimation of the temperature.

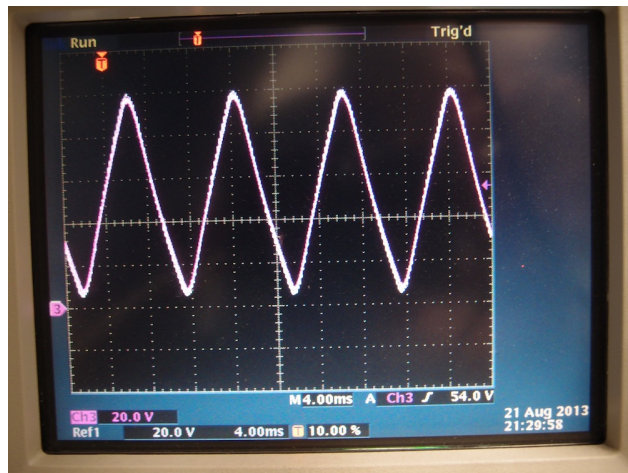


Figure 41: PZT endurance test: Driving voltage monitor.

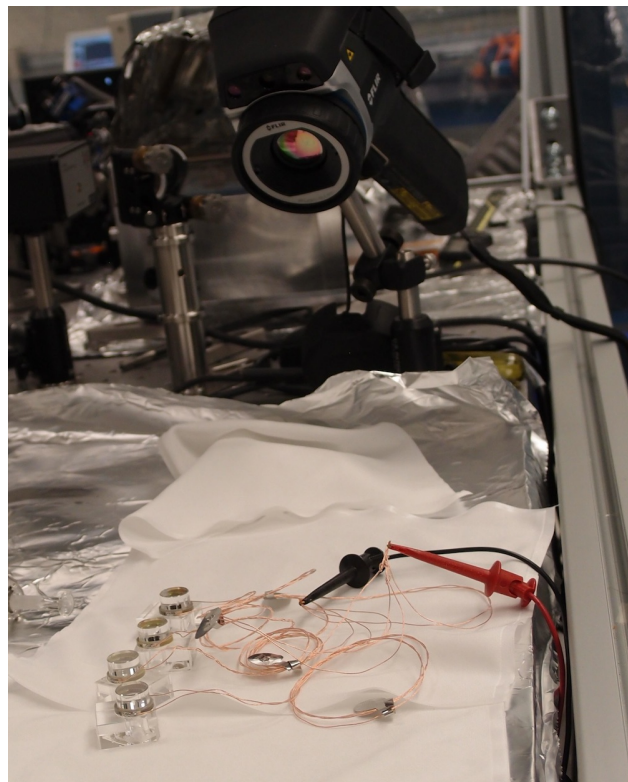


Figure 42: PZT endurance test: Temperature monitor setup.

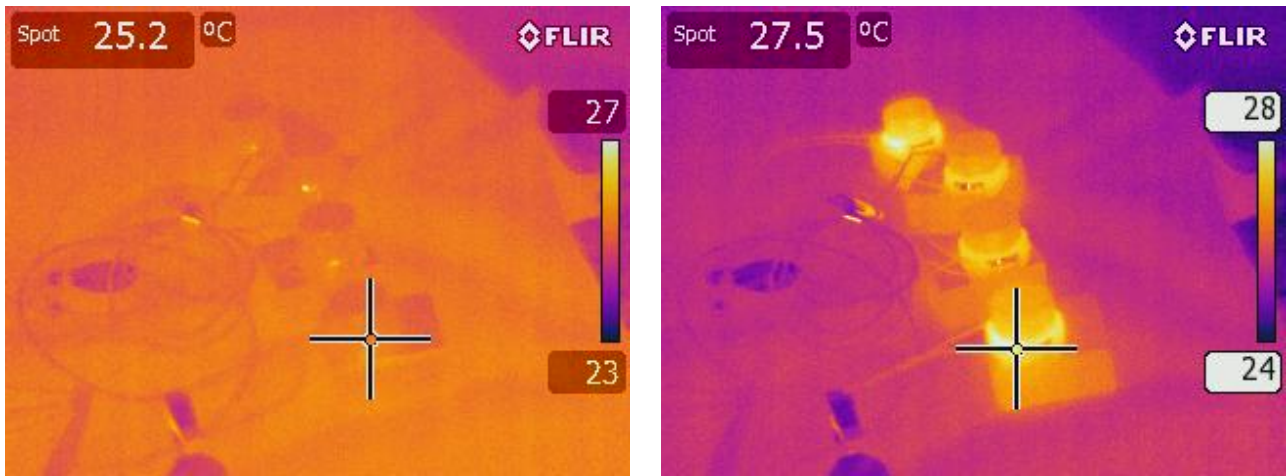


Figure 43: Thermal vision of the PZTs before the actuation.

Figure 44: Thermal vision of the PZTs during the actuation.

[Result]

The temperature change of the PZT was tracked for an hour (below). Fitting of the points indicated that the temperature rise is 2.3 degC and the time constant of 446 sec. This level of temperature rise is totally OK. Note that the fitting function was $T = 27.55 - 2.31 \exp(-t/446)$.

For the 1st day, the actuation was applied for 70 minutes (i.e. 4.2×10^5 cycles). No sign of degradation was observed.

For the 2nd and 3rd day, the actuation was continuously applied for about 28 hours. This yielded total 10.65 Mcycles. **No sign of degradation was observed.**

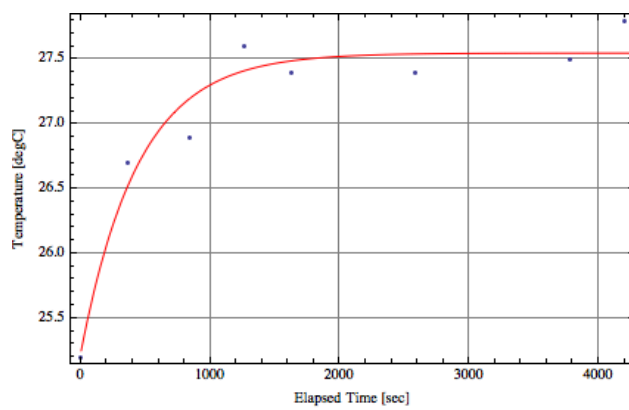


Figure 45: Teperature change of the PZTs

2.3.5 PZT endurance test 2: Reverse voltage test

This is a test of the PZTs to make sure small (10V) reverse voltage does not break the PZTs.

[External Link]

http://nodus.ligo.caltech.edu:8080/OMC_Lab/157

[Description]

At the Livingston site, we decided to use one of the two OMC PZTs, which is still alive, for the HV and LV actuation. The HV actuation is limited to 0 to 100V while the LV actuation is 10Vdc with 1Vpp fast dithering. This means that a reverse voltage upto 10.5V will be applied to the PZT at the worst case.

From the technical note of Noliac, this level of reverse voltage does not induce polarization of the PZT. The test is to ensure the PZT is not damaged or degraded by this small reverse voltage.

[Experimental method]

HV and LV drives are simultaneously applied. (See Figure 46)

HV drive: Thorlabs HV amp ($G=15$) driven with DS345 function generator (3.5Vpp+1.7Vdc, 0.1Hz). This provides 0~100V signal at 0.1Hz. The hot side of the potential is connected to the positive side of the PZT.

LV drive: Phillips function generator (1Vpp at 1kHz +9.5Vdc offset). The driving frequency is limited by the current output of the function generator. The hot side of the potential is connected to the negative side of the PZT.

These drives shares the common ground.

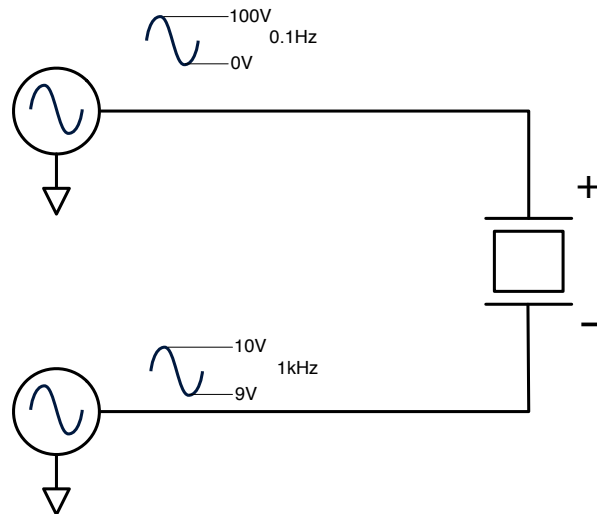


Figure 46: Reverse voltage test of the PZT

[Result]

- First, spare PZTs were tested.

The actuation has been applied for 48 hours and 52 minutes, which corresponds to 17600 and 176M cycles for the 0.1Hz and 1kHz drives, respectively.

After the actuation, the impedance of the PZTs were measured. When 100Vdc was applied via a 1kOhm resister, 0V (0.001V resolution) was detected across the 1kOhm resister. This corresponds to the upper limit of the 1MOhm resistance.

- Next the PZT subassemblies were tested.

After the sme actuation for 39.5 hours, no impedance change was detected.

Thus it was concluded that the PZT were unchanged after the reverse voltage test.

2.4 Photodiode and photodetector test

2.4.1 DCPD diode test

[External Link]

http://nodus.ligo.caltech.edu:8080/OMC_Lab/73

LIGO-T1100208: Photodiodes Pulse Damage Testing - status report, a.k.a. “Totally Awesome Diode Blasting Experiment” (by Frank Seifert)

LIGO-T1300321: OMC DCPD Test Result - InGaAs PD C30665GH

[Description]

The photodiodes for the OMC DCPDs are the photodiodes that the gravitational wave signals will eventually appear. Therefore they have to be carefully selected and characterized.

[Experimental method]

Measurement setup was inherited from the diode blasting experiment (see above T1100208). Here is the brief description.

- The dark current was measured with a sourcemeter (Keithley 2635A Sorcemeter).
- The RF impedance was measured with a network analyzer (Agilent 4395A Network Analyzer + 43961A RF impedance test adapter)
- The dark noise was measured with a low noise current amplifier (FEMTO DLPCA-200) and FFT analyzer (Stanford Research SR785).

Some remarks on the setup:

- For the dark noise measurement, the lid of the die-cast case should also contact to the box for better shielding. This made the 60Hz lines almost completely removed, although unknown 1kHz harmonics remains.
- The diode characteristics with the impedance kit was measured between 10MHz and 100MHz.
- The impedance of the diodes could not be obtained when Frank’s measurement box was used. The cables between the diode and the network analyzer was too long to allow precise impedance measurement. Instead, the diode impedances were measured directly on the impedance measurement kit at the network analyzer. With this setup, the reverse bias voltage of 5V was applied on the network analyzer.

[Result]

- Impedance measurement

For comparison, 1mm and 2mm diameter photodiodes brought from the 40m lab were also tested. In total, 30 photodiodes were measured. The breakdown of the tested diodes are as follows:

- 3mm InGaAs photodiodes: C30665GH, Serial 1~13.
- 2mm InGaAs photodiodes: C30642G, Serial 20~29.
- 1mm InGaAs photodiodes: C30641GH, Serial 30~36.

The photodiode impedances are listed as Table 13. The DCPDs employ 3mm photodiodes. The PD #1~#13 showed basically identical performance in terms of the impedance.

- Dark current / dark noise measurement

Table 14 shows the result of the dark noise and current measurement for the 3mm InGaAs photodiodes. The dark current is represented at the value at 5V reverse bias. The dark noise is represented by the average between 1 Hz and 10 Hz, and between 200 Hz and 290 Hz.

Three out of 13 PDs showed abnormal dark current or noise and rejected for the use for the OMC purpose.

Typical performance of a “good” diode is shown in Figures 47. The measured data for the other PDs are attached as Figures 48~59. The same figures are also available in T1300321 (linked above).

Diode	LIGO Serial	Vendor Serial	R_s [Ω]	C_d [pF]	Source
C30665GH	1	0782	8.3	219.9	Peter King
C30665GH	2	1139	9.9	214.3	Peter King
C30665GH	3	0793	8.5	212.8	Peter King
C30665GH	4	0732	7.4	214.1	Peter King
C30665GH	5	0791	8.4	209.9	Peter King
C30665GH	6	0792	8.0	219.0	Peter King
C30665GH	7	0787	9.0	197.1	Peter King
C30665GH	8	0790	8.4	213.1	Peter King
C30665GH	9	0781	8.2	216.9	Peter King
C30665GH	10	0784	8.2	220.0	Peter King
C30665GH	11	1213	10.0	212.9	40m
C30665GH	12	1208	9.9	216.8	40m
C30665GH	13	1209	10.0	217.5	40m
C30642G	20	2484	12.0	99.1	40m, EG&G
C30642G	21	2487	14.2	109.1	40m, EG&G
C30642G	22	2475	13.5	91.6	40m, EG&G
C30642G	23	6367	9.99	134.7	40m, ?
C30642GH	24	1559	8.37	94.5	40m, Perkin-Elmer
C30642GH	25	1564	7.73	94.5	40m, Perkin-Elmer
C30642GH	26	1565	8.22	95.6	40m, Perkin-Elmer
C30642GH	27	1566	8.25	94.9	40m, Perkin-Elmer
C30642GH	28	1568	7.83	94.9	40m, Perkin-Elmer
C30642GH	29	1575	8.32	100.5	40m, Perkin-Elmer
C30641GH	30	8983	8.19	25.8	40m, Perkin-Elmer
C30641GH	31	8984	8.39	25.7	40m, Perkin-Elmer
C30641GH	32	8985	8.60	25.2	40m, Perkin-Elmer
C30641GH	33	8996	8.02	25.7	40m, Perkin-Elmer
C30641GH	34	8997	8.35	25.8	40m, Perkin-Elmer
C30641GH	35	8998	7.89	25.5	40m, Perkin-Elmer
C30641GH	36	9000	8.17	25.7	40m, Perkin-Elmer

Table 13: Measured impedances of the 3mm, 2mm, and 1mm photodiodes.

Diode P/N	LIGO Serial	Vendor Serial	Dark Current @5V[nA]	Dark Noise 1-10 Hz _{Avg} [pA/ $\sqrt{\text{Hz}}$]	Dark Noise 200-290 Hz _{Avg} [pA/ $\sqrt{\text{Hz}}$]	Note
C30665GH	1	0782	6.74	6.504	1.452	Too high D.N.
C30665GH	2	1139	5.19	2.031	0.205	Too high D.N.
C30665GH	3	0793	4.83	1.473	0.269	OK
C30665GH	4	0732	2.19	0.051	0.107	good
C30665GH	5	0791	2.33	0.048	0.115	good
C30665GH	6	0792	2.76	0.077	0.111	good
C30665GH	7	0787	2.01	0.223	0.143	OK
C30665GH	8	0790	5.87	0.911	0.177	OK
C30665GH	9	0781	1131.96	0.011	0.005	Broken
C30665GH	10	0784	2.09	0.062	0.111	good
C30665GH	11	1213	3.48	0.674	0.128	OK
C30665GH	12	1208	2.19	0.076	0.096	good
C30665GH	13	1209	2.15	0.077	0.097	good

Table 14: Dark noise/current measurement for the 3mm InGaAs photodiodes

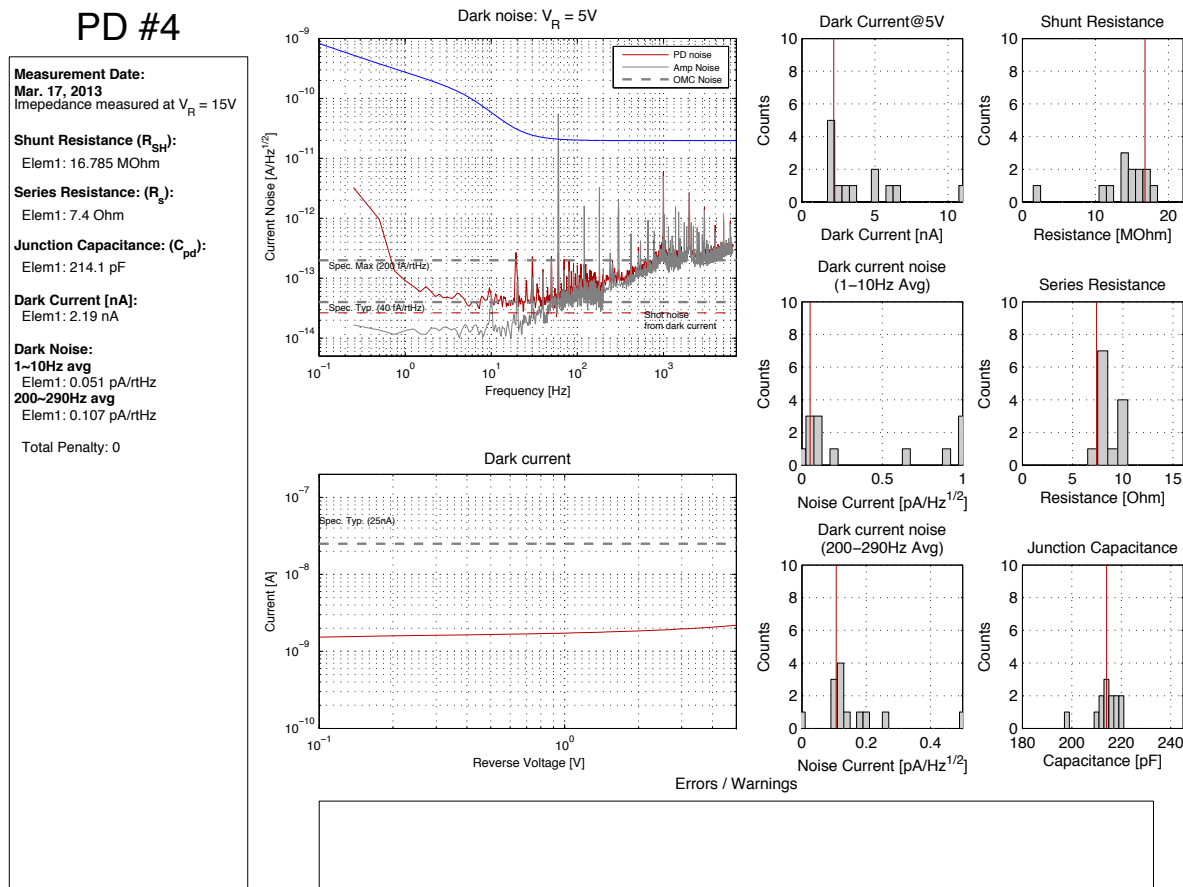


Figure 47: Test result of DCPD SN:4, typical good diode performance

LIGO-T1500060-v1

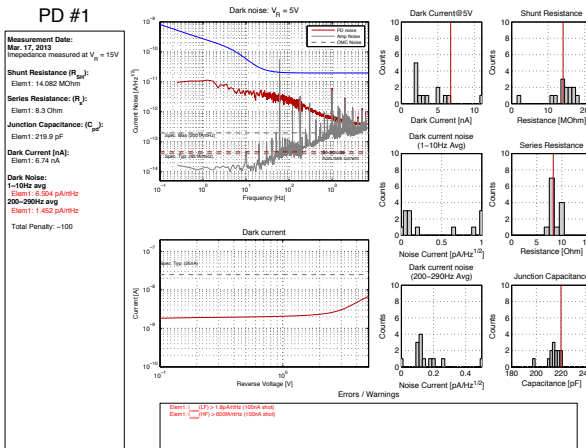


Figure 48: Test result of DCPD SN:1

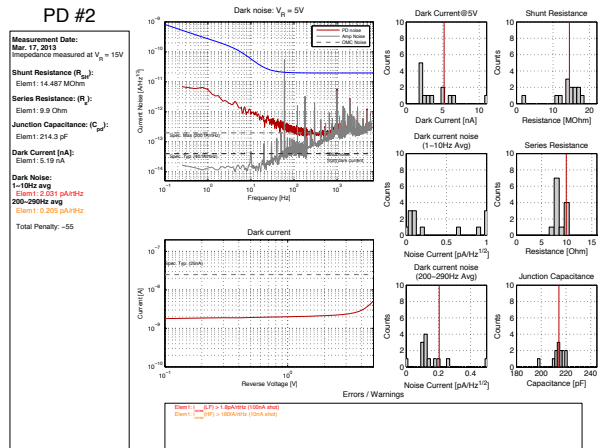


Figure 49: Test result of DCPD SN:2

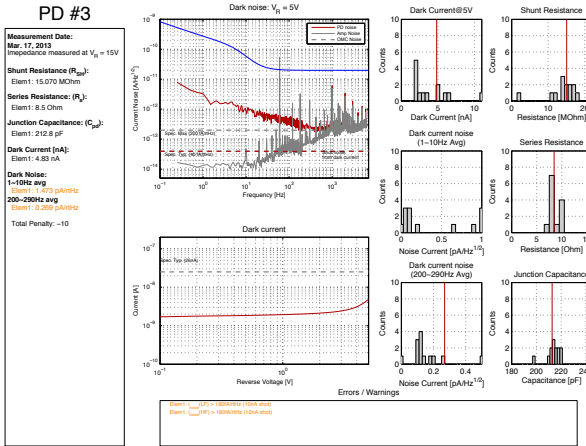


Figure 50: Test result of DCPD SN:3

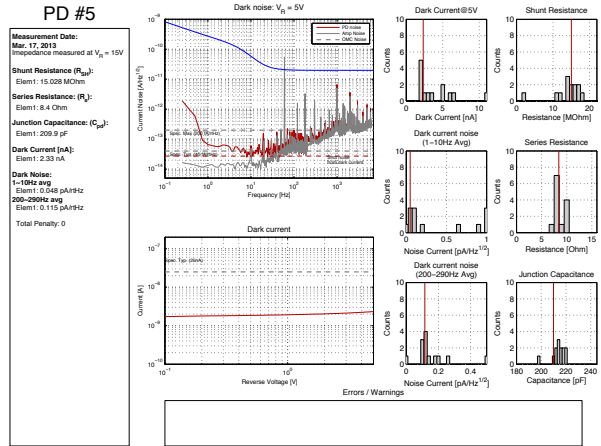


Figure 51: Test result of DCPD SN:5

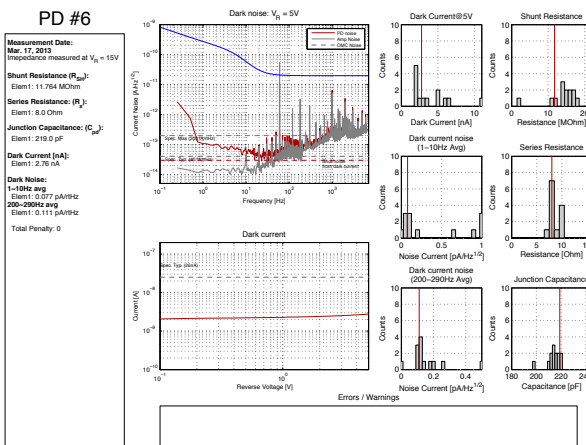


Figure 52: Test result of DCPD SN:6

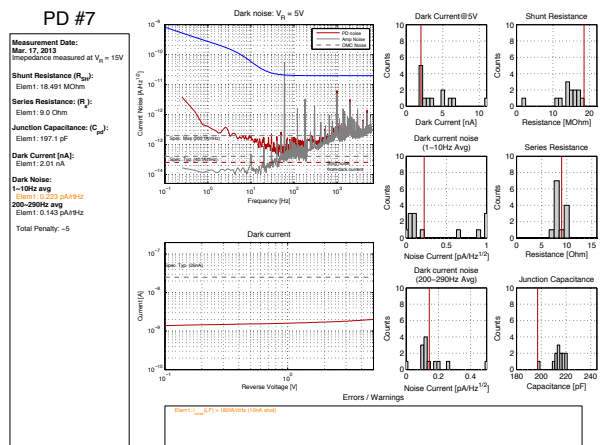


Figure 53: Test result of DCPD SN:7

LIGO-T1500060-v1

PD #8

Measurement Date: Mar. 17, 2013
Impedance measured at $V_R = 15V$
Shunt Resistance (R_{sh}):
Elem1: 11.269 MΩ
Series Resistance: (R_s):
Elem1: 8.4 Ohm
Junction Capacitance: (C_j):
Elem1: 215.1 pF
Dark Current [nA]:
Elem1: 5.87 nA
Dark Noise:
1-10Hz avg: 0.0001 pA/Hz
200-250Hz avg: 0.0001 pA/Hz
Element: 0.177 pA/Hz
Total Penalty: -6

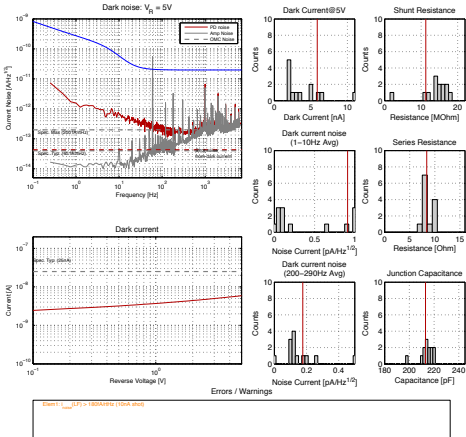


Figure 54: Test result of DCPD SN:8

PD #9

Measurement Date: Mar. 17, 2013
Impedance measured at $V_R = 15V$
Shunt Resistance (R_{sh}):
Elem1: 3.272 MΩ
Series Resistance: (R_s):
Elem1: 8.2 Ohm
Junction Capacitance: (C_j):
Elem1: 216.9 pF
Dark Current [nA]:
Elem1: 0.131 36 nA
Dark Noise:
1-10Hz avg: 0.001 pA/Hz
200-250Hz avg: 0.005 pA/Hz
Element: 0.005 pA/Hz
Total Penalty: -105

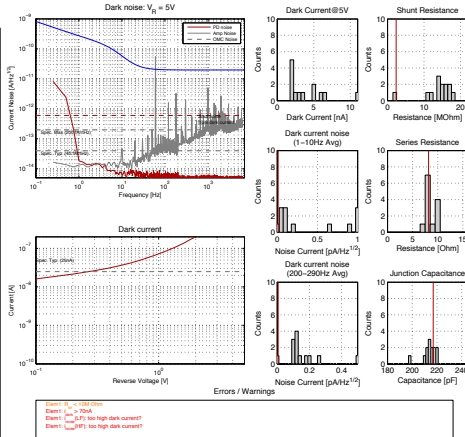


Figure 55: Test result of DCPD SN:9

PD #10

Measurement Date: Mar. 17, 2013
Impedance measured at $V_R = 15V$
Shunt Resistance (R_{sh}):
Elem1: 17.106 MΩ
Series Resistance: (R_s):
Elem1: 8.2 Ohm
Junction Capacitance: (C_j):
Elem1: 220.0 pF
Dark Current [nA]:
Elem1: 2.09 nA
Dark Noise:
1-10Hz avg: 0.0002 pA/Hz
200-250Hz avg: 0.0002 pA/Hz
Element: 0.111 pA/Hz
Total Penalty: 0

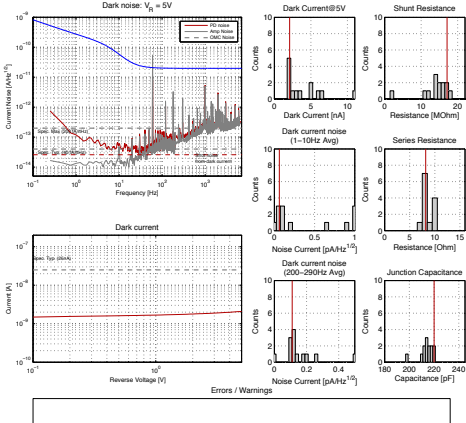


Figure 56: Test result of DCPD SN:10

PD #11

Measurement Date: Mar. 17, 2013
Impedance measured at $V_R = 15V$
Shunt Resistance (R_{sh}):
Elem1: 13.052 MΩ
Series Resistance: (R_s):
Elem1: 10.0 Ohm
Junction Capacitance: (C_j):
Elem1: 212.9 pF
Dark Current [nA]:
Elem1: 1.48 nA
Dark Noise:
1-10Hz avg: 0.004 pA/Hz
200-250Hz avg: 0.020 pA/Hz
Element: 0.120 pA/Hz
Total Penalty: -5

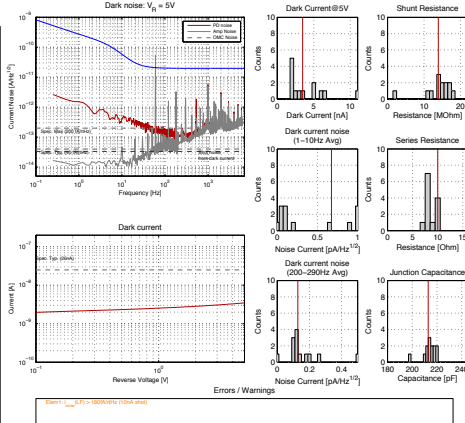


Figure 57: Test result of DCPD SN:11

PD #12

Measurement Date: Mar. 17, 2013
Impedance measured at $V_R = 15V$
Shunt Resistance (R_{sh}):
Elem1: 15.749 MΩ
Series Resistance: (R_s):
Elem1: 9.9 Ohm
Junction Capacitance: (C_j):
Elem1: 216.8 pF
Dark Current [nA]:
Elem1: 2.153 nA
Dark Noise:
1-10Hz avg: 0.001 pA/Hz
200-250Hz avg: 0.006 pA/Hz
Element: 0.096 pA/Hz
Total Penalty: 0

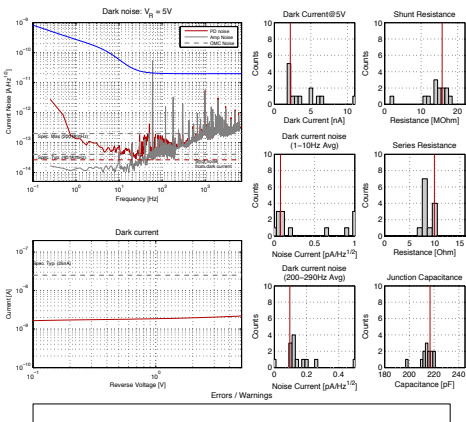


Figure 58: Test result of DCPD SN:12

PD #13

Measurement Date: Mar. 17, 2013
Impedance measured at $V_R = 15V$
Shunt Resistance (R_{sh}):
Elem1: 16.201 MΩ
Series Resistance: (R_s):
Elem1: 10.1 Ohm
Junction Capacitance: (C_j):
Elem1: 217.3 pF
Dark Current [nA]:
Elem1: 2.153 nA
Dark Noise:
1-10Hz avg: 0.007 pA/Hz
200-250Hz avg: 0.009 pA/Hz
Element: 0.097 pA/Hz
Total Penalty: 0

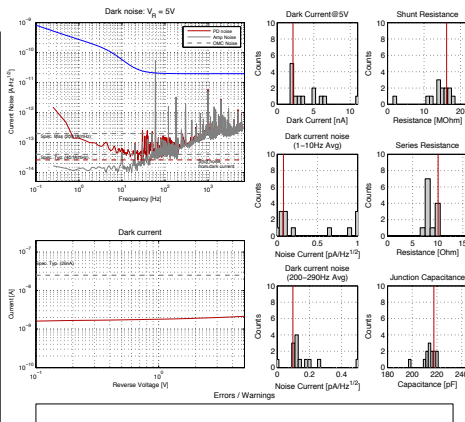


Figure 59: Test result of DCPD SN:13

2.4.2 DCPD diode response test

[External Link]

http://nodus.ligo.caltech.edu:8080/OMC_Lab/78

LHO iLog Aug 24, 2009

LLO iLog Sep 5, 2009

LIGO-T0900420: H1 OMC DC PDs

[Description]

The responsivities (i.e. quantum efficiencies) of the C30665GH diodes were measured.

[Experimental method]

The photodiode under test was reverse-biased by FEMTO DLPCA-200, transimpedance amplifier (TIA). The diode pin 1 (anode) was connected to the signal input of the amplifier. The diode pin 2 (cathode) was the shield side of the amplifier input and was set to be +5V. The pin 3 (case) was left open. The amplifier gain was 10^3 V/A.

P-polarized light is focused on the diode. The diode angle was adjusted to be the incident angle of 10 deg with a rotation stage. The diodes had their glass windows on. Therefore this significantly reduces the quantum efficiency. The output from the TIA V_{out} , the power of the incident beam P_{inc} and the prompt reflection $P_{refl,prompt}$, and the total reflected power from the photodiode $P_{refl,total}$, are measured (Figure 60). The power measurements have been done with Thorlabs S130C, which has the measurement uncertainty of $\pm 7\%$ at 1064nm.

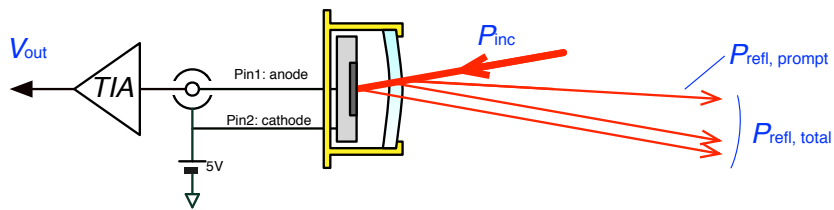


Figure 60: Measured quantities on the photodiode efficiency.

[Result]

The raw results of the measurements are shown in Table 15. From the numbers, some properties of the photodiodes are extracted.

- R_{ON} , Responsivity with the glass window on:

$$R_{ON} = \frac{V_{out}}{G_{TIA} P_{inc}} \text{ [A/W]} ,$$

where G_{TIA} is the transimpedance of the TIA ($1k\Omega$).

LIGO SN	Vendor SN	Power measurements [mW]			PD output
		P_{inc}	$P_{\text{refl},\text{total}}$	$P_{\text{refl},\text{prompt}}$	$V_{\text{out}} [\text{V}]$
1	0782	12.82 ± 0.02	1.168	0.404	9.161 ± 0.0005
2	1139	12.73 ± 0.02	0.937	0.364	9.457 ± 0.0005
3	0793	12.67 ± 0.02	1.272	0.383	9.114 ± 0.001
4	0732	12.71 ± 0.02	1.033	0.393	9.307 ± 0.0005
5	0791	12.69 ± 0.02	1.183	0.401	9.107 ± 0.005
6	0792	12.65 ± 0.02	1.306	0.395	9.031 ± 0.01
7	0787	12.67 ± 0.02	1.376	0.411	9.059 ± 0.0005
8	0790	12.63 ± 0.01	1.295	0.420	9.079 ± 0.0005
9	0781	12.67 ± 0.02	1.091	0.384	9.208 ± 0.0005
10	0784	12.70 ± 0.01	1.304	0.414	9.088 ± 0.001
11	1213	12.64 ± 0.01	1.152	0.416	9.286 ± 0.0005
12	1208	12.68 ± 0.02	1.057	0.419	9.365 ± 0.001
13	1209	12.89 ± 0.01	1.047	0.410	9.386 ± 0.001

Table 15: Measurement of the quantum efficiencies for the DCPD photodiodes. P_{inc} : Incident power on a photodiode. $P_{\text{refl},\text{total}}$: Total reflected power from a photodiode. $P_{\text{refl},\text{prompt}}$: The reflected power in a first spot. $V_{\text{out}} [\text{V}]$: PD output voltage with a transimpedance of $10^3[\Omega]$.

- η_{ON} , Quantum efficiency with the glass window on:

$$\eta_{\text{ON}} = R_{\text{ON}} \times \frac{hc}{e\lambda} ,$$

where h and e are the Planck constant and the electron charge, respectively. λ is the wavelength of the laser.

- R_{OFF} , Estimated responsivity when the glass window is removed:

$$R_{\text{OFF}} = \frac{V_{\text{out}}}{G_{\text{TIA}} P_{\text{inc}} (1 - P_{\text{refl},\text{prompt}}/P_{\text{inc}})^2} [\text{A/W}] ,$$

This assumes two glass reflections are reflected with the same reflectivities.

- η_{OFF} , Estimated quantum efficiency with the glass window off:

$$\eta_{\text{OFF}} = R_{\text{OFF}} \times \frac{hc}{e\lambda} .$$

Table 16 shows the summary of these values for the DCPD photodiodes. Note that the quantum efficiency of the diodes are distributed around 90%.

2.4.3 Dependence of the photodiode response on the incident angle

[External Link]

LIGO-T1100564: E.G.&G. Photodiode angular response (S. Waldman)

[Description]

LIGO SN	Vendor SN	With window			Without window		
		R_{ON} [A/W]	Q.E.	η_{ON}	R_{OFF} [A/W]	Q.E.	η_{OFF}
1	0782	0.715	± 0.001	0.833	± 0.001	0.762	± 0.001
2	1139	0.743	± 0.001	0.866	± 0.002	0.787	± 0.001
3	0793	0.719	± 0.001	0.838	± 0.001	0.765	± 0.001
4	0732	0.732	± 0.001	0.853	± 0.001	0.780	± 0.001
5	0791	0.718	± 0.001	0.836	± 0.002	0.765	± 0.001
6	0792	0.714	± 0.001	0.832	± 0.002	0.761	± 0.001
7	0787	0.715	± 0.001	0.833	± 0.001	0.764	± 0.001
8	0790	0.7188	± 0.0006	0.8376	± 0.0006	0.7691	± 0.0006
9	0781	0.727	± 0.001	0.847	± 0.001	0.773	± 0.001
10	0784	0.7156	± 0.0006	0.8340	± 0.0006	0.7646	± 0.0006
11	1213	0.7347	± 0.0006	0.8562	± 0.0006	0.7855	± 0.0006
12	1208	0.739	± 0.001	0.861	± 0.002	0.790	± 0.001
13	1209	0.7282	± 0.0006	0.8487	± 0.0006	0.7768	± 0.0006

Table 16: Estimated responsivities and quantum efficiencies of the DCPD photodiodes.

It's worth to mention that there is a document by S. Waldman about measured angular response of 2mm InGaAs photodiodes distributed by EG&G (i.e. = Perkin Elmer = Excelitas).

Note that the aLIGO OMC PDs have the AOI of $\sim 10\text{deg}$. The AOI is well within the central flat region according to the document.

2.4.4 DCPD preamp test

[External Link]

LIGO-E1600013: OMC DCPD characterization for aLIGO transition (W.Z. Korth, K. Arai)

[Description]

For the L1 and H1 OMC, we transitioned the eLIGO OMC DCPD preamps for aLIGO use. This document summarizes the electrical performance of these preamps. Refer the external link for the details.

2.4.5 High QE DCPD diode test

[External Link]

LIGO-E1600013: aLIGO OMC: Handling procedure for high quantum efficiency photodiodes
LIGO-Dxxxxxxxx: Cage

[Description]

Based on the quantum efficiency defect of C30665 photodiodes (Table 16), LIGO asked Laser Components to produce custom high Q.E. photodiodes that has the same dimentions (Section B)and pinouts. This diode IGHQE3000 is supposed to have Q.E. of 99%. The

following sections describe the characteristic of the photodiodes.

E1600013 describes the handling procedure of the photodiodes based on the following background.

A special care is necessary for handling of the photodiodes because they are expensive and precious products that were customly ordered and not off-the-shelf. The custom photodiodes are particularly prone to be damaged by ESD shock, according to the manufacturer.

Also it turned out that the manufacturer used Eccobond CE3103WLV and EPO-TEK H70E-4 in this batch of the photodiodes. These adhesives are not LIGO-approved ones. Therefore, a careful procedure for the outgassing reduction is necessary as well as performance check before and after the bake process.

2.4.6 High QE DCPD response measurement

2.4.7 High QE DCPD dark current measurement

2.4.8 High QE DCPD dark noise measurement

2.4.9 Effect of air-baking on high QE DCPD

2.5 Miscellaneous measurements

2.5.1 Breadboard size measurement

[External Link]

http://nodus.ligo.caltech.edu:8080/OMC_Lab/27

[Description]

The OMC glass breadboards were inspected. The size and mass of them were measured.

[Experimental method]

The scale of the 40m bake lab (max 60kg, min resolution of 1g) was brought and used. The dimensions were measured by a huge caliper which was brought from Downs.

[Result]

Results are shown in Table. 17

Height measurements were made twice, once at each end.

S/N 01, 03, 04 look pretty similar. They should be the primary candidates.

2.5.2 UV epoxy thickness

http://nodus.ligo.caltech.edu:8080/OMC_Lab/62

[Description]

Thickness of the UV epoxy was measured upon gluing test with UV-cure epoxy Optocast 3553-LV-UTF-HM.

S/N #	Mass [g]	Length [mm]	Width [mm]	Height [mm]	Notes
01	6146	449.66	149.85	41.42, 41.42	for LLO
02	6126	449.66	149.97	41.32, 41.32	for LHO
03	6143	449.76	149.98	41.39, 41.43	
04	6139	449.78	149.81	41.40, 41.40	for 3IFO
05	6132	449.76	150.03	41.27, 41.31	corner chip, front-bottom-left*
06	6138	449.84	149.71	41.42, 41.42	

Table 17: The dimensions and mass of the OMC glass breadboards. * Orientation of the chipping is relative to "front" face, i.e. long-short face with S/N on it, with S/N upright.

The thickness of a pair of fused silica substrates (no coating) was measured without any glue. The total thickness before the gluing was 12.658 mm.

Then the UV epoxy was applied and the UV light was illuminated for curing. The thickness after the gluing was 12.663 mm. This indicates the glue thickness is $5 \pm 1\mu\text{m}$.

3 Test of the integrated OMC breadboards

During the OMC building, the parameters of the cavity geometry was necessary to be continuously monitored. In addition, various parameters of the OMC breadboards needed to be characterized after the assembling.

These tests of the integrated OMC have been done using a cavity locking setup built in the OMC lab at Caltech. This section explains the setup and the tests performed there.

3.1 Experimental setup

The test setup is similar to the one in Section 2.1.1. The setup has been built on the optical table at Room 056 in West Bridge, Caltech.

The schematic diagram of the optical setup is shown in Figure 61. The main difference from the RoC measurement setup is listed below:

- The input mode to the cavity was confined by a polarization-maintaining single-mode fiber (Thorlabs P3-1064PM-FC-5). Each fiber end has a collimation lens (Thorlabs CFC-2X-C) on a fiber mount (Thorlabs K6X) so that we can easily mode-match the input beam to the fiber, as well as the output from the fiber to the OMC.
- The input beam to the OMC cavity was elevated by a periscope to the optical height of the OMC cavity on the transport fixture.
- The photodetector for the PDH locking was replaced with PDA100CF, instead of PDA255. In addition, the transmission RF detector was replaced with Newfocus 1611FS (InGaAs, 1GHz BW), instead of 1801FS (Si, 125MHz BW).
- The reflection and transmission of the OMC cavity were monitored by CCDs.

The OMC itself was mounted on the transport fixture. The transport fixture was rigidly mounted on the optical table so that the OMC cavity does not shift during assembling and testing.

Mode-matching of the input beam to the OMC cavity was the crucial part of this optical setup in order to make the power budget measurement precise. The mode-matching telescope is consist of two plano-convex lenses ($f = 35\text{mm}$ and $f = 125\text{mm}$). The distances of the lenses from the fiber coupler is shown in 62. This mode-matching telescope resulted the beam profile as shown in 64. This mode-matching solution was estimated to have the mode-matching of 99.8%. The actual beam had the mode-matching of about 99%, which seemed not limited by the second-order higher-order mode (Figure 66). Since the mode-matching telescope was built on a separate sub-breadboard (Figure 63), the same mode-matching quality of the beam can be reproduced by maintaining the optics on this sub-breadboard including the fiber and the coupler.

The electrical setup is shown in Figure 67. For the measurement of the FSR and TMS of the cavity, the technique in Section 2.1.1 was used again. Therefore the electrical setup is

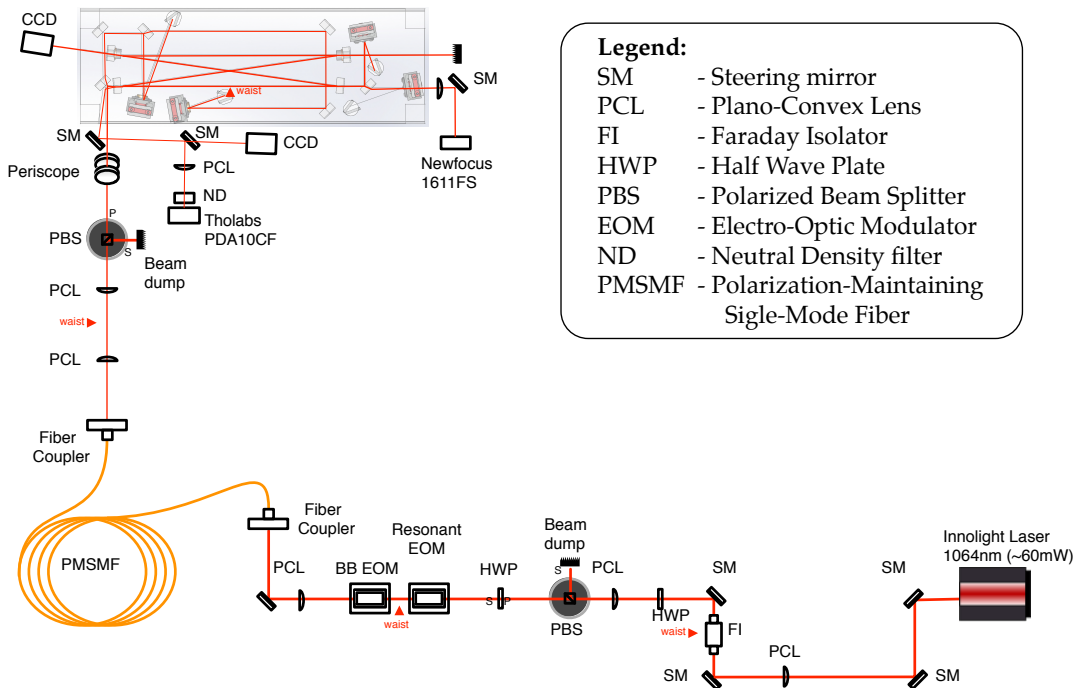


Figure 61: Optical setup for the OMC test.

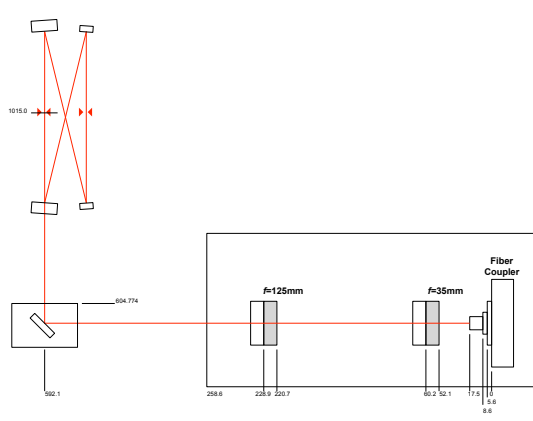


Figure 62: Mode-matching telescope for the OMC cavity. The small numbers indicates the distance of the optics from the body of the fiber coupler in the unit of mm. The waist is located at the distance of 1015.0 mm.

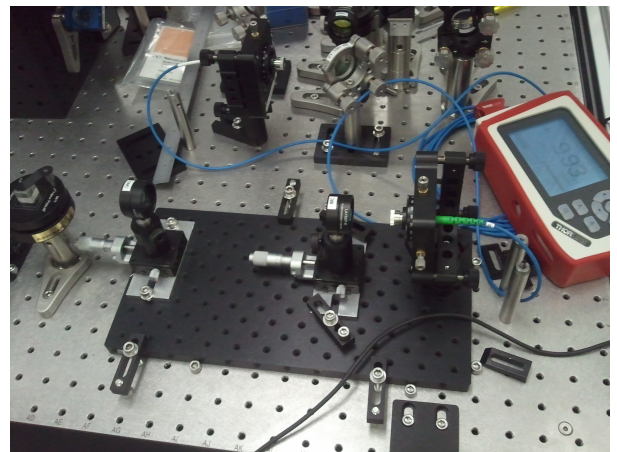


Figure 63: The actual setting of the mode matching telescope.

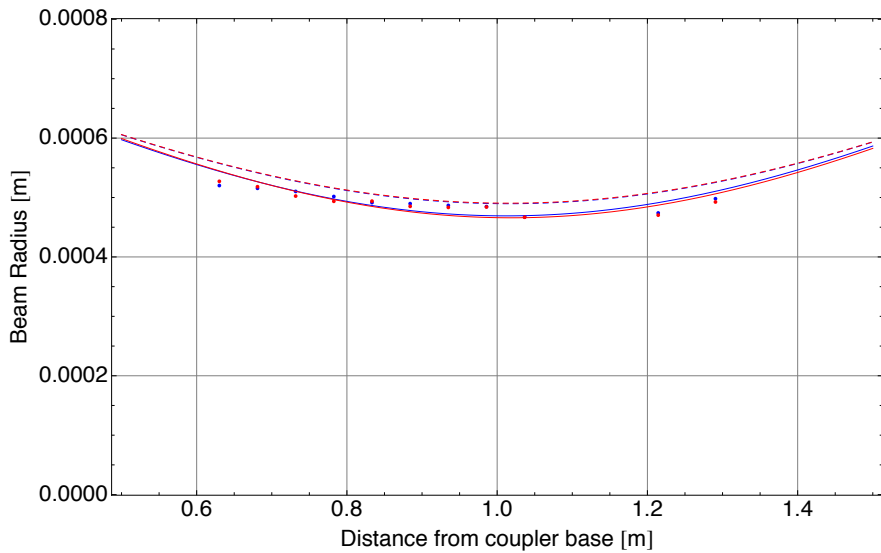


Figure 64: Beam profile measurement for the OMC cavity mode-matching. The blue and red dots indicate the measured horizontal and vertical beam radius. The solid lines indicate the estimated mode profile with curve fitting. The dashed lines indicate the calculated OMC modes.

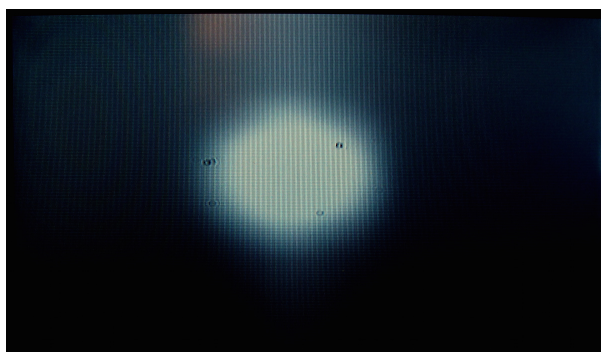


Figure 65: Photo of the transmission monitor CCD when the cavity is locked.

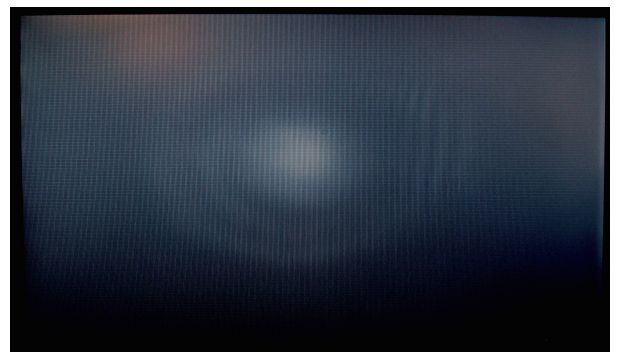


Figure 66: Photo of the reflection monitor CCD when the cavity is locked.

basically same as the one in the RoC measurement (Figure 2) with some improvement of the components. Particularly, the cavity is now just locked with laser PZT via a high-voltage driver.

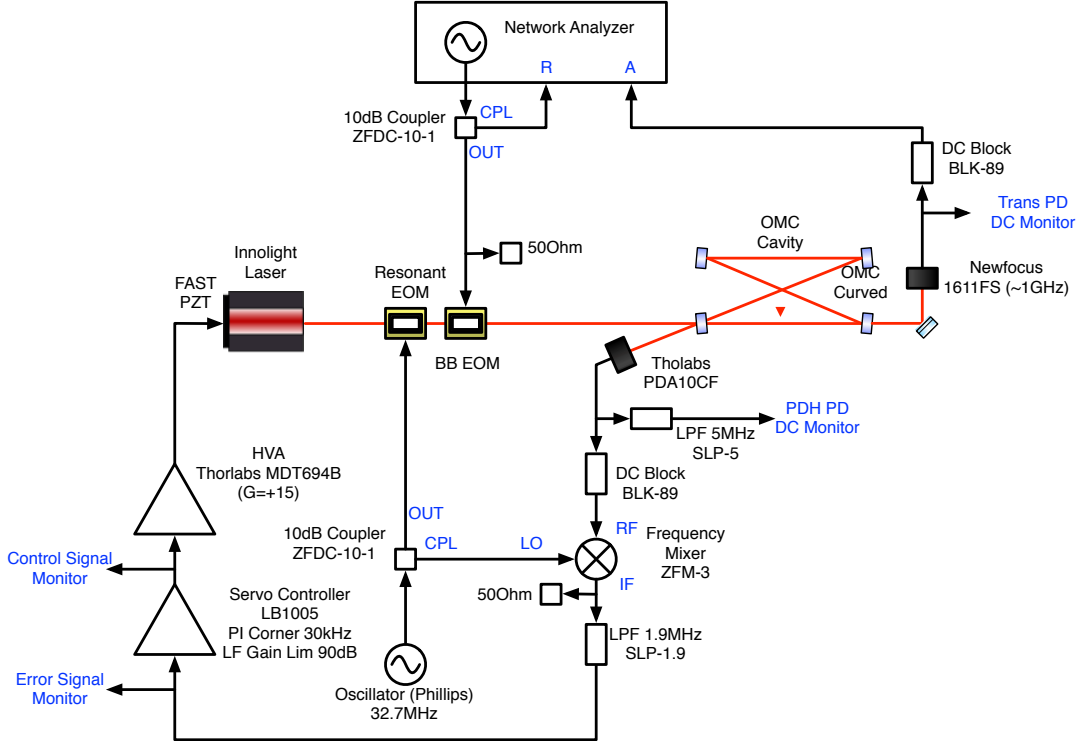


Figure 67: Electrical setup for the OMC test.

3.2 Cavity geometry test

3.2.1 Cavity absolute length measurement with detuned locking

[Description]

When a cavity is locked with an error signal offset, the detuning imposes frequency-modulation to amplitude-modulation (FM-AM) conversion. This conversion does not happen when the modulation frequency is at the free spectral range. Therefore the transfer function from the phase modulation at an EOM to amplitude modulation at the transmission RF PD has a dip at the FSR. This effect is described in [1].

[Experimental method]

This test has been done with the following procedure:

- Lock the OMC cavity and maximize the transmission by aligning the input beam. Align the transmission and reflection PDs too.
- Adjust the input signal offset of the LB1005 servo module.

- Measure the transfer function between R channel (modulation signal for the BB EOM) and A channel (transmission PD RF). The twin-peak structure should be present at around 265MHz (or 262MHz for H1 OMC).

- Adjust the offset so that the structure is maximized.

[Result]

By fitting the dip in the transfer function we can determine the location of the FSR. The fitting function is

$$f(a, f_0, \phi, dT, f) = a e^{-i2\pi f dT} (f - e^{i\phi} f_0) , \quad (1)$$

where f is the variable (frequency) and the others are fitting parameters: f_0 corresponds to the FSR. The other parameters a, ϕ, dT are related to an amplitude, a complex constant offset, and a time delay of the measurement.

The measurement and fitting results are summarized in Sections [3.2.4](#) (L1), [3.2.5](#) (H1), and [3.2.6](#) (3IFO).

3.2.2 Cavity length and finesse measurement with RFAM injection

[Description]

Another technique to characterize the cavity length is the amplitude modulation injection. The similar measurement can be done with the injection of the frequency shifter carrier using an AOM. In our case, the frequency shifter AOM was broken, and the AM injection technique was needed.

[Experimental method]

When the input polarization to the EOM is rotated, the actuation on the EOM produces voltage dependent birefringence. This is converted to the amplitude modulation via polarization optics between the EOM and the OMC. Therefore the EOM works as the AM injector.

One problem of this technique is that this RFAM cause the offset in the PDH signal as the polarization was rotated before the EOM for the PDH signal. If we have the offset in the PDH locking, this causes FM-AM conversion around the FSR frequency and confuses the response of the AM injection method. The PDH offset was cancelled by the input offset of the servo filter so that the line width of the response is minimized.

[Result]

The measured transfer function was fitted by the following model function:

$$f(a, f_{\text{FSR}}, F, dT, f) = a \left[\frac{1 - r(F)}{1 - r(F)e^{-i2\pi f/f_{\text{FSR}}}} \right]^2 e^{-i2\pi f dT} , \quad (2)$$

where $r(F)$ is the inverse function of

$$F = \frac{\pi\sqrt{r}}{1-r}, 0 < r < 1. \quad (3)$$

f is the variable (frequency) and the others are fitting parameters. f_{FSR} and F correspond to the FSR and the finesse of the cavity. The other parameters a, dT are related to an amplitude, and a time delay of the measurement.

The measurement and fitting results are summarized in Sections 3.2.4 (L1), 3.2.5 (H1), and 3.2.6 (3IFO).

3.2.3 Transverse-mode spacing measurement

[Description]

The transverse mode spacing of the OMC cavity was measured. The vertical and horizontal modes have different TMSs as expected. It was found that the TMSs depend on the PZT voltages.

[Experimental method]

Similarly to the measurement in Section 2.1.1, the transverse mode spacing (TMS) of each OMC cavity was measured. Because of the intrinsic astigmatism of the ring cavity, the TMSs for the vertical and horizontal directions were measured independently.

It is also found that the TMS is dependent on the PZT voltage. This is probably due to the three dimensional deformation of the ring PZT with the voltage applied. The TMSs in both directions were measured with each PZT voltage swept from 0V to 200V with 50V increment.

[Result]

The measured transfer function has three peaks associated with the 1st order modes. Each peak was fitted by the following function:

$$f(a_R, a_I, f_0, \Gamma, dT, f) = (a_R + i a_I) e^{-i 2\pi f dT} \frac{\Gamma}{\Gamma + i(f - f_0)} \quad (4)$$

where f is the variable (frequency) and the others are fitting parameters. f_0 and Γ correspond to the peak frequency and the half line width. The other parameters a_R, a_I, dT are related to the real and imaginary parts of the amplitude, and a time delay of the measurement.

The measurement and fitting results are summarized in Sections 3.2.4 (L1), 3.2.5 (H1), and 3.2.6 (3IFO).

3.2.4 Cavity geometry test results: L1 OMC

HOM 5/30

http://nodus.ligo.caltech.edu:8080/OMC_Lab/134

dependence on PZT 5/31

http://nodus.ligo.caltech.edu:8080/OMC_Lab/135

FSR measurement with the detuned locking technique
 (Section 3.2.1, Figure 91)

FSR	264.967	± 0.002	[MHz]
Cavity roundtrip length	1.131433	± 0.000007	[m]

FSR/Finesse measurement with the RFAM injection
 (Section 3.2.2, Figure 92)

FSR	264.9694	± 0.0003	[MHz]
Cavity roundtrip length	1.131423	± 0.000001	[m]
Finesse	405.3	± 0.3	

Table 18: Summary of the cavity geometry tests for L1 OMC

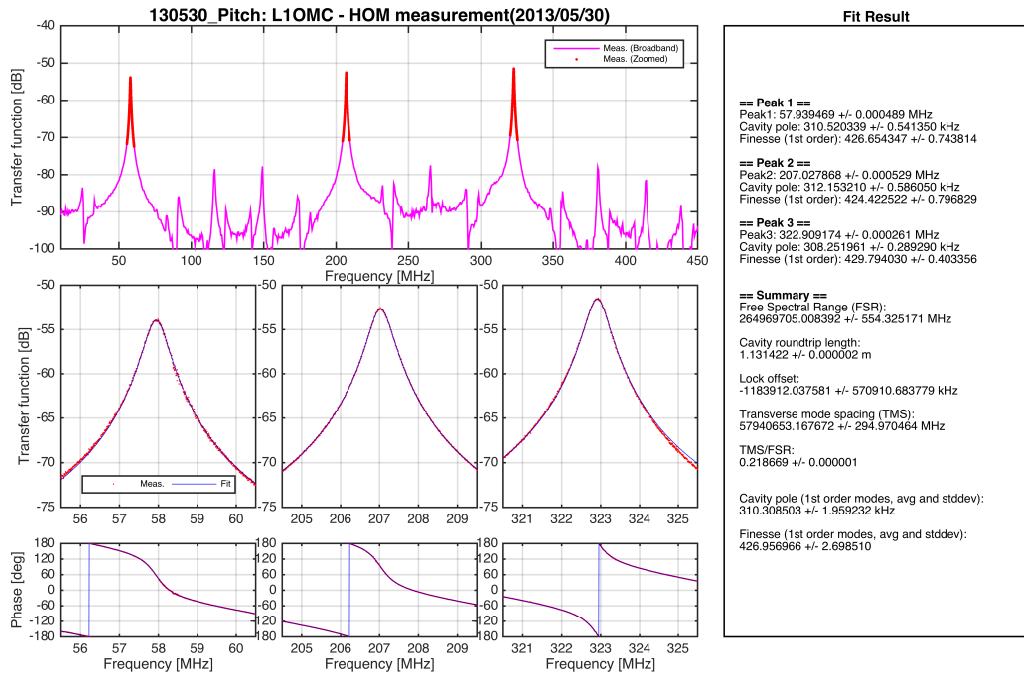


Figure 68: Electrical setup for the OMC test.

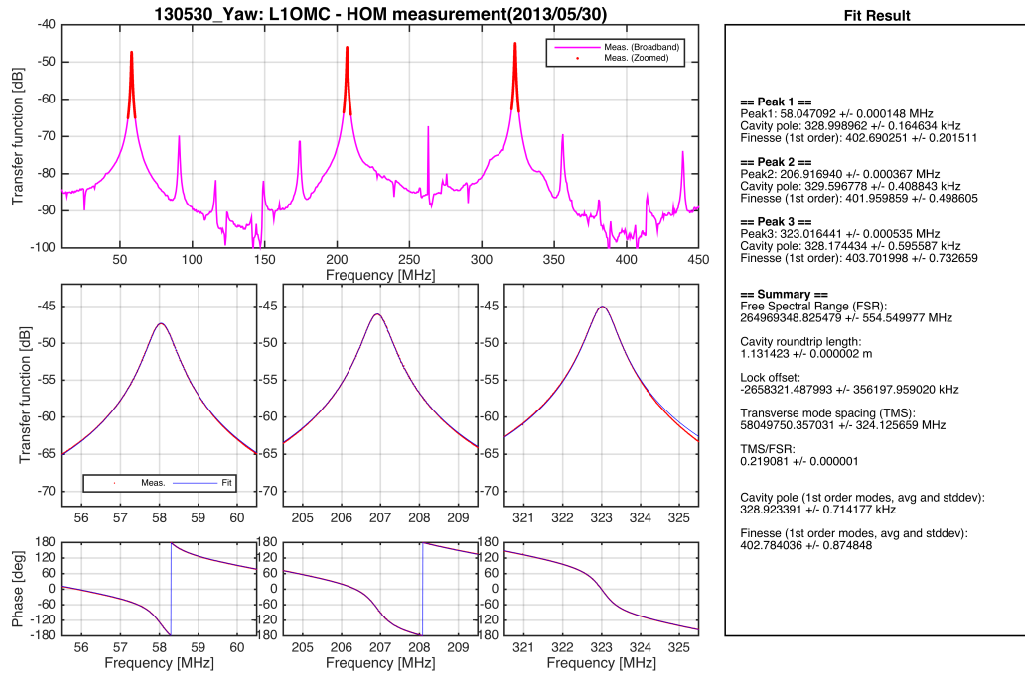


Figure 69: Electrical setup for the OMC test.

3.2.5 Cavity geometry test results: H1 OMC

FSR measurement with the detuned locking technique (Section 3.2.1, Figure 93)

FSR	261.710	± 0.003	[MHz]
Cavity roundtrip length	1.14552	± 0.000001	[m]

FSR/Finesse measurement with the RFAM injection (Section 3.2.2, Figure 94)

FSR	261.7104	± 0.0003	[MHz]
Cavity roundtrip length	1.145512	± 0.000001	[m]
Finesse	375.7	± 0.3	

Table 19: Summary of the cavity geometry tests for H1 OMC

http://nodus.ligo.caltech.edu:8080/OMC_Lab/134

H1 HOM

ELOG 159@PZT1 50V ELOG 161@PZT1 50V ELOG 162@PZT1 50V

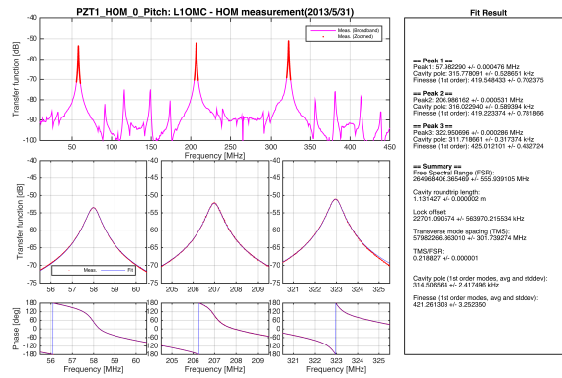


Figure 70: L1 OMC Vertical HOM measurement with $V_{\text{PZT}1} = 0\text{V}$ and $V_{\text{PZT}2} = 0\text{V}$

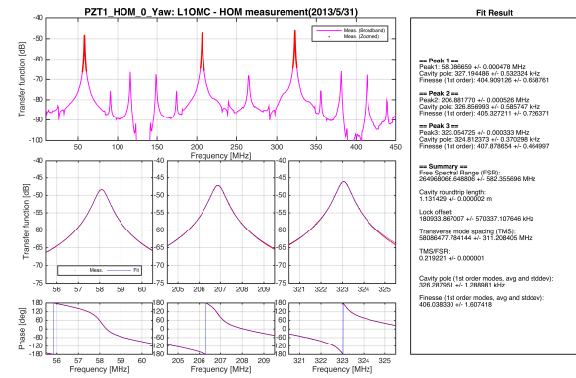


Figure 71: L1 OMC Horizontal HOM measurement with $V_{\text{PZT}1} = 0\text{V}$ and $V_{\text{PZT}2} = 0\text{V}$

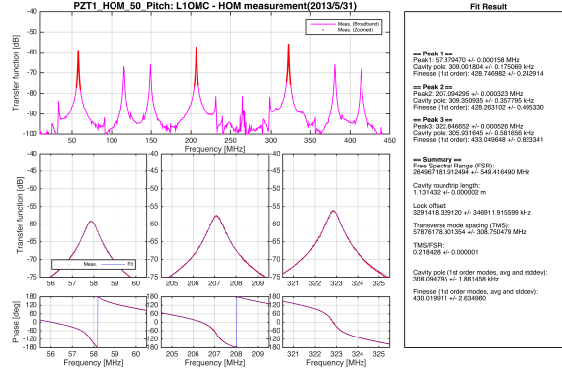


Figure 72: L1 OMC Vertical HOM measurement with $V_{\text{PZT}1} = 50\text{V}$ and $V_{\text{PZT}2} = 0\text{V}$

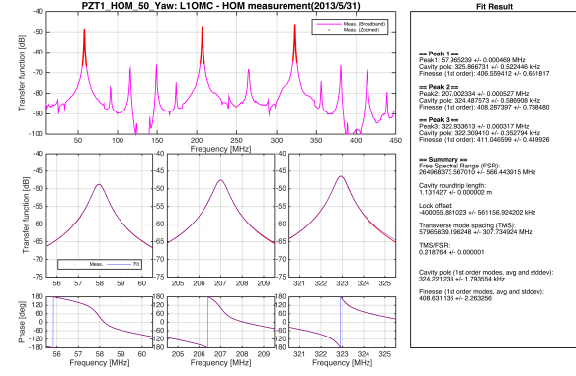


Figure 73: L1 OMC Horizontal HOM measurement with $V_{\text{PZT}1} = 50\text{V}$ and $V_{\text{PZT}2} = 0\text{V}$

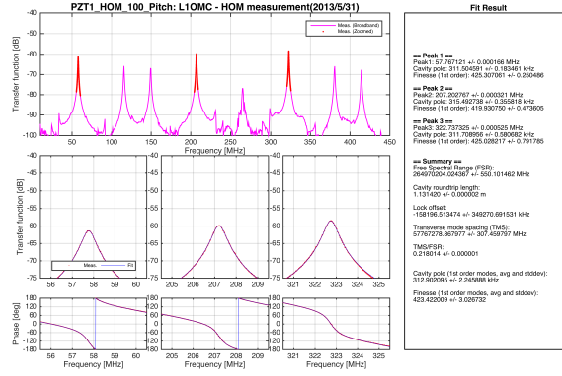


Figure 74: L1 OMC Vertical HOM measurement with $V_{\text{PZT}1} = 100\text{V}$ and $V_{\text{PZT}2} = 0\text{V}$

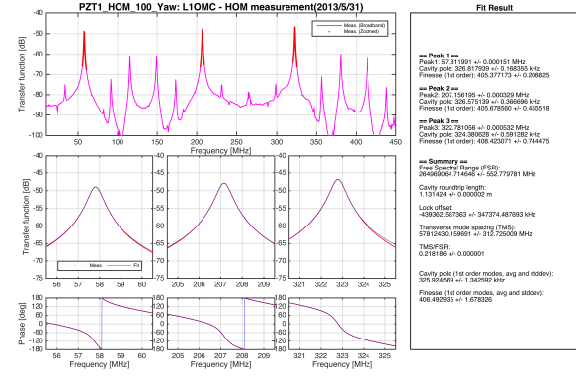


Figure 75: L1 OMC Horizontal HOM measurement with $V_{\text{PZT}1} = 100\text{V}$ and $V_{\text{PZT}2} = 0\text{V}$

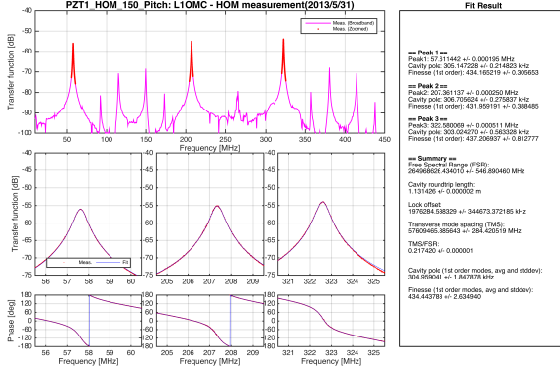


Figure 76: L1 OMC Vertical HOM measurement with $V_{\text{PZT}1} = 150\text{V}$ and $V_{\text{PZT}2} = 0\text{V}$

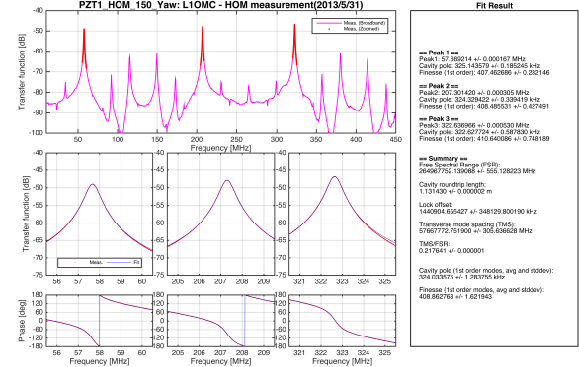


Figure 77: L1 OMC Horizontal HOM measurement with $V_{\text{PZT}1} = 150\text{V}$ and $V_{\text{PZT}2} = 0\text{V}$

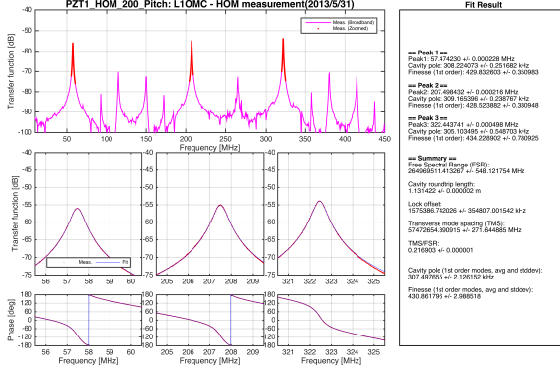


Figure 78: L1 OMC Vertical HOM measurement with $V_{\text{PZT}1} = 200\text{V}$ and $V_{\text{PZT}2} = 0\text{V}$

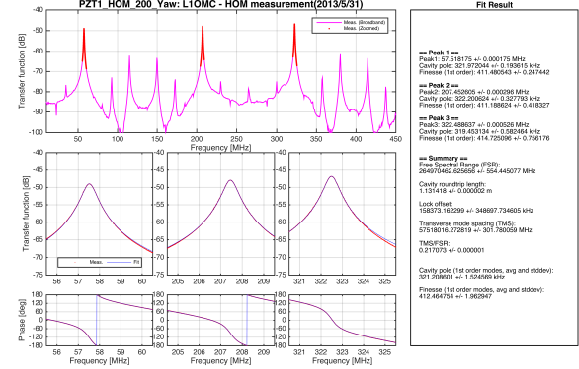


Figure 79: L1 OMC Horizontal HOM measurement with $V_{\text{PZT}1} = 200\text{V}$ and $V_{\text{PZT}2} = 0\text{V}$

FSR measurement with the detuned locking technique (Section 3.2.1, Figure 95)

FSR	264.819 ± 0.001	[MHz]
Cavity roundtrip length	1.132065 ± 0.000004	[m]

FSR/Finesse measurement with the RFAM injection (Section 3.2.2, Figure 96)

FSR	264.8121 ± 0.0003	[MHz]
Cavity roundtrip length	1.132095 ± 0.000001	[m]
Finesse	399.0	± 0.3

Table 20: Summary of the cavity geometry tests for 3rd IFO OMC

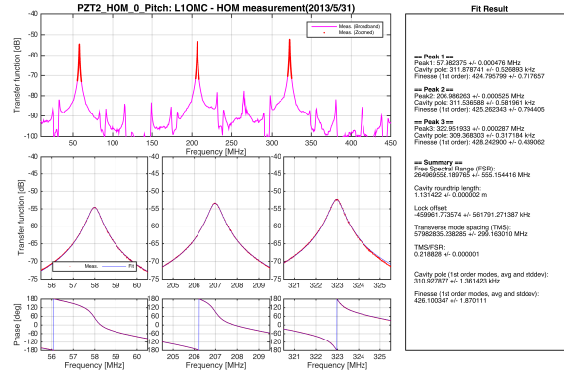


Figure 80: L1 OMC Vertical HOM measurement with $V_{\text{PZT}1} = 0\text{V}$ and $V_{\text{PZT}2} = 0\text{V}$

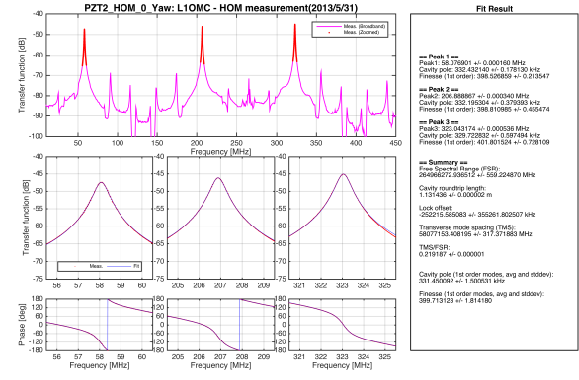


Figure 81: L1 OMC Horizontal HOM measurement with $V_{\text{PZT}1} = 0\text{V}$ and $V_{\text{PZT}2} = 0\text{V}$

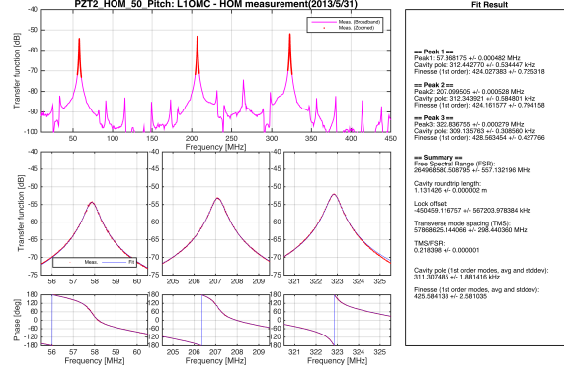


Figure 82: L1 OMC Vertical HOM measurement with $V_{\text{PZT}1} = 0\text{V}$ and $V_{\text{PZT}2} = 50\text{V}$

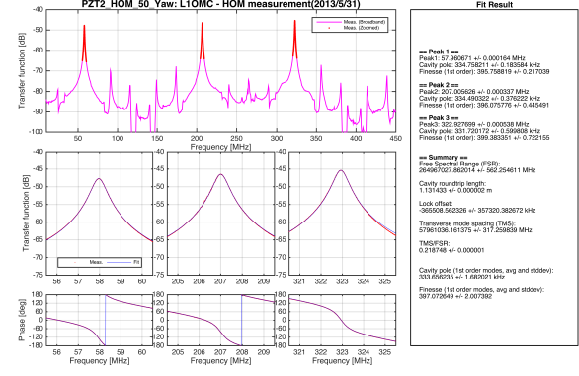


Figure 83: L1 OMC Horizontal HOM measurement with $V_{\text{PZT}1} = 0\text{V}$ and $V_{\text{PZT}2} = 50\text{V}$

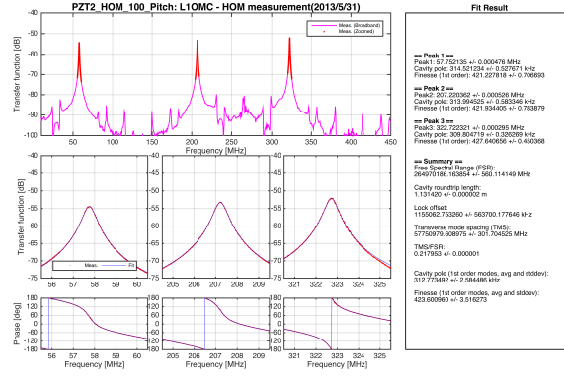


Figure 84: L1 OMC Vertical HOM measurement with $V_{\text{PZT}1} = 0\text{V}$ and $V_{\text{PZT}2} = 100\text{V}$

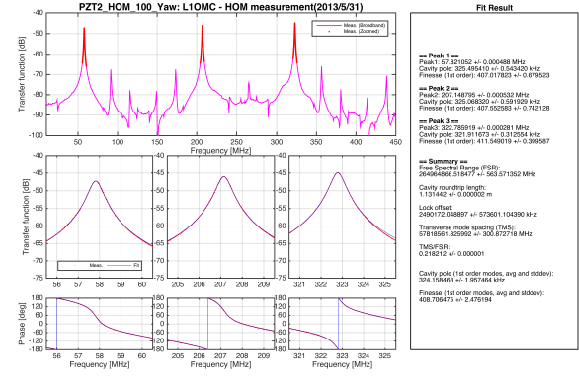


Figure 85: L1 OMC Horizontal HOM measurement with $V_{\text{PZT}1} = 0\text{V}$ and $V_{\text{PZT}2} = 100\text{V}$

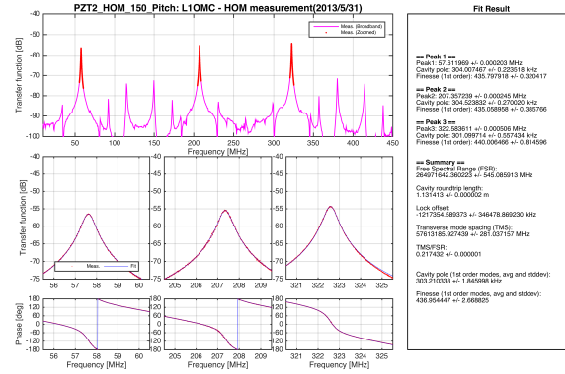


Figure 86: L1 OMC Vertical HOM measurement with $V_{\text{PZT}1} = 0\text{V}$ and $V_{\text{PZT}2} = 150\text{V}$

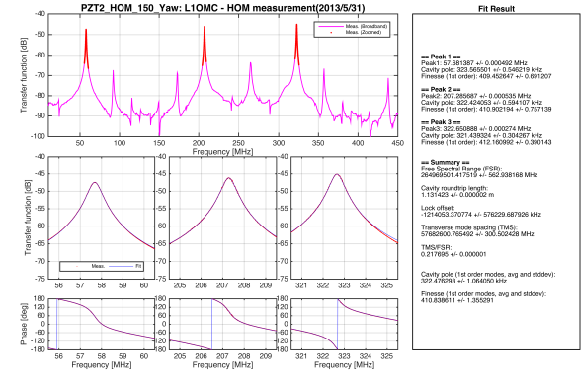


Figure 87: L1 OMC Horizontal HOM measurement with $V_{\text{PZT}1} = 0\text{V}$ and $V_{\text{PZT}2} = 150\text{V}$

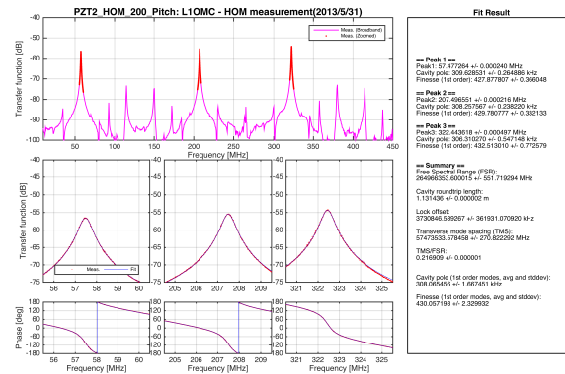


Figure 88: L1 OMC Vertical HOM measurement with $V_{\text{PZT}1} = 0\text{V}$ and $V_{\text{PZT}2} = 200\text{V}$

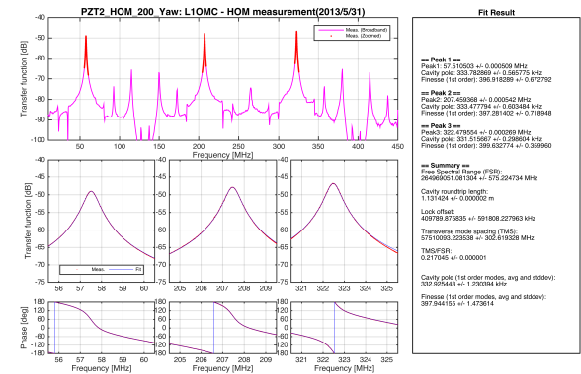


Figure 89: L1 OMC Horizontal HOM measurement with $V_{\text{PZT}1} = 0\text{V}$ and $V_{\text{PZT}2} = 200\text{V}$

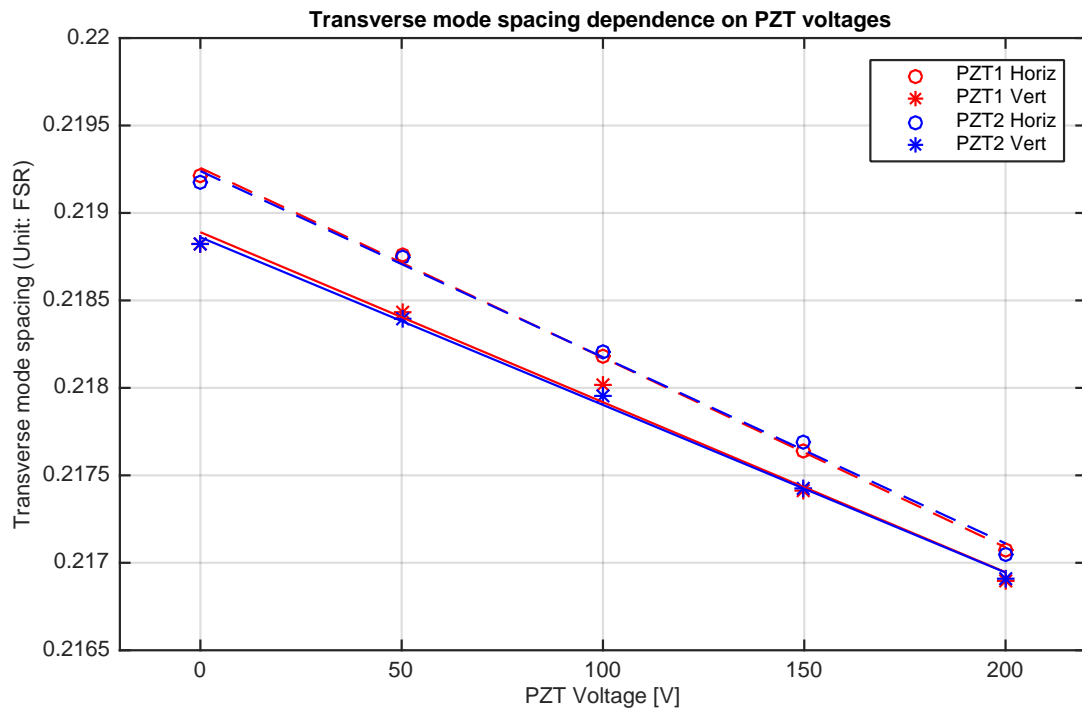


Figure 90: Electrical setup for the OMC test.

3.2.6 Cavity geometry test results: 3rd IFO OMC

http://nodus.ligo.caltech.edu:8080/OMC_Lab/198
http://nodus.ligo.caltech.edu:8080/OMC_Lab/199

GOLDEN ARCH

AMINJ

HOM

3.3 Power budget

[External Link]

http://nodus.ligo.caltech.edu:8080/OMC_Lab/135
http://nodus.ligo.caltech.edu:8080/OMC_Lab/170
http://nodus.ligo.caltech.edu:8080/OMC_Lab/186
http://nodus.ligo.caltech.edu:8080/OMC_Lab/197
http://nodus.ligo.caltech.edu:8080/OMC_Lab/217

3.4 PZT characterization

3.4.1 PZT response

L1 ELOG 148

3IFO ELOG 202

3.5 Diode alignment

3.5.1 SHIM HEIGHT MEASUREMENT

L1 ELOG 120/121 L1 invar reinforcement shim 125

H1 163 H1 DCPD 172

3IFO ELOG 206

DCPD#	DCPD1	DCPD2	
Housing#	#009	#010	
Diode#	#07	#10	
Shim	1.00mm 01	1.00mm 02	(1.00mm = D1201467-09)
<hr/>			
Power Incident	11.1 mW	10.6 mW	
Vout	7.65 V	7.33 V	
Responsivity[A/W]	0.69	0.69	
Q.E.	0.80	0.81	
<hr/>			
photo	2nd	1st	

PD alignment confirmation

3.5.2 PD/QPD ALIGNMENT photos

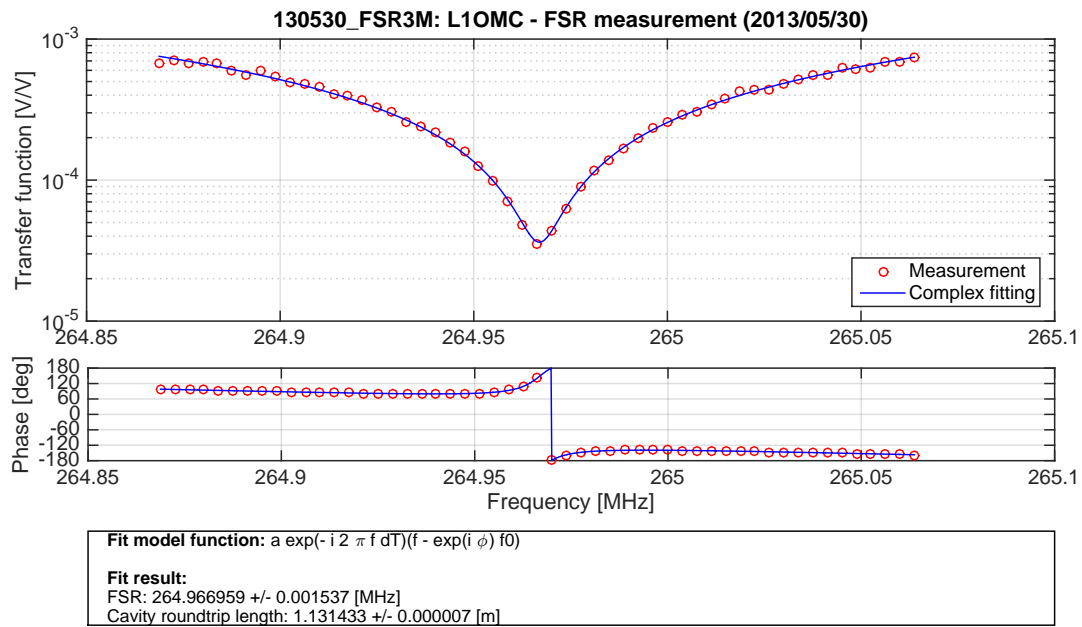


Figure 91: FSR/DETUNING L1

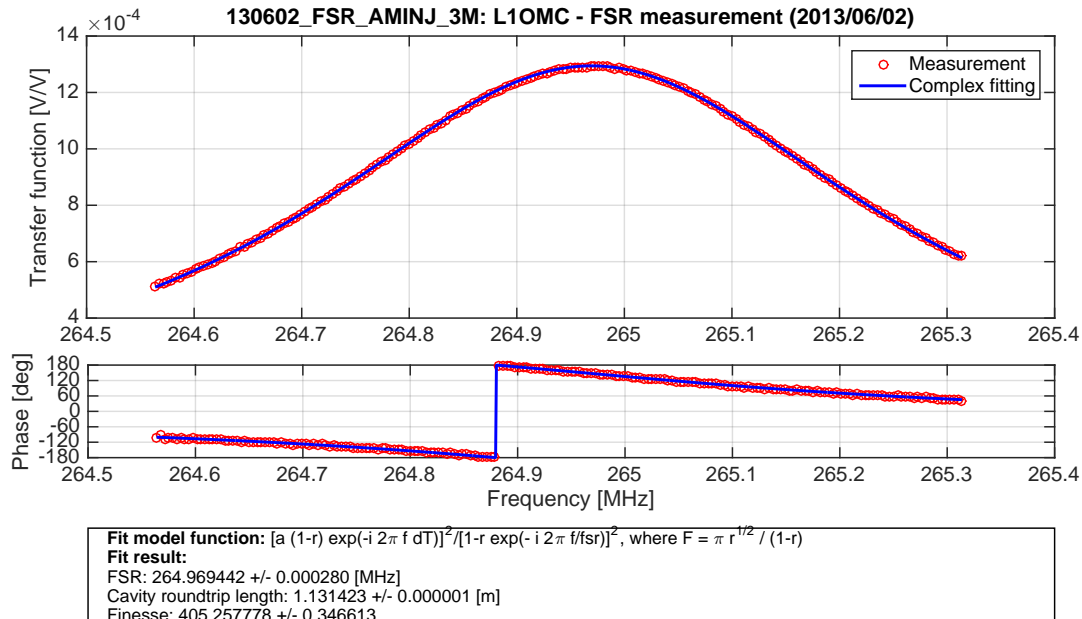


Figure 92: AM INJ L1

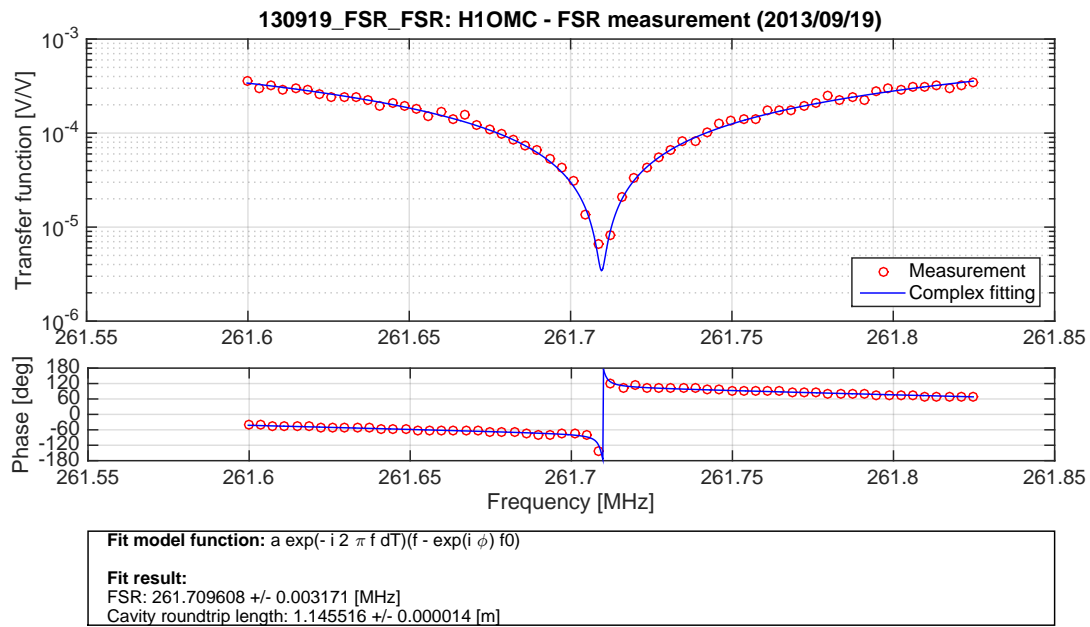


Figure 93: FSR/DETUNING H1

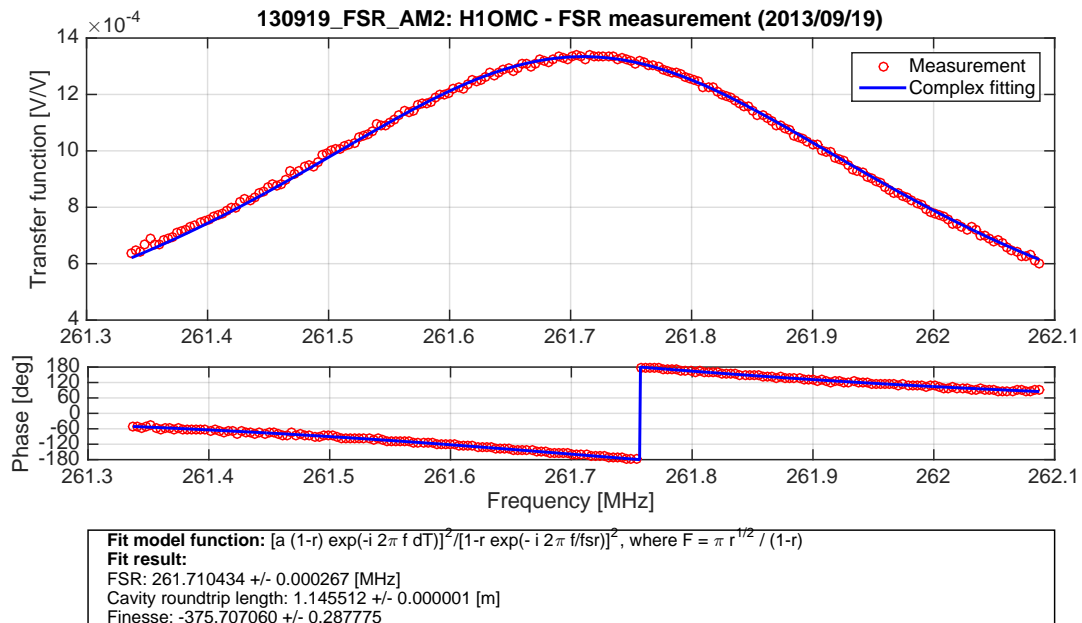


Figure 94: AM INJ H1

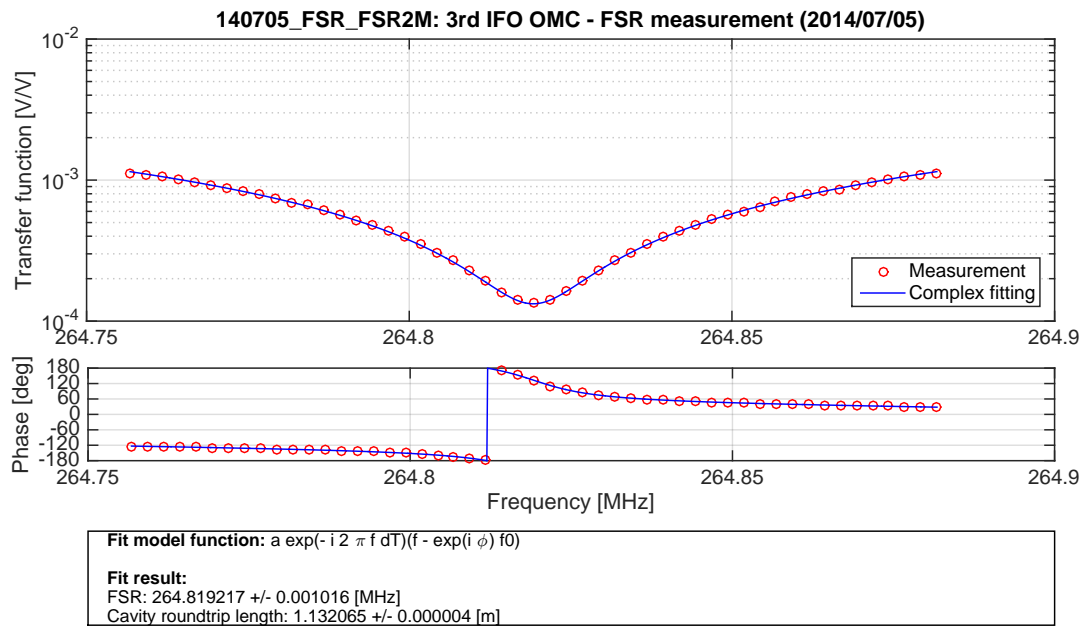


Figure 95: FSR/DETUNING 3IFO

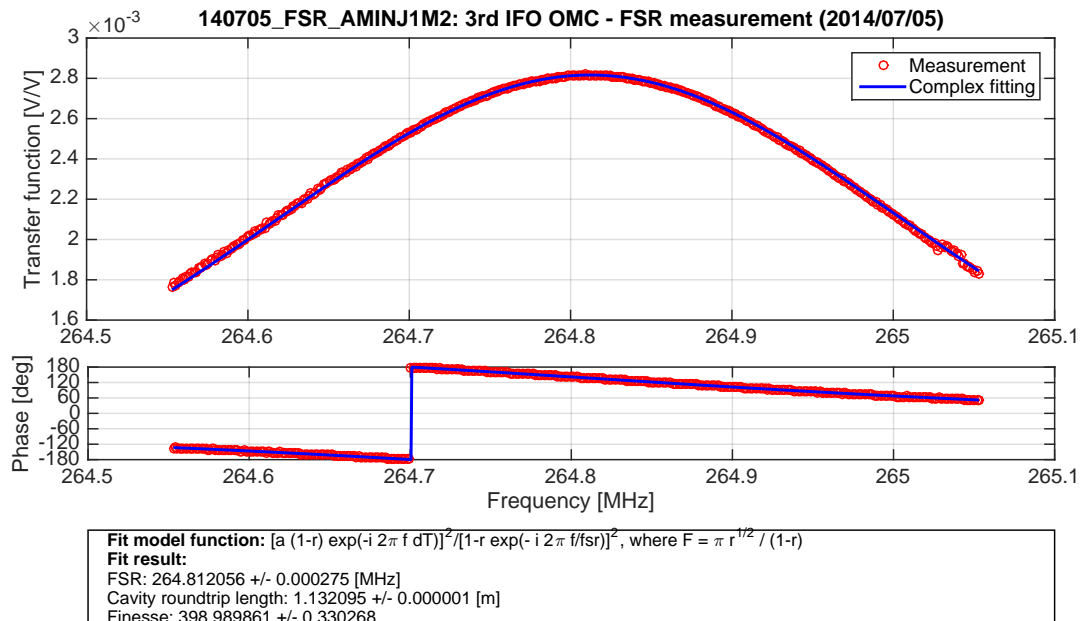


Figure 96: AM INJ 3IFO

3.5.3 QPD ALIGNMENT

The QPD alignment was adjusted using the aligned beam to the cavity and the 4ch transimpedance amplifier.

As I have a test cable for the QPD, I attached a DB9 connector on it so that I can use the QPD transimpedance amplifier to read the photocurrent. The transimpedance of the circuit is 1kV/A. As this board (D1001974) does not have X/Y/SUM output, I quickly made the summing circuit on a universal board I took from Japan a while ago.

The spot on the QPD1 (shorter arm side) seems too low by 0.64mm. It seems that the QPD is linearly responding to the input misalignment, so there is no optical or electrical problem.

As I wonder how much I can improve the situation by replacing the diodes, I swapped the diodes between QPD1 and QPD2. Now QPD1 and QPD2 have the diode #43 and #38, respectively. It improved the situation a little (about 60um). But the beam is still 0.58mm too low. 95% of the power is on the upper two elements. Of course this is at the edge of the linear range. I confirmed we still can observe the cavity is fringing even with the beam is aligned on this QPD. So this may be sufficient for the initial alignment.

The QPD2 was in a better situation. The spot is about 100um too low but this is still well within the linear range.

The incident powers on the diodes were also measured. The estimated responsivities and Q.E.s are listed below. The reflection from the diode is adjusted to hit the beam dump properly.

Here are the raw numbers

Once these burrs were removed, the spots were found on the right position of each diode. From the measurement of the power on each segment, the positions of the spots were estimated. (listed in the table) They indicate that the spots are within 0.1mm from the center. This is good enough.

The quantum efficiency was measured from the incident power and the sum output. It seems that there are some difference between the diodes. The numbers are consistent with the measurement the other day.

L1

ELOG 133

QPD#	QPD1	QPD2
Diode#	#43	#38
<hr/>		
Power Incident	84.7 uW	86.2 uW
Sum Out	56 mV	61 mV
Vertical Out	-6.8 mV	10 mV
Horizontal Out	4.2 mV	8.8 mV
SEG1	-17 mV	-15 mV

SEG2	-14.5	mV	-11	mV
SEG3	-11	mV	-15	mV
SEG4	-13	mV	-20	mV

Spot position X	+25	um	+46	um	(positive = more power on SEG1 and SEG4)
Spot position Y	-42	um	+46	um	(positive = more power on SEG3 and SEG4)

Responsivity[A/W]	0.66	0.71
Q.E.	0.77	0.82

Arrangement of the segments

View from the beam

```
/ 2 | 1 X
|---+---|
\ 3 | 4 /
```

$$I(w,x,y) = \text{Exp}[-2(x^2 + y^2)/w^2]/(\text{Pi } w^2/2)$$

$$(\text{SEG_A+SEG_B-SEG_C-SEG_D})/(\text{SEG_A+SEG_B+SEG_C+SEG_D}) = \text{Erf}[\sqrt{2} d/w]$$

d: distance of the spot from the center

w: beam width

ELOG 172

- 1) Deburr the bottom surfaces of the QPD housings
- 2) Aligned the QPDs

QPD#	QPD1	QPD2
Housing#	#004	#008
Diode#	#44	#46
Shim	1.75mm 001	1.25mm 001

Power Incident	125.7	uW	126.4	uW
Sum Out	80.1	mV	78.9	mV
Vertical Out	+ 3.4	mV	0	mV
Horizontal Out	-23.7	mV	-26	mV
SEG1	-15.6	mV	-13.2	mV
SEG2	-13.1	mV	-13.3	mV

SEG3	-29.0	mV	-26.4	mV
SEG4	-23.2	mV	-26.3	mV

Spot position X	-13	um	- 0.8	um	(positive = more power on SEG1 and SEG4)
Spot position Y	+93	um	+107	um	(positive = more power on SEG3 and SEG4)

Responsivity [A/W]	0.64	0.62
Q.E.	0.74	0.73

Arrangement of the segments

View from the beam
/ 2 | 1 X
|---+---|
\ 3 | 4 /

$$I(w, x, y) = \text{Exp}[-2(x^2 + y^2)/w^2]/(\text{Pi } w^2/2)$$

$$(\text{SEG_A} + \text{SEG_B} - \text{SEG_C} - \text{SEG_D}) / (\text{SEG_A} + \text{SEG_B} + \text{SEG_C} + \text{SEG_D}) = \text{Erf}[\sqrt{2} d/w]$$

d: distance of the spot from the center
w: beam width

ELOG205

QPD#	QPD1	QPD2	
Housing#	#006	#007	
Diode#	#50	#51	
Shim	1.25mm 03	1.25mm 02	(1.25mm = D1201467-10)

Power Incident	123.1-13.0	uW	124.5-8.0	uW
Sum Out	77.0	mV	82.5	mV
Vertical Out	-24.0	mV	- 8.8	mV
Horizontal Out	4.2	mV	9.0	mV
SEG1	-11.6	mV	-16.0	mV
SEG2	-12.6	mV	-18.0	mV
SEG3	-25.2	mV	-24.4	mV
SEG4	-21.4	mV	-21.4	mV

Spot position X	-21	um	-19	um	(positive = more power on SEG1 and SEG4)
Spot position Y	+102	um	+47	um	(positive = more power on SEG3 and SEG4)

Responsivity [A/W]	0.70	0.71
Q.E.	0.82	0.83

Arrangement of the segments

View from the beam

```
/ 2 | 1 X
|---+---|
\ 3 | 4 /
```

$$I(w, x, y) = \text{Exp}[-2(x^2 + y^2)/w^2]/(\text{Pi } w^2/2)$$

$$(SEG_A+SEG_B-SEG_C-SEG_D)/(SEG_A+SEG_B+SEG_C+SEG_D) = \text{Erf}[\sqrt{2} d/w]$$

d: distance of the spot from the center

w: beam width

3.6 Misc measurement

3.6.1 Weight

L1 ELOG 144

Weights:

Suspension cage and transportation box: 250.8lb Suspension cage and transportation box:
150.2lb ==> 100.6lb ==> 45,630 g

Metal Breadboard: 7261 g

Glass Breadboard and transportation fixture: 16382 g Transportation fixture only: 9432 g
==> 6950 g Added mass (up to now): 300 g ==> 7250 g

3.6.2 Spot positions

3IFO OMC

ELOG181

alignment effort ELOG 182

3.7 Backscatter measurement

[External Link]

http://nodus.ligo.caltech.edu:8080/OMC_Lab/207

http://nodus.ligo.caltech.edu:8080/OMC_Lab/208

http://nodus.ligo.caltech.edu:8080/OMC_Lab/209

[Description]

[Experimental method]

[Result]

3.8 Vibrational test

[External Link]

http://nodus.ligo.caltech.edu:8080/OMC_Lab/210

http://nodus.ligo.caltech.edu:8080/OMC_Lab/211

[Description]

[Experimental method]

[Result]

Appendices

A Mirror List

[External Link]

http://nodus.ligo.caltech.edu:8080/OMC_Lab/152

Breadboard	
SN	Location
BB 1	L1 OMC
BB 2	H1 OMC
BB 3	-
BB 4	3IFO OMC
BB 5	-
BB 6	-

Mounting Prisms	
SN	Location
M 1	
M 2	
M 6	H1 CM1 (PZT ASSY #6)
M 7	
M 10	3IFO CM1 (PZT ASSY #5)
M 11	H1 CM2 (PZT ASSY #4)
M 12	
M 13	3IFO CM2 (PZT ASSY #3)
M 14	
M 15	
M 16	L1 CM1 (PZT ASSY #1)
M 17	
M 20	L1 CM2 (PZT ASSY #2)
M 21	
M 22	

Table 21: List and location for OMC breadboards and Mounting Prisms

Prism Mirror A	
SN	Location
A 1	faux OMC FM1
A 2	@ Fullerton
A 3	faux OMC FM2
A 4	
A 5	
A 6	3IFO FM2
A 7	L1 FM2
A 8	L1 FM1
A 9	H1 FM1
A 10	
A 11	
A 12	3IFO FM1
A 13	H1 FM2
A 14	

Prism Mirror B	
SN	Location
B 1	
B 2	
B 3	L1 BS2 (QPD)
B 4	
B 5	3IFO BS2 (QPD)
B 6	
B 7	L1 BS3 (DCPD)
B 8	
B 9	H1 BS2 (QPD)
B 10	H1 BS3 (DCPD)
B 11	
B 12	3IFO BS3 (DCPD)

Table 22: List and location for Mirror A & B

Prism Mirror C	
SN	Location
C 1	3IFO CM1 (PZT ASSY #5)
C 2	@Fullerton
C 3	3IFO CM2 (PZT ASSY #3)
C 4	H1 CM2 (PZT ASSY #4)
C 5	L1 CM2 (PZT ASSY #2)
C 6	L1 CM1 (PZT ASSY #1)
C 7	faux OMC CM1
C 8	faux OMC CM2 - <i>&</i> H1 CM1 (with PZT ASSY #6)
C 9	H1 CM1 (PZT ASSY #6) - <i>&</i> BURNT
C 10	Liyuan tested
C 11	Liyuan tested
C 12	Curvature untested, faux OMC CM2
C 13	Curvature untested

PZT	
SN	Location
PZT 11	
PZT 12	
PZT 13	
PZT 14	3IFO CM1 (PZT ASSY #5)
PZT 15	3IFO CM2 (PZT ASSY #3)
PZT 21	H1 CM1 (PZT ASSY #6)
PZT 22	
PZT 23	L1 CM2 (PZT ASSY #2)
PZT 24	
PZT 25	H1 CM2 (PZT ASSY #4)
PZT 26	L1 CM1 (PZT ASSY #1)

Table 23: List and locations for Mirror C & PZTs

Prism Mirror E	
SN	Location
E 1	H1 SM2
E 2	H1 SM3
E 3	H1 BS1
E 4	L1 SM2
E 5	H1 SM1
E 6	
E 7	3IFO BS1
E 8	3IFO SM1
E 9	
E 10	L1 BS1
E 11	
E 12	L1 SM1
E 13	3IFO SM2
E 14	
E 15	
E 16	L1 SM3
E 17	3IFO SM3
E 18	

Table 24: List and locations for Mirror E

B DCPD dimensions

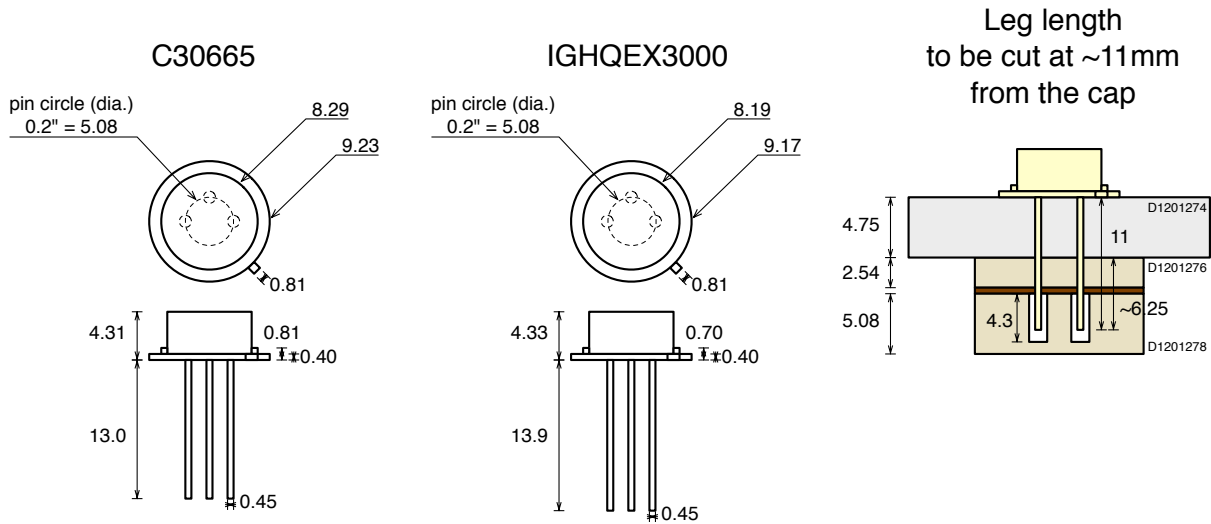


Figure 97: DCPD dimensions

C Cavity axis alignment

[External Link]

http://nodus.ligo.caltech.edu:8080/OMC_Lab/179

LIGO Document T0900647: Ray optics calculations of alignment matrices (by Sam Waldman).

[Description]

Relationship between mirror misalignment in yaw and the shift of the cavity mode was calculated.

[Experimental method]

The calculation technique is described in T0900647. The angles and displacement of the mirrors and beams are defined in Figure 98. Here only the misalignment in the horizontal plane is considered.

[Result]

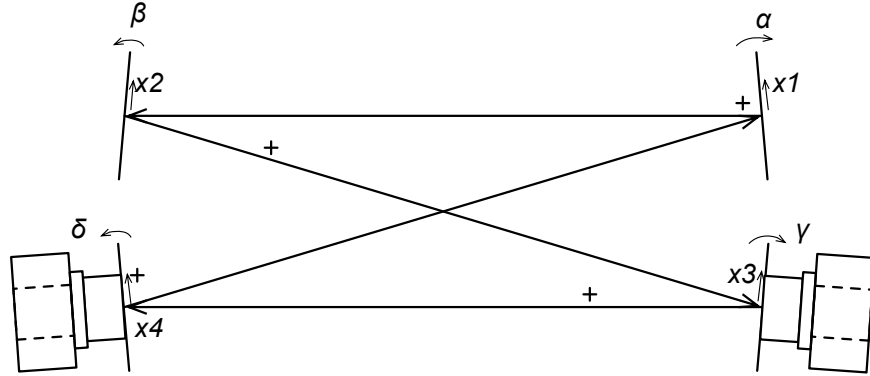


Figure 98: Definition of the parameters for the cavity axes and mirror alignment

$$\begin{pmatrix} x_1 \\ \theta_1 \\ x_2 \\ \theta_2 \\ x_3 \\ \theta_3 \\ x_4 \\ \theta_4 \end{pmatrix} = \begin{pmatrix} 0.893 & 1.107 & 1.323 & 1.246 \\ 0.759 & -0.759 & -0.271 & 0.271 \\ 1.107 & 0.893 & 1.246 & 1.323 \\ 0.759 & 1.241 & -0.271 & 0.271 \\ 1.323 & 1.246 & 1.169 & 1.400 \\ -0.271 & 0.271 & 0.819 & -0.819 \\ 1.246 & 1.323 & 1.400 & 1.169 \\ -1.241 & -0.759 & -0.271 & 0.271 \end{pmatrix} \begin{pmatrix} \alpha \\ \beta \\ \gamma \\ \delta \end{pmatrix}$$

Example:

Assuming the flat mirrors are fixed, if I want to move the x_3 spot up by 1mm without moving x_4 , the solution is

$$\begin{pmatrix} \alpha \\ \beta \\ \gamma \\ \delta \end{pmatrix} = \begin{pmatrix} 0 \\ 0 \\ -1.97 \text{ mrad} \\ +2.36 \text{ mrad} \end{pmatrix} \quad (5)$$

This yields:

$$\begin{pmatrix} x_1 \\ \theta_1 \\ x_2 \\ \theta_2 \\ x_3 \\ \theta_3 \\ x_4 \\ \theta_4 \end{pmatrix} = \begin{pmatrix} +0.33 \text{ mm} \\ +1.18 \text{ mrad} \\ +0.67 \text{ mm} \\ +1.18 \text{ mrad} \\ +1.00 \text{ mm} \\ -3.55 \text{ mrad} \\ +0.00 \text{ mm} \\ +1.18 \text{ mrad} \end{pmatrix}$$

D DCPD/QPD/PZT/Preamplifier arrangement

[External Link]

H1 PD arrangement: http://nodus.ligo.caltech.edu:8080/OMC_Lab/176

L1 PD arrangement: http://nodus.ligo.caltech.edu:8080/OMC_Lab/144

L1 PD arrangement: <https://alog.ligo-la.caltech.edu/aLOG/index.php?callRep=26476>

L1 PZT failure: <https://alog.ligo-la.caltech.edu/aLOG/index.php?callRep=8366>

[Description]

LIGO-D060572 In-vacuum DCPD (preamplifier) for OMC

L1 OMC preamps are arranged as shown in Figure 99.

- DCPD response (LLO ALOG 26476):
 - Illuminate DCPD1 (T) \Rightarrow DCPD **B** responded in MEDM
 - Illuminate DCPD2 (R) \Rightarrow DCPD **A** responded in MEDM
- QPD response (LLO ALOG 26476):
 - Illuminate QPD1 \Rightarrow QPD A responded in MEDM
 - Illuminate QPD2 \Rightarrow QPD B responded in MEDM
- PZT arrangement:
 - One of the PZTs is broken. (LLO ALOG 8366)

H1 OMC preamps are arranged as shown in Figure 100.

- DCPD response:
 - Illuminate DCPD1 (T) \Rightarrow DCPD **B** responded in MEDM
 - Illuminate DCPD2 (R) \Rightarrow DCPD **A** responded in MEDM
- QPD response:
 - Illuminate QPD1 \Rightarrow QPD A responded in MEDM
 - Illuminate QPD2 \Rightarrow QPD B responded in MEDM
- PZT arrangement:
 - Mighty Mouse Pin1&2 \Rightarrow PZT2 (DCPD side)
 - Mighty Mouse Pin3&4 \Rightarrow PZT1 (QPD side)

List of installed photodiodes: as of March 14, 2015

- L1 OMC

Top View

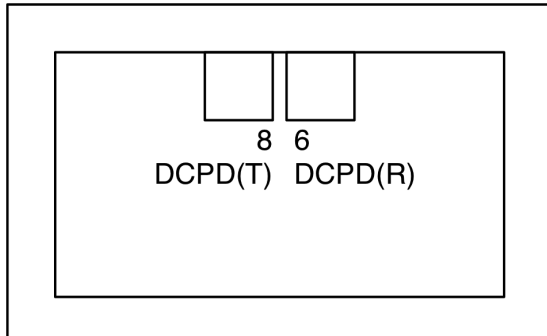


Figure 99: Preamp SNs and arrangement at LLO

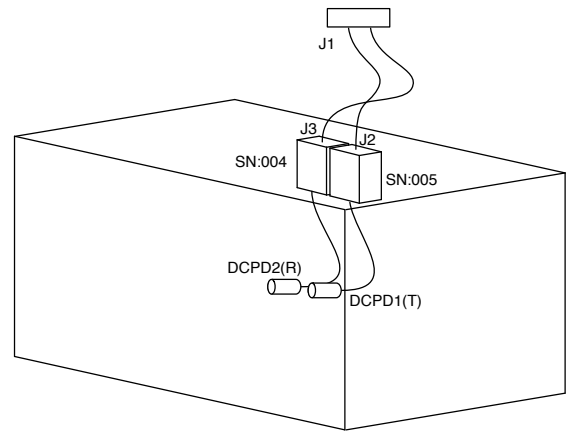


Figure 100: Preamp SNs and arrangement at LHO

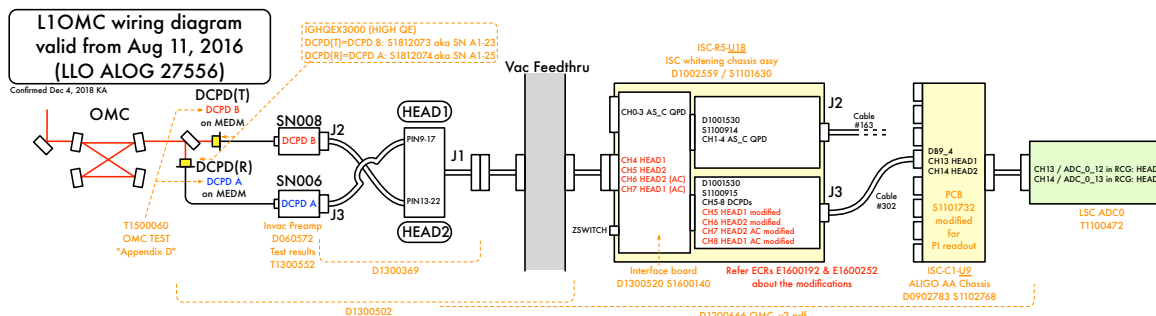
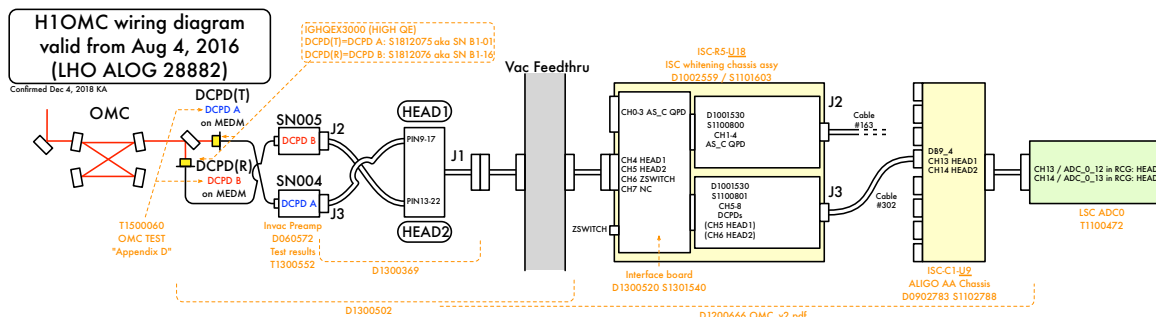


Figure 101: OMC Wiring - diagram as built

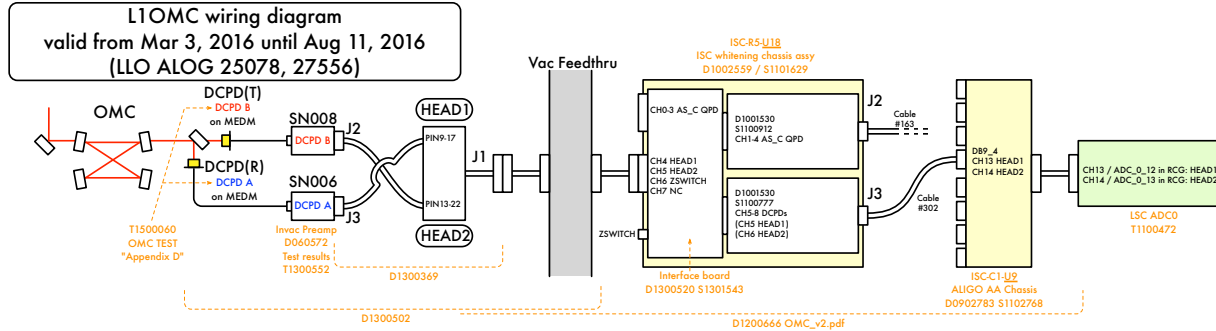


Figure 102: OMC Wiring - diagram as built (OLD)

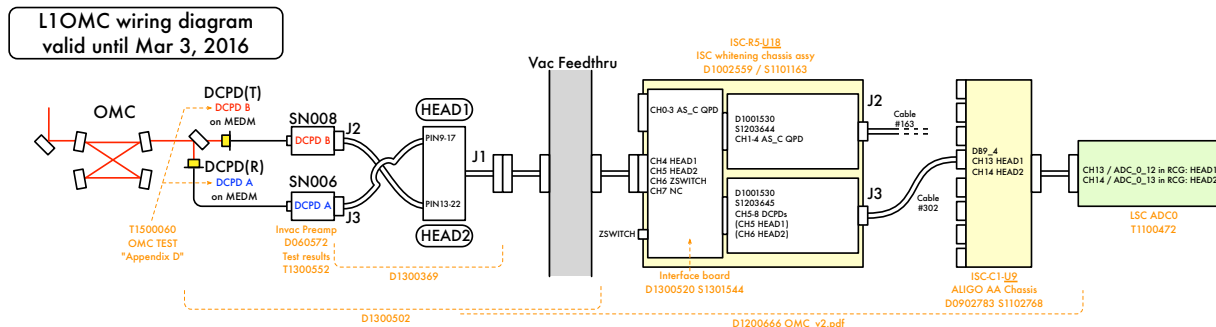
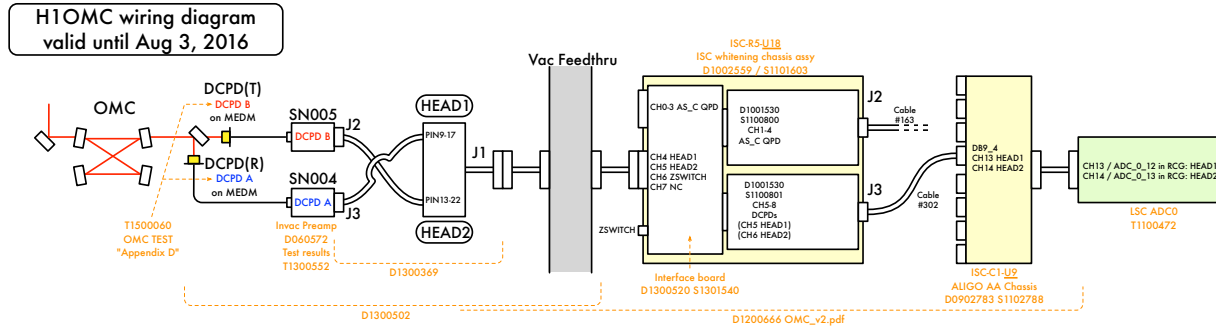


Figure 103: OMC Wiring - diagram as built (OLD)

- DCPD1 (Trans): eLIGO diode, Vendor SN unknown, Preamp SN 008, Connected to J2
- DCPD2 (Refl): eLIGO diode, Vendor SN unknown, Preamp SN 006, Connected to J3
- QPD1: LIGO SN 43
- QPD2: LIGO SN 38
- H1 OMC
 - DCPD1 (Trans): eLIGO diode, Diode Marked “A”, Vendor SN 0288, Preamp SN 005, Connected to J2
 - DCPD2 (Refl): eLIGO diode, Diode Marked “B”, Vendor SN 0721, Preamp SN 004, Connected to J3
 - QPD1: LIGO SN 44
 - QPD2: LIGO SN 46
- 3IFO OMC
 - DCPD1 (Trans): new diode with a glass window, LIGO SN 11, Vendor SN 1213
 - DCPD2 (Refl): new diode with a glass window, LIGO SN 12, Vendor SN 1208
 - QPD1: LIGO SN 50
 - QPD2: LIGO SN 51

List of installed photodiodes: as of June 10, 2016

- L1 OMC
 - DCPD1 (Trans): High QE diode IGHQEX3000, Vendor SN A1-23, Preamp SN 008, Connected to J2
 - DCPD2 (Refl): High QE diode IGHQEX3000, Vendor SN A1-25, Preamp SN 006, Connected to J3

References

- [1] N. Uehara and K. Ueda, *Accurate measurement of the radius of curvature of a concave mirror and the power dependence in a high-Finesse Fabry-Perot interferometer*, Appl. Opt., **34** (1995) 5611-5619.
- [2] K. Arai, J. Lewis, P. Fritschel, *Output Mode Cleaner Assembly Procedure LIGO Document T1300201*, (2015).
- [3] K. Arai, S. Barnum, P. Fritschel, J. Lewis, S. Waldman, *Output Mode Cleaner Design, LIGO Document T1000276*, (2013).